Fatigue in Wood

An investigation in tension perpendicular to the grain

Clorius, Christian Odin

Publication date:
2001

Document Version
Publisher's PDF, also known as Version of record

Christian Odin Clorius

Fatigue in Wood

An investigation in tension perpendicular to the grain

BYG•DTU

DANMARKS
TEKNISKE
UNIVERSITET

Rapport
BYG•DTU R-038
2002
ISBN 87-7877-096-3

Fatigue in Wood

An investigation in tension perpendicular to the grain

Christian Odin Clorius

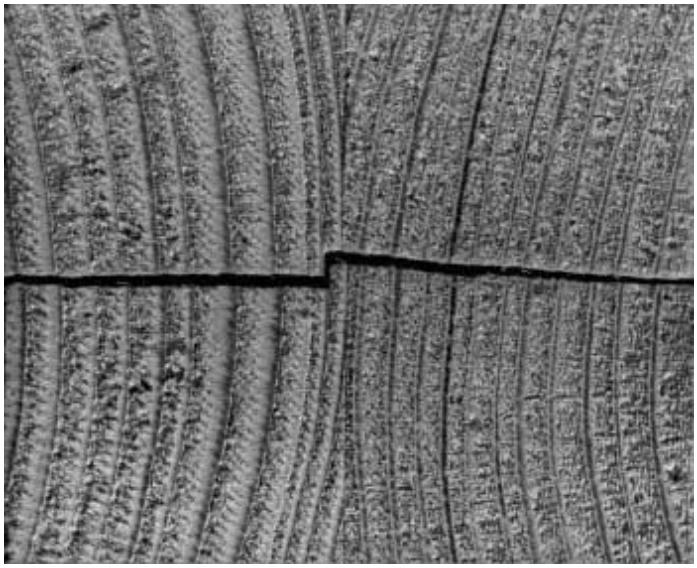

Department of Civil Engineering
DTU-building 118
2800 Kgs. Lyngby
http://www.byg.dtu.dk

2002

Preface

This thesis is submitted as a partial fulfilment of the requirements for the Danish Ph.d. degree.

The work has been carried out at the Department of Structural Engineering and Materials (BKM), Technical University of Denmark (DTU), during 1996 to 2000. Associate Professor, Ph.D. Preben Hoffmeyer and Associate Professor, Ph.D. Lars Damkilde have supervised the study. I would like to thank my supervisors, my colleague Martin Pedersen and the staff at the Department for their support throughout the project.

The project period has been interrupted at several occasions, where I in cooperation with my colleague Martin Pedersen have solved design assignments for the Danish glulam industry. Though this work for Limtræ Danmark A/S has prolonged the project it has also made my time at the Department very dynamic.

Part of the test setup was realized through a participation in the fatigue programme of the Nordic Wood project "Bridges in Wood" for which Nordic Wood is acknowledged.

Abstract

Wood fatigue is of interest in regular fatigue loaded structures such as wood bridges but wood fatigue also covers low cycle fatigue encountered in ordinary structures. The study concentrates entirely on fatigue in tension perpendicular to the grain as this strength parameter often is strength limiter in critical details.

Small clear specimens have been taken to failure in fatigue loading at stress levels of 50% and 65% of the short term strength and at frequencies of loading ranging from 1 Hz to 0.01 Hz and at dead load condition. Square wave load shape was used. The specimens were tested with a moisture content in equilibrium with either 65% or 85% relative humidity, RH. In total approximately 300 small specimens were fatigue tested.

The objective of the investigation was to search for an interaction between number of cycles and time under load to failure. Such an interaction corresponds to frequency dependent fatigue. The main experimental observations from testing of small specimens are:

- At RH 65% number of cycles to failure depends only on stress level and is invariant to frequency.
- At RH 85% number of cycles to failure is highly influenced by frequency corresponding to interaction between number of cycles and time under load to failure.

In order to model the experimental observations a model comprising both a time dependent term and a term related to the number of load oscillations is needed. This is offered by the theory of wood as a damaged viscoelastic material, the DVM theory. Essentially the DVM theory predicts a frequency range where failure is governed by interaction between number of cycles and time under load. Above this frequency range failure is due to number of cycles and below due to time under load. By use of standard values for the model parameters, the model predicts the same order of magnitude of number of cycles to failure as found from the tests. Further the model is able to correctly predict tests at RH 85% to be in the frequency range with interaction.

Resumé

Udmattelse i træ har interesse i regulært udmattelsesbelastede konstruktioner som f.eks. træbroer, men dækker også udmattelse ved få gentagelser i almindelige trækonstruktioner. Undersøgelsen koncentrerer sig udelukkende om udmattelse i træk på tværs af fiberretningen, da denne styrkeparameter ofte er styrkebegrænsende i kritiske detaljer.

Små, fejlfrie prøver er blevet belastet til udmattelsesbrud ved lastniveauer på 50% og 65% af korttidsstyrken ved frekvenser fra 1 Hz til 0.01 Hz samt ved dødlast betingelser. De anvendte lastcykler var firkantformede. Prøvelegemerne blev undersøgt ved fugtniveauer i ligevægt med 65% eller 85% relativ luftfugtighed, RF. Omkring 300 prøvelegemer blev udmattelsesundersøgt.

Målet med undersøgelsen var at søge efter en interaktion mellem antal cykler og tid under last til brud. En sådan interaktion svarer til frekvensafhængig udmattelse. De eksperimentelle hovedobservationer fra prøvning af små prøvelegemer er:

- Ved 65% RF er antallet af cykler til brud uafhængigt af frekvensen og afhænger udelukkende af lastniveauet.
- Ved 85% RF er antallet af cykler til brud meget påvirket af frekvensen, svarende til interaktion mellem antal cykler og tid under last til brud.

For at kunne modellere de eksperimentelle observationer kræves en model, der både indeholder tidsafhængighed og afhængighed af antal last-oscillationer. Dette er indeholdt i teorien om træ som et skadet viscoelastisk materiale, DVM-teorien. DVM-teorien forudsiger et frekvensområde, hvor brud styres af interaktion mellem antal cykler og tid under last. Over dette frekvensområde skyldes brud udelukkende antal cykler og under udelukkende tid under last. Under anvendelse af standardværdier for modellens parametre forudsiger modellen den samme størrelsesorden af antal cykler til brud som fundet eksperimentelt. Yderligere er modellen i stand til korrekt at forudsige, at 85% RF forsøgene er i frekvensområdet med interaktion.

Table of Contents

Chapter 1

Introduction

Wood structures are not the first in mind when fatigue is discussed. And at a conversational level the author of the present work has often been let to feel that the subject indeed were among the more exotic. However, fatigue loaded wood constructions exists and the timber construction code includes an informative annex on fatigue.

An interesting Danish example of fatigue loaded wood structures is the rotor blades of the Nibe windmills. These glulam constructions were erected in the mid 1980'ties and were in operation in approximately 10 years until they were demounted. The critical blade to hub connection was made with glued in rods. This connection was fatigue tested in accelerated tests in the design phase, however, after demounting there was interest to know whether the in-situ loads have had a more severe impact than expected. The residual strength was determined and is reported in (Pedersen, Clorius, Damkilde & Hoffmeyer 1999). The interest in the residual strength was due to the reluctancy to extrapolate from accelerated fatigue tests to the influence of the in-situ fatigue impacts also involving a duration of load phenomenon. In other words does e.g. 10 Hz accelerated fatigue testing yield the same number of cycles to failure as 0.5 Hz in situ fatigue loading.

Bridges are another example of fatigue loaded structures. In wood bridges the attention does not concentrate on the average cross section but on the details. The detailing, i.e. the connections, notches and other disturbances of the cross sections, all unite in a common tendency to introduce stress singularities often with stresses utilizing the weak and brittle shear and tension perpendicular to grain strengths.

Further, fatigue also includes the problem of low cycle fatigue. Viewed from the duration of load perspective low cycle fatigue is the natural next step after mechano-sorptive mechanisms have been included. Even so it is of course a long-term goal to unite the understanding of the phenomena of duration of load, mechano-sorptive mechanisms

and fatigue.

This work contributes with one stone in the understanding of the problem between duration of load and fatigue. It concentrates entirely on tension perpendicular to the grain. This limitation has been chosen as tension perpendicular to the grain is the most fragile of the strength parameters utilized in critical details. Fatigue is within the work understood as a phenomenon to be studied together with duration of load. Hence, the objective has not been to seek stress levels below which a specified high number of load cycles can be survived, but to seek for interaction between duration of load and number of load cycles. This is of course a limited perspective on fatigue, however, fatigue design diagrams, traditionally known as Wöhler diagrams or $S - N$ curves, do start in some point and the work tries to asses to what extend such design diagrams can be blurred by duration of load phenomena.

The work concentrates on reporting a test series which in time was extended over 3 years. For the purpose of the low frequency tests a special set of test rigs was constructed in the cellar of the department. The reader shall be spared for all the troubles involved in making this "automized-pneumato-mechanical" system work. But the author could not withstand the temptation to show an assorted assembly of unintended fatigue failures gained in various parts of the test rig during construction and testing of the system as shown in Figure 1.1.

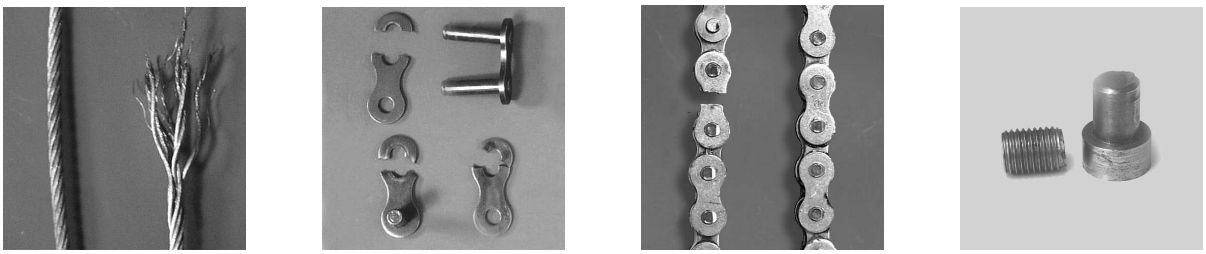

(a) Steel wire (b) Chain lock (c) Chain (d) Bolt

Figure 1.1: *Assorted assembly of unintended fatigue failures in parts of test rig gained during construction and testing of system.*

Chapter 2

Background on fatigue

Fatigue is generally understood as failure of a material due to repeated load oscillations below the static strength of the material. Normally fatigue is described by number of load oscillations to failure at a given stress level. In wood where the static strength is a function of the duration of load, fatigue may also comprise static fatigue, i.e. fatigue where the failure is obtained within the first load cycle. Static fatigue is not just a special case of fatigue; when the strength depends on the duration of load the number of cycles to failure will depend on the load frequency.

2.1 Wood Fatigue Modelling

The influence of duration of load divides the literature on wood fatigue into two fundamentally different main lines. The first main approach is a traditional number of cycles, NOC, quantification. According to this approach Wöhler curves can be used to state fatigue resistance in NOC and stress level. The second main approach is a traditional duration of load, DOL, quantification. According to this approach fatigue failure is not directly a function of the number of load oscillations counted by NOC, but is explained by the total accumulated time under load, TUL, summarized over all load cycles. However, the truth may be in between, i.e. wood fatigue is governed by a combination of number of cycles and time under load.

As a crude but instructive first approximation it may be assumed that fatigue failure can be described by a failure surface in a coordinate system spanned by stress level, number of cycles and time; similar thoughts are presented in (Mohr 1996). A schematic linearisation of such a failure surface is shown in Figure 2.1. The plane spanned by stress level and number of cycles contains the Wöhler curve for "unit frequency", the curve is assumed to have a fatigue threshold for stresses below a certain non-critical level. The

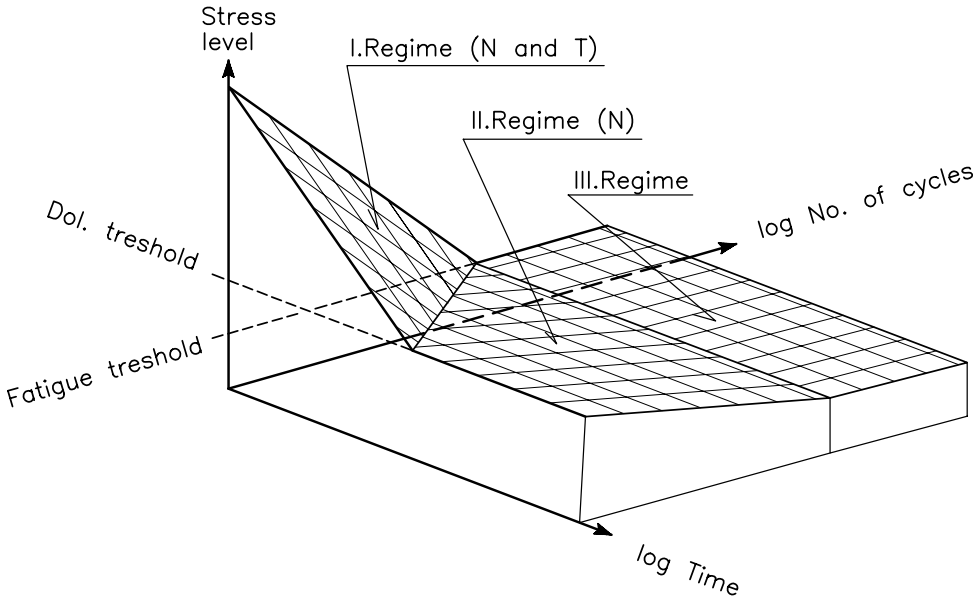

Figure 2.1: *Combined fatigue and duration of load failure surface divided into three possible failure regimes.*

plan spanned by stress level and time contains a schematic version of the *Madison curve* which for the sake of simplicity is given a duration of load threshold for stresses below a certain non-critical level. The failure surface can now be divided into the following three regimes.

I. Regime: In this regime the failure is both dependent on time and number of cycles, i.e. the fatigue resistance cannot alone be quantified in number of cycles as the number of cycles to failure will decrease when the load cycle frequency is lowered.

II. Regime: In this regime the surface lies below the duration of load threshold and the failure is solely dependent on number of cycles.

III. Regime: In this regime the surface lies below both the duration of load threshold and the fatigue threshold and failures are not encountered.

In the following sections some of the available wood failure models are briefly presented and discussed with respect to their ability to account for failures influenced as well by number of cycles as by duration of load. The following models are presented:

- Damage accumulation laws
- Polymer debonding
- Energy based models

- Number of cycles criterion
- Damaged viscoelastic material model

2.1.1 Damage accumulation

Damage accumulation laws have been proposed in various forms in order to model time to failure at ramp loading and constant load. The main target for these models is to model the duration of load phenomenon adequately. The simplest form of damage accumulation laws is proposed by Gerhards, implemented in e.g. (Gerhards & Link 1986). The rate of damage is expressed as:

$$\frac{d\alpha}{dt} = \exp\left(-a + b\,\frac{\sigma(t)}{\sigma_s}\right), \tag{2.1}$$

where α is the damage degree ($0 \leq \alpha \leq 1$), t is time, $\sigma(t)$ is load history, σ_s is strength, and a and b are empirically constants for a given wood population. When neglecting the initial ramp loading the time to failure, T_c, at constant load conditions, σ_c, can be expressed as:

$$T_c = \exp(a - b\,\frac{\sigma_c}{\sigma_s}), \tag{2.2}$$

Barrett & Foschi (1978*a*) presents a damage accumulation law where the rate of damage growth is also dependent on the damage degree:

$$\frac{d\alpha}{dt} = a\left(\frac{\sigma(t)}{\sigma_s} - \frac{\sigma_0}{\sigma_s}\right)^b + \lambda\,\alpha(t), \tag{2.3}$$

where σ_0 is a stress threshold below which no damage occurs, and the parameters a, b and λ are empirical constants for a given wood population. In this model the damage rate is dependent on the degree of damage due to the term $\lambda\,\alpha(t)$. As pointed out by Foschi & Yao (1986) this term leads to exponential growth of damage when damage is present and the load is just larger than the threshold value. In order to avoid this the model is improved by letting λ be a function of stress level:

$$\frac{d\alpha}{dt} = a\left(\frac{\sigma(t)}{\sigma_s} - \frac{\sigma_0}{\sigma_s}\right)^b + c\left(\frac{\sigma(t)}{\sigma_s} - \frac{\sigma_0}{\sigma_s}\right)^n \alpha(t), \tag{2.4}$$

where c and n are empirical constants for a given wood population.

Irrespective of the different forms of the damage accumulation laws, the models (2.1), (2.3) and (2.4) unite in seeing damage rate as being only time dependent. With respect to fatigue this may be a model flaw as damage introduced due to repetitive loading is only accounted for by time dependent damage. This is evident from a discussion of cyclic

loading at constant amplitude in (Barrett & Foschi 1978*b*) where it is explicitly stated that number of cycles to failure is proportional to the frequency of the load cycles. Hence, an ideal square load cycle only contributes to damage due to the time under constant load. In other words, the models cannot account for the effect due to the load oscillation phenomenon usually associated with fatigue.

2.1.2 Polymer debonding

A wood fatigue model applied to wood under sinusoidal fatigue loading is presented in (Liu, Zahn & Schaffer 1994). The general setting of the model is within a frame of bond breaking energy of polymers. In the model f is the fraction of unbroken bonds in the material and a function of orientation and time. The rate of change of f is expressed as:

$$\frac{df}{dt} = K_r(1-f) - K_b\, f, \tag{2.5}$$

where K_r is the rate of reformation of broken bonds and K_b is the rate of bond breaking. These parameters can be expressed as functions of thermodynamical parameters and parameters expressing stress. Assuming that $K_r \simeq 0$ the rate of change is:

$$\frac{df}{dt} = -\omega_b\, f\, \exp\left[-\frac{E}{RT} + \frac{\beta\,\sigma}{f}\right], \tag{2.6}$$

where ω_b is the frequency of bond jump motion with respect to bond breaking processes, E is the activation energy, R the gas constant, T the absolute temperature, β a coefficient that modifies the energy barrier due to applied stress and σ is the applied stress. Under a couple of assumptions, (2.6) can be solved for a sinusoidal stress history with mean stress σ_c and stress amplitude σ_0:

$$\sigma = \sigma_c + \sigma_0 \sin \Omega t \tag{2.7}$$

When solving the differential equation (2.6) for the load history (2.7) the frequency of loading, Ω, disappears and hence the time to failure is independent of the loading frequency. This contradicts the usual view that fatigue life can be stated in number of cycles to failure.

2.1.3 Energy based models

Fatigue models exploiting energy based failure criteria have been applied to wood by e.g. Bach (1975) and Philpot, Fridley & Rosowsky (1994). Energy based failure criteria are

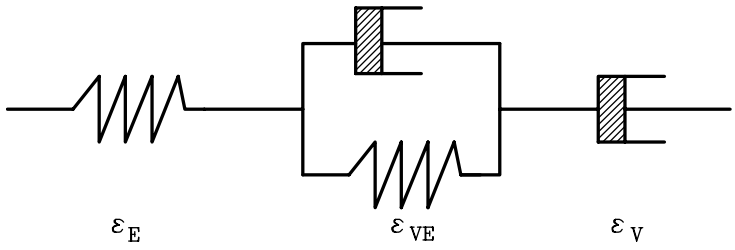

Figure 2.2: *Four element viscoelastic model, the Burger model.*

expressed as a critical value of a specific energy quantity, w, which is calculated as an integral of a stress component times the corresponding strain increment:

$$w = \int \sigma \, d\varepsilon \tag{2.8}$$

The stress component can be identified with the stress in an element of a rheological model. Due to the time dependent properties of wood, energy based failure criteria can be expressed in rates of stress, $\dot{\sigma}$, and strain, $\dot{\varepsilon}$, or generally stress work rate, $\dot{w}$:

$$w(t_f) = \int_0^{t_f} \dot{\sigma}\,\varepsilon + \sigma\,\dot{\varepsilon}\,dt = \int_0^{t_f} \dot{w}\,dt \tag{2.9}$$

A simple theoretical basis can be a four element viscoelastic rheological material model, Figure 2.2, representing the three strain components: elastic strain, ε_E, viscoelastic strain, ε_{VE} and viscous strain, ε_V. Integrating all stress and strain components of the model in Figure 2.2 yields the total stress work (2.9). An elaborate energy failure criterion was put forward by Reiner & Weisenberg (1939). The criterion has recently been theoretically exploited by Liu & Ross (1995). According to the Reiner-Weisenberg theory failure will occur when the strain work, w_c, due to the recoverable part of the deformation attains a critical value. Hence, the dissipation rate of non-elastic energy, $\dot{D}$, is subtracted from the work integral:

$$w_c(t_f) = \int_0^{t_f} (\dot{w} - \dot{D})\,dt \tag{2.10}$$

The Reiner-Weisenberg theory, (2.10), states failure at a critical value of the energy stored due to ε_E and ε_{VE}. However, the Reiner-Weisenberg theory does not include stress relaxation failure as observed by Bach (1967). Stress relaxation failure occurs at constant strain condition due to redistribution of the strain components. To include stress relaxation failure Bach (1973) proposed a modification of (2.10). The modified criterion

includes only the energy stored due to ε_{VE}, hence the instantaneously recoverable elastic energy at failure, $w_c^E(t_f)$, is excluded. The criterion takes the form:

$$w_c^{VE}(t_f) = -w_c^E(t_f) + \int_0^{t_f} (\dot{w} - \dot{D})\, dt \tag{2.11}$$

Bach (1975) attempted to verify the criterion (2.11) experimentally in low cycle fatigue testing. However, Bach found that failure was best expressed by a time under load criterion. Philpot et al. (1994) discuss energy based failure models. In a work density model failure is suggested identified with a critical value of the total work, (2.9), due to all strain components in Figure 2.2. However, this model has the theoretical obstacle of rupture at almost any magnitude of load under repeated loading due to creep recovery, i.e. regain of ε_{VE} in periods without load. Hence, a modification is suggested which omits the work corresponding to creep recovery, i.e. the energy corresponding to the closed part of the hysteresis loop in a load cycle. The modification takes an empirical form and essentially the modified work density model in (Philpot et al. 1994) is a stress level dependent criterion on the maximum strain.

2.1.4 Number of cycles criterion

Fatigue characterization in number of cycles to failure is the traditional approach to fatigue in engineering materials. In the NOC-approach Wöhler curves, or $S-N$ diagrams, describe fatigue resistance by a critical number of load cycles, N, leading to failure at a given stress level, SL, i.e.:

$$log(N) = A + B \cdot log(SL), \tag{2.12}$$

where the coefficients A and B depend on the factor R, which is determined as $R = \sigma_{min}/\sigma_{max}$, where σ_{min} and σ_{max} are the minimum respectively maximum stress level in a cycle. The approach origins from empirical observation that number of cycles to failure in dependency of stress level can be described by a relation of the form (2.12). However, steady state crack growth due to stress variations can be given an interpretation within linear elastic fracture mechanics. Paris law assumes a relation between crack growth rate and the stress intensity factor of the following form:

$$\frac{da}{dn} = C\,(\Delta K)^m, \tag{2.13}$$

where a is crack length, n is number of cycles, ΔK is the variation of the stress intensity factor in the crack tip, and both C and m are constants. If ΔK is given as function of

stress variation and number of cycles as a continuous variable an integration of (2.13) will give the number of cycles corresponding to catastrophic crack length.

$$N = C' \left(\Delta\sigma\right)^m \tag{2.14}$$

This form of relation between number of cycles and stress level or stress level variation is equivalent to (2.12), and gives a linear relation between number of cycles to failure and stress level in a double logarithmic diagram. Wöhler curves of this form establish the design basis at constant amplitude conditions. For load conditions with different amplitudes the Palmgren Miner summation rule is often assumed. The summation rule states that the fatigue life consumed due to n cycles at condition i, n_i, is a fraction of the number of cycles to failure at this condition, N_i. The impact at k different stress levels is safe if:

$$\sum_{i=0}^{k} \frac{n_i}{N_i} \leq 1 \tag{2.15}$$

A wood fatigue life prediction analysis based on Wöhler curves is presented in (Bonfield 1991). An explanation of the fatigue phenomena is not established, but the underlying theory for the empirical fits is a Paris law relation, placing all emphasis on N according to the fracture mechanical approach presented in (Ansell 1987).

However, the Wöhler approach is not able to distinguish between fatigue loading at different frequencies. That is the crack length grows with the number of cycles irrespective of the duration of each load cycle. This is a problem with respect to wood fatigue where duration of load phenomena may also be present.

Code rules

In the bridge part of the Eurocode, (EC5-2 1997), an informative annex gives guidelines for a simplified fatigue verification method. The method considers only number of cycles. According to the method it should be verified that:

$$\Delta\sigma \leq f_{fat,d}, \tag{2.16}$$

where the stress range of the fatigue loading is determined of $\Delta\sigma = \sigma_{max} - \sigma_{min}$. The fatigue strength $f_{fat,d}$ is determined in dependency of the number of imposed load cycles according to:

$$f_{fat,d} = \frac{k_{fat}\, f_k}{\gamma_{M,fat}} \tag{2.17}$$

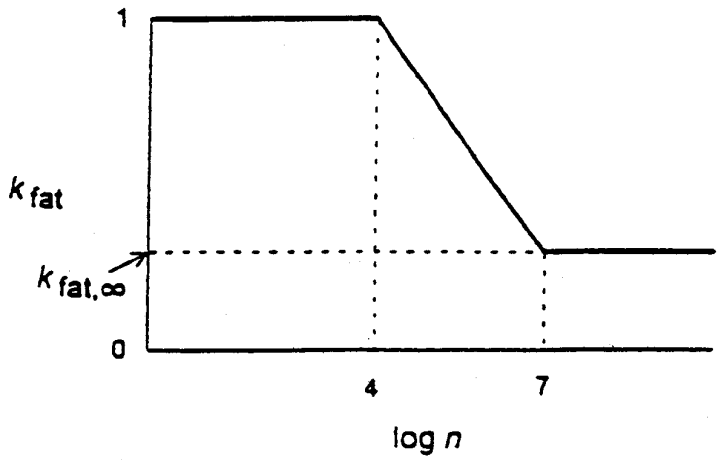

Figure 2.3: *Fatigue reduction factor in the Eurocode.*

The fatigue strength reduction factor, k_{fat}, is determined of the diagram shown in Figure 2.3, and values for $k_{fat,\infty}$ corresponding to the fatigue limit is given with the value 0.6 for compression perpendicular and parallel to grain, 0.3 for bending, tension and reversed tension/compression and 0.2 for shear.

2.1.5 Damaged viscoelastic material theory

Nielsen (1979) first introduces the Damaged cracked Viscoelastic Material (DVM) theory to describe the mechanical behaviour of wood subjected to constant loads. In a number of papers, most recently (Fuglsang Nielsen 2000*a*) and (Fuglsang Nielsen 2000*b*), the theory is further developed to cover harmonic load variations. A basic assumption behind the theory is that all mechanical behaviour of wood is governed by fracture mechanics, irrespective of loading mode. This assumption may be too bold, e.g. in compression parallel to grain the damage morphology is such that no free surfaces are produced and hence the concept of strain energy release rate should not be invoked. However, in tension perpendicular to grain, which is the subject of this thesis, fracture mechanics seems most appropriate.

Intrinsic creep

Unlike the elastic fatigue approach used for steel, the DVM theory includes creep to consider viscoelasticity. It is included by use of an elastic - viscoelastic analogy, i.e. in an

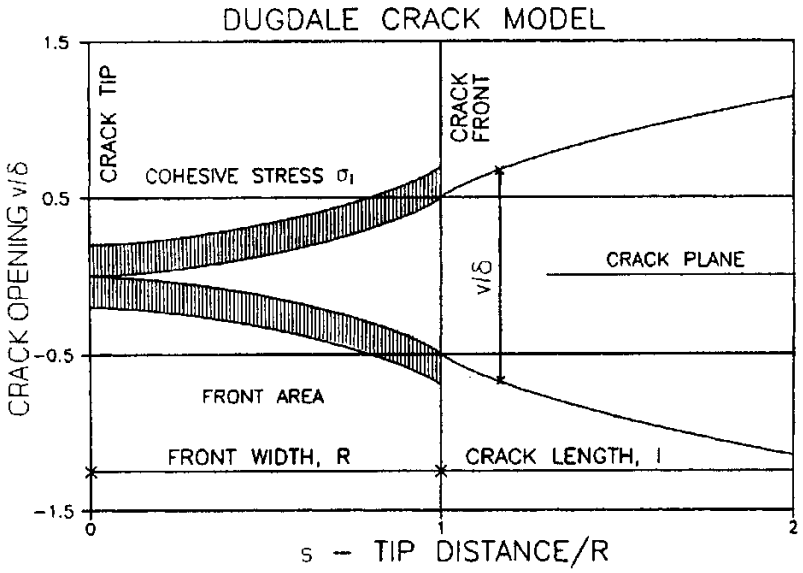

Figure 2.4: *Dugdale crack and crack front, from (Nielsen 2000a).*

elastic solution of fracture development under pulsating load the coefficients of elasticity are replaced by their viscoelastic counterparts. It is assumed that creep of wood follows a power law expression, i.e. creep is described by the normalized creep function $C(t)$:

$$C(t) = 1 + \left(\frac{t}{\tau}\right)^b, \tag{2.18}$$

where τ is the creep doubling time and b is the creep power. In (Fuglsang Nielsen 2000a) creep is referred to as *"a small areas big events phenomenon"*, meaning that creep takes place in weak areas in the microstructure and is hence an intrinsic property that cannot be determined from direct measurement.

Elastic fracture mechanical basis

For the elastic fracture mechanical description the Dugdale crack model, (Dugdale 1960), is chosen with modifications by Rice (1967) to cover pulsating load. Figure 2.4 shows the crack front of a Dugdale crack. The following quantities are defined in the figure: The width of the crack front zone, R, the crack opening, v, the opening at the front, δ, the crack length, l, and the relative distance from the crack tip, s. From the definitions it

follows that $v/\delta \simeq s^2$ and in (Dugdale 1960) it is further given that:

$$\frac{R}{l} = \frac{\pi^2}{8}\left(\frac{\sigma}{\sigma_l}\right)^2 \tag{2.19}$$

$$\frac{\delta}{l} = \frac{\pi\sigma^2}{E\sigma_l} \tag{2.20}$$

The material is loaded with the tension stress σ perpendicular to the crack plane infinite away from the crack. The resulting uniformly distributed cohesive stress, σ_l, at the crack front is an intrinsic property just as creep is. It may be thought of as the theoretical strength of the uncracked material. In the same way the reference strength, σ_{cr}, is the strength of the material with an initial damage, i.e. crack, of length l_0. In order to describe the development of damage three more quantities are introduced; strength level, FL, load level, SL, and damage ratio, κ:

$$FL = \frac{\sigma_{cr}}{\sigma_l} \tag{2.21}$$

$$SL = \frac{\sigma}{\sigma_{cr}} \tag{2.22}$$

$$\kappa = \frac{l}{l_0}, \text{ where } 1 \leq \kappa \leq \kappa_{cr} \tag{2.23}$$

For a given stress level SL the material will fail when it reaches the critical damage ratio κ_{cr}. From the definition of the critical strain energy release rate, $\Gamma_{cr} = \sigma_l\delta_{cr}$, it follows that:

$$\begin{aligned} \Gamma_{cr} = \sigma_l\delta_{cr} = \frac{\pi\sigma_{cr}^2 l_0}{E} \Rightarrow \sigma_{cr} = \sqrt{\frac{E\Gamma_{cr}}{\pi l_0}} \\ SL = \frac{\sigma}{\sigma_{cr}} = \frac{\sqrt{\frac{E\Gamma_{cr}}{\pi l}}}{\sqrt{\frac{E\Gamma_{cr}}{\pi l_0}}} = \sqrt{\frac{l_0}{l}} \Rightarrow \kappa = \frac{l}{l_0} = \frac{1}{SL^2} \end{aligned} \tag{2.24}$$

Rice modifications

In the Dugdale model the material in the crack area is assumed ideal plastic and load monotone increasing. Rice (1967) modified the assumption in order to describe oscillating load. For a load ranging from σ_{min} to σ_{max} a distant load of $-\Delta\sigma$, where $\Delta\sigma = \sigma_{max} - \sigma_{min}$, and a cohesive stress of $-2\sigma_l$ at the crack front is superimposed the original stress state. Up to the relative distance s_0 from the crack tip the material in the crack area is still assumed incompressible, but from s_0 until the crack front, $s = 1$, the crack width changes while the load oscillates and the cohesive stresses changes from σ_l to $-\sigma_l$. For $s > 1$

the crack width changes but the crack surfaces are assumed never to contact each other, hence no stresses are obtained. The value of s_0 is by Rice given as:

$$1 - s_0 = \frac{1}{4}(1-p)^2, \tag{2.25}$$

where $p = \sigma_{min}/\sigma_{max} = SL_{min}/SL_{max}$ is the load ratio (often denoted R in fatigue literature). Further, the normalised change in crack width, Δ_0, is defined as $\Delta_0 = \Delta\delta/\delta_{max}$. Nielsen (1986) introduces a contact parameter Z that groups the crack closure quantities:

$$Z = \Delta_0(1 - s_0) \text{ and } 1 - s_0 = \sqrt{\frac{Z}{2}} \tag{2.26}$$

In (Nielsen 1996) an expression for Z that allows crack surface contact is given:

$$Z = \frac{C}{8}\left[\frac{U(1-p)}{2}\right]^M \left[\kappa SL_{max}^2\right]^{M/2-2}, \; U = \frac{1+p}{2}, \tag{2.27}$$

where C is a damage constant and M is a damage rate power. According to (Nielsen 1996) the expression considers the texture of the fracture surfaces as M should increase with increasing failure surface roughness.

Damage rate

If the rate of crack propagation is assumed constant during a period of time, Ω, and the crack expands R_{max} during this period of time the crack rate is:

$$\frac{dl}{dt} = \frac{R_{max}}{\Omega} \tag{2.28}$$

A point which is at the crack tip at time $t = 0$ will be at the crack front at time $t = \Omega$. The strain energy release rate for this point is determined from two contributions. The first contribution, Γ_1, takes the crack width from $\delta = 0$ at time $t = 0$ to δ_{max} at time $t = \Omega$ and the second contribution, Γ_2, is from the oscillating load that at time $t = s_0\Omega$ starts with amplitude 0 and at time $t = \Omega$ ends with amplitude $\Delta\delta$. The period length of one load cycle is denoted T.

$$\Gamma_1 = \sigma_l \cdot \delta_{max} \tag{2.29}$$

$$\Gamma_2 = \sigma_l \Delta\delta(1 - s_0)\frac{\Omega}{T} \tag{2.30}$$

$$\Gamma = \Gamma_1 + \Gamma_2 = \sigma_l\delta_{max}\left(1 + \frac{\Delta\delta}{\delta_{max}}(1-s_0)\frac{\Omega}{T}\right) = \sigma_l\delta_{max}\left(1 + Z\frac{\Omega}{T}\right) \tag{2.31}$$

In order to express Γ_{cr} (2.22) is first rearranged:

$$SL = \frac{\sigma}{\sigma_{cr}} = \sqrt{\frac{\delta l_0}{\delta_{cr} l}} \Rightarrow \frac{\delta}{\delta_{cr}} = \kappa S L^2 \tag{2.32}$$

The critical strain energy release rate Γ_{cr} can then be written as:

$$\Gamma_{cr} = \frac{\sigma_l \delta_{max}}{\kappa S L_{max}^2} \tag{2.33}$$

Setting $\Gamma = \Gamma_{cr}$ in (2.31) gives:

$$\frac{\sigma_l \delta_{max}}{\kappa S L_{max}^2} = \sigma_l \delta_{max} \left(1 + Z\frac{\Omega}{T}\right) \Rightarrow Z\frac{\Omega}{T} = \frac{1}{\kappa S L_{max}^2} - 1 = \frac{1 - \kappa S L_{max}^2}{\kappa S L_{max}^2} \tag{2.34}$$

The damage accumulation rate $d\kappa/dN$ can by use of (2.20), (2.23) and (2.28) be expressed as:

$$\begin{aligned} \frac{d\kappa}{dN} = \frac{dl/l_0}{dt/T} = \frac{R_{max} T}{l_0 \Omega} = \frac{\pi^2}{8}\left(\frac{\sigma_{max}}{\sigma_l}\right)^2 \frac{lT}{l_0 \Omega} = \frac{\pi^2}{8}\left(\frac{\sigma_{max}}{\sigma_{cr}}\frac{\sigma_{cr}}{\sigma_l}\right)^2 \frac{\kappa T}{\Omega} \\ = \frac{\pi^2}{8}(S L_{max} F L)^2 \frac{\kappa T}{\Omega} \end{aligned} \tag{2.35}$$

Combining (2.34) and (2.35) gives:

$$\frac{d\kappa}{dN} = \frac{\pi^2 F L^2}{8} \frac{(S L_{max})^4 \kappa^2}{1 - \kappa S L_{max}^2} Z \tag{2.36}$$

Introducing (2.27) gives:

$$\frac{d\kappa}{dN} = \frac{C \pi^2 F L^2}{64} \frac{(U \Delta S L)^M}{1 - \kappa (S L_{MAX})^2} \kappa^{M/2}, \;\; U = \frac{1+p}{2} \tag{2.37}$$

The equation (2.37) forms the elastic basis for damage rate prediction in the DVM theory.

Viscoelastic solution

In order to make an elastic - viscoelastic analogy a revised creep function is introduced; the crack closure creep function, C_{cl}, that envelopes the viscoelastic peaks of the displacement history:

$$\begin{aligned} &C_{cl}(t) \approx C_{cl}(t/h) = 1 + \left(\frac{t}{h\tau}\right)^b, \;\; h \approx \begin{cases} 0.8 + 0.2\mu & \text{for} \;\; \Delta' \leq 1 - p^2 \\ 1 & \text{for} \;\; \Delta' > 1 - p^2 \end{cases} \\ &\text{with } \mu = \left[\beta^b + (\Delta' - \Delta_0)\langle f \rangle^b\right]^{-1/b} \text{ and } \Delta' \approx \frac{1 - \beta^b + \Delta_0 \langle f \rangle^b}{\langle f \rangle^b + (1-\beta)^b}, \end{aligned} \tag{2.38}$$

where $\langle f \rangle = f \cdot \tau$ is a normalization of the frequencies. The critical strain energy release rate for the viscoelastic material with C_{cl} included is:

$$\Gamma_{cr} = \sigma_l \delta_{max} \left[C_{cl} \left(\frac{\Omega}{q} \right) + \frac{\Delta\delta}{\delta_{max}} (1 - s_0) \frac{\Omega}{T} \right] = \sigma_l \delta_{max} \left[C_{cl} \left(\frac{\Omega}{q} \right) + Z \frac{\Omega}{T} \right] \tag{2.39}$$

The factor q supposedly compensates for the maximum crack opening not occurring instantly in a given point penetrated by the crack. In Madsen (1992) it is given the value:

$$q = \left[\frac{(1+b)(2+b)}{2} \right]^{1/b} \tag{2.40}$$

Introducing (2.33) and (2.38) in (2.39) gives:

$$\frac{1 - \kappa S L_{max}^2}{\kappa S L_{max}^2} = \left(\frac{1}{qh\langle f \rangle} \right)^b \left(\frac{\Omega}{T} \right)^b + Z \frac{\Omega}{T} \tag{2.41}$$

By use of (2.35) and (2.27) Ω and Z may be eliminated from (2.41):

$$\begin{aligned} \left[\frac{\pi^2/8 \cdot \kappa S L_{MAX}^2}{qh < f >} \right]^b \left[F L^2 \frac{dN}{d\kappa} \right]^b \\ + \frac{C \pi^2 \kappa S L_{MAX}^2}{64} \left[U (1-p) \right]^M \left[\kappa (S L_{MAX})^2 \right]^{(M/2-2)} F L^2 \frac{dN}{d\kappa} \\ - \frac{1 - \kappa (S L_{MAX})^2}{\kappa (S L_{MAX})^2} = 0 \end{aligned} \tag{2.42}$$

This differential equation in N and κ has to be solved numerically to determine the lifetime.

Determining lifetime using DVM

Equation (2.42) may be given the form:

$$Y = A_1 X^b + A_2 X - A_3 = 0 \quad \text{with:} \quad \begin{cases} X = F L^2 \frac{dN}{d\kappa} \\ A_1 = \left(\frac{\Phi}{qh\langle f \rangle} \right)^b \\ A_2 = \Phi Z \\ A_3 = \frac{1 - \kappa S L_{max}^2}{\kappa S L_{max}^2} \\ \Phi = \frac{\pi^2}{8} \kappa S L_{max}^2 \end{cases} \tag{2.43}$$

The equation may be solved by Newtons principle of iteration. In Chapter 8 lifetimes are predicted by use of (2.43) for the different test conditions in the tension perpendicular to grain investigation.

2.2 Experimental Wood Fatigue

2.2.1 Influence of time and frequency

The influence of the loading frequency is reported in an investigation by Bach (1975). Bach investigated the influence of frequency, FQ, on fatigue failure. Compressive square wave shaped load cycles were imposed parallel to grain on small clear specimens at frequencies ranging from 0.1 Hz to 10^{-6} Hz spaced by one decade. The number of cycles to failure was reduced from several hundreds to one in the frequency range investigated. It was concluded that failure is best predicted by TUL determined as:

$$TUL = \frac{NOC}{2FQ}, \tag{2.44}$$

where $1/2FQ$ is the time under load in each cycle and NOC is total number of cycles to failure. Hence, according to this investigation wood fatigue is suggested reduced to a duration of load phenomenon.

In (Kohara, Kanayama, Nakai, Nagata & Okuyama 1997) compressive damage failure morphology of small fatigue failed beam samples in bending is studied. Square wave loading at 1 Hz and 0.1 Hz is used. For tests at 0.1 Hz variations are made to the duty factor, e, defined as the ratio between period of maximum load, τ_D, and the duration of the whole cycle, τ:

$$e = \frac{\tau_D}{\tau}.$$

The number of load cycles to generate cracks on the compressive side is reported uninfluenced by the frequency but is on the other hand found to fall for higher values of the duty factor. The latter finding points at an effect of time when the effect of a load cycle is evaluated.

In (Okuyama, Itoh & Marsoem 1984) tensile and compressive fatigue failures are realised on small clear spruce specimens loaded parallel to grain. The loading is sinusoidal and the frequency is either 0.1 Hz or 10 Hz. Compressive tests have been made at stress levels ranging from 80% to 125% of the short term static strength. The logarithm of the number of cycles to failure is found to decrease linearly within stress levels in the tested region. The number of cycles to failure increases approximately two decades when the frequency is raised from 0.1 Hz to 10 Hz, i.e. this finding corresponds to failure explained by duration of load. The tensile tests have been made at stress levels from 60% to 100% of the short term strength. The number of cycles to failure increases less than two decades when the frequency is raised from 0.1 Hz to 10 Hz indicating that each cycle contributes to the damage accumulation irrespective of its duration, Figure 2.5.

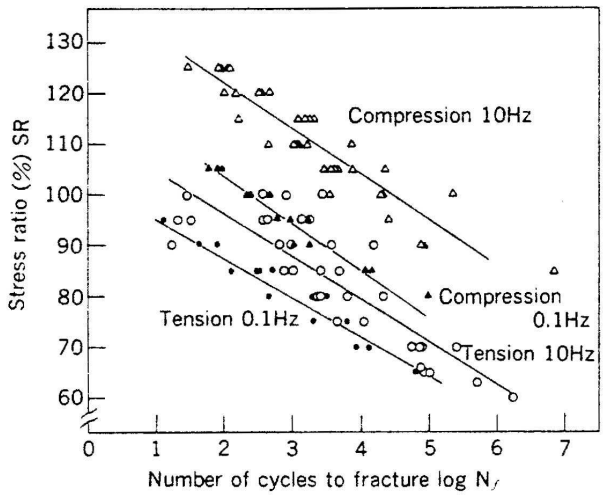

Figure 2.5: *S–N diagrams in compression and tension for 10 Hz and 0.1 Hz sinusoidal fatigue loading from (Okuyama et al. 1984).*

The effect of frequency on bending fatigue strength of chipboard is investigated in (Thompson, Bonfield, Dinwoodie & Ansell 1996). Small samples are taken to failure in bending at stress levels from 30% to 80% of the reference strength. The influence of frequency is investigated for frequencies in three ranges, low (0.015-0.15 Hz), medium (0.15-3 Hz) and high (3-15.0 Hz). The reason for the vague frequency limitation is probably that load is applied at tree different constant rates whereby the frequency becomes a function of stress level. However, the work shows that the number of cycles to failure increase for increasing frequency.

In (Norlin, Norlin & Lam 1999) the shear behaviour of laminated Douglas fir veneer is fatigue tested in 3-point bending tests using trapezoidal load shape with a frequency of 0.033 Hz and stress levels above 80%. The objective is to test the damage accumulation law by Foschi & Yao (1986) given in (2.4). The damage accumulation parameters are calibrated at one stress level, with these values the model is subsequently used to predict failures in the whole stress range investigated. The damage model is found to yield good predictions of failure times. However, is should be observed that the test frequency is confounded with the model parameter calibration. Hence, a different outcome could be expected at a different frequency, if the frequency of loading affects the fatigue life.

In (Cai, Bradtmueller, Hunt, Fridley & Rosowsky 1996) the response to five-point fatigue bending is mapped as S-N curves for OSB at 70% to 100% SL. The influence of frequency is partly examined at 80% SL as tests are run at both 1 Hz and 0.5 Hz. No

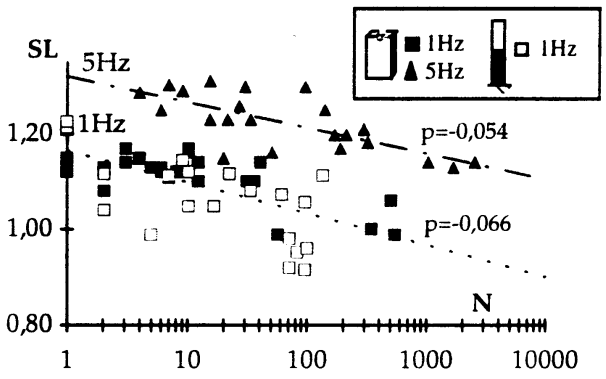

Figure 2.6: *Number of cycles to failure for embedment and embedment like single dowel fatigue tests at 1 Hz and 5 Hz, from (Chaplain et al. 1996).*

statistical significant difference in number of cycles to failure is observed between the two frequencies.

The key objective in (Chaplain, Fournely & Vergne 1996) and (Chaplain, Valentin & Fournely 1999) is to explain the frequency dependency of number of cycles to failure for embedment type tests of single dowel connections, Figure 2.6. Sinusoidal load is applied to the embedment parallel to the grain above 100% SL at either 1 Hz or 5 Hz. At 115% SL the 5 Hz tests are reported to have 60 times longer time to failure than the 1 Hz tests. The damage accumulation laws by Foschi, Barrett, Yao and Gerhards are not able to take into account the effect of frequency as the integration of periodic stress functions is independent of frequency. In order to cope with the frequency dependency observed the damage model by Barrett & Foschi (1978a) given in (2.3) is rewritten in the following form:

$$\frac{d\alpha}{dt} = a\left[\frac{\sigma_D(t) - \sigma_0}{\sigma_s}\right]^b - \lambda\,\alpha(t), \tag{2.45}$$

The model in (2.45) replaces the stress history, $\sigma(t)$, of the original model in (2.3) with the frequency dependent stress history, $\sigma_D(t)$. The stress history, $\sigma_D(t)$, is evaluated in the elastic spring of a material analogy consisting of a parallel spring and a dashpot. As the stress, $\sigma_D(t)$, in the spring element decreases for increasing load frequency, increasing the frequency entails a longer fatigue life according to the model. The model is able to explain the difference between the two frequencies, at least for the highest stress levels.

Experimental evidence for the exact opposite influence of frequency is found in (Clorius, Pedersen, Hoffmeyer & Damkilde 2000). The investigation covers the interaction of a duration of load mechanism and a number of cycles mechanism in fatigue in compression

Frequency [Hz]	No. of specimens		Mean no. of cycles to failure $N\bar{O}C$		Standard deviation s_{NOC}		Mean time under load $T\bar{U}L$ [sec]	
RH▶	65%	85%	65%	85%	65%	85%	65%	85%
0.01	12	12	48	26	35	41	2421	1308
0.1	14	12	284	98	262	81	1420	490
1	12	11	3048	367	3569	213	1524	183
10	11	11	21749	4431	29905	7529	1087	222

Table 2.1: *Number of cycles to failure and time under load to failure for small specimens in compression parallel to the grain.*

parallel to grain. Small clear specimens of spruce (*Picea abies*) are taken to failure in square wave formed fatigue loading at a stress excitation level corresponding to 80% of the short term strength. Four frequencies ranging from 0.01 Hz to 10 Hz are used and the whole test is reproduced at two levels of moisture content.

The number of cycles to failure, NOC, increase significantly with increase in test frequency. In Figures 2.7 and 2.8 NOC and TUL for specimens taken to failure are shown in a normal probability plot. The scatter within frequencies is significantly smaller than the scatter between frequencies and increasing the frequency from e.g. 0.01 Hz to 0.1 Hz corresponds to an increase in NOC from about 50 to about 300. The mean values of number of cycles to failure and total accumulated time to failure, calculated as in equation (2.44), are given in Table 2.1. The data presented in Table 2.1 accentuates that while the number of cycles to failure decreases for increased frequency the accumulated time under load to failure decreases. Hence, the failures recorded must be an effect of some interaction of number of cycles and duration of load and lie in the 1.st regime in Figure 2.1. In (Clorius et al. 2000) the outline of a model explaining the interaction of the effect of load duration and the effect of the loading sequences is presented.

2.2.2 Number of cycles

The early 20th century's use of wood and wood based materials in fatigue loaded airplane structures is seen from e.g. (Küch 1939), where improvements of the mechanical and hygroscopical properties of wood and plywood is discussed with respect to use in airplane structures. In (Küch 1942) bending and tension fatigue strength of plywood for airplanes is determined. The frequency is not reported, but is probably high as 20 10^6 cycles is

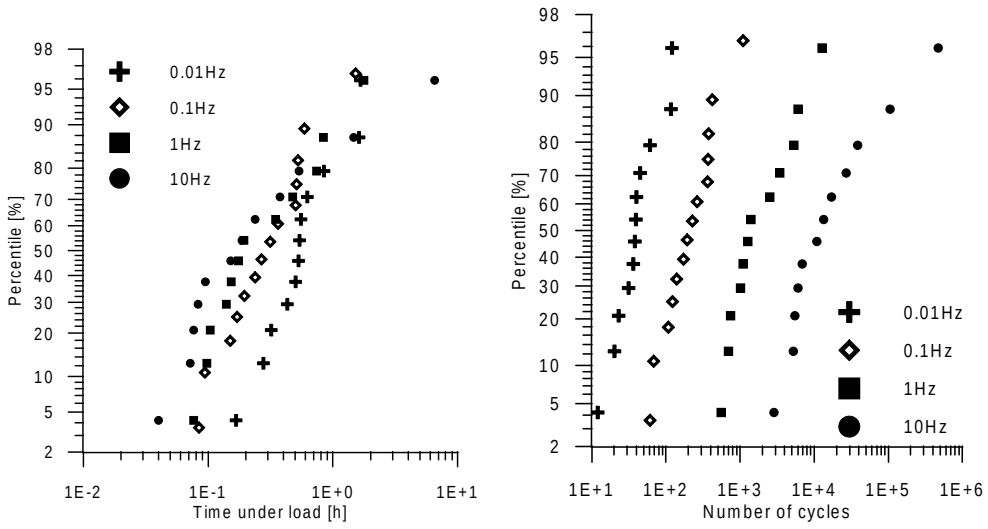

(a) Time to failure at different frequencies

(b) Number of cycles to failure at different frequencies

Figure 2.7: *Log-normal probability ranking of failures at different frequencies for compressive fatigue at SL=80 % and RH=65 %.*

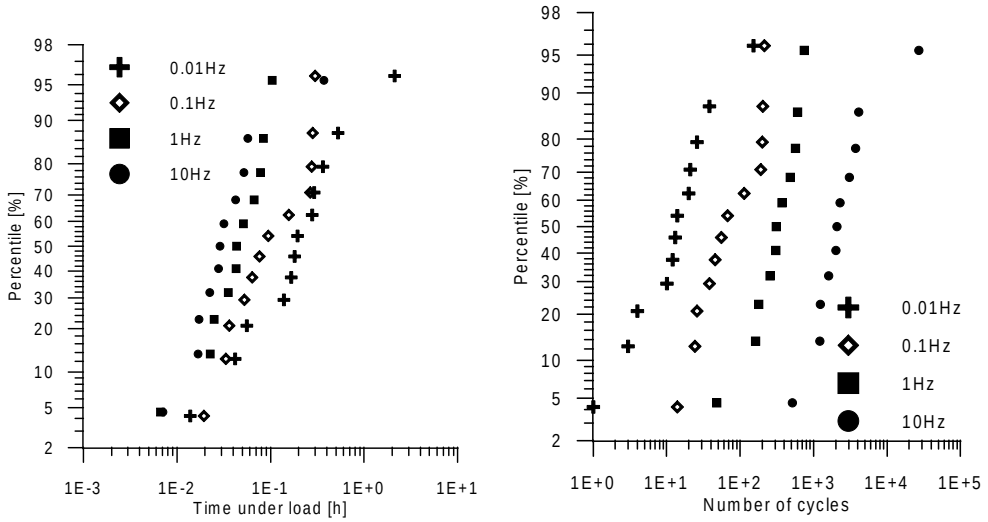

(a) Time to failure at different frequencies

(b) Number of cycles to failure at different frequencies

Figure 2.8: *Log-normal probability ranking of failures at different frequencies for compressive fatigue at SL=80 % and RH=85 %.*

reached. In bending the plywood is found to survive 20 10^6 at 30% stress level and in tension this number of cycles is reached at a stress level of 52% of the short term strength.

In (Rose 1965) tension and compression fatigue tests on clear pine heartwood are reported. The aim is to determine the effect of fatigue load on the mechanical properties of wood, i.e. the modulus of elasticity and residual strength after fatigue loading. The compression tests are made at approximately 41-42 Hz sinusoidal load oscillation between 2-3 MPa and an upper load value. For an upper value below 75 % of the static short term strength, determined in a ramp with a load application rate of 0.8 MPa/s, no failures were observed before 3.5 10^6 load cycles corresponding to a total test duration of approximately 24 hours. For higher load levels only specimens with a high moisture content are reported to survive until 3.5 10^6 load cycles.

Studies of microscopic cell wall creases in the compression side of small beams due to low cycle fatigue is presented in eg. (Kitahara, Tsutsumi & Matsumoto 1981). The observation laid forward is an increase in damage degree with stress level and number of load oscillations.

Reversed bending fatigue on sugi, (*Cryptomeria japonica*), is studied in (Imayama & Matsumuto 1970). Small beams are taken to fatigue failure at 40 Hz and stress levels ranging from 35% to 60% of the short term bending strength. A linear S-N curve is established. No study of the influence of frequency is made, but stiffness and other deformation related quantities are surveyed throughout the tests. A closer analysis of the temperature development is offered in (Imayama & Matsumuto 1974). The temperature rise is divided into 4 regions correlated with the damage development.

In (Bohannan & Kanvik 1969) fatigue strength of small finger jointed Douglas-Fir specimens is determined at 15 Hz. The joints are tested at stress levels from 40% to 90% and the results are presented in S-N diagrams. At 40% SL failure is met after approximately 30 10^6 cycles.

The work by Bonfield is probably the most extensive recent experimental wood fatigue study existing and this work is based on a number of cycles approach to fatigue. The number of cycles to failure is determined in constant amplitude tests at a number of different stress levels with varying R values as reported in Bonfield (1991). This leads to empirical relations of the form given in (2.12). In order to verify the Palmgren-Miner summation rule Bonfield carried out tests where each specimen was subjected to different stress levels. The main results from (Bonfield 1991) are presented in (Bonfield & Ansell 1991). Based on these results a life prediction analysis is presented in (Bonfield, Ansell & Dinwoodie 1994). The nature of Bonfield's life prediction analysis based on Wöhler

curves is presented in (Ansell 1995).

2.2.3 Load shape

In (Bordonné, Okuyama & Marsoem 1987) the effect of waveform is discussed. Tension fatigue specimens, same as reported in (Okuyama et al. 1984), were instrumented with gauges and exposed to fatigue loading at 0.5 Hz at different stress levels. Each specimen was exposed to loading of sinusoidal, periodic triangular, periodic sawtooth and periodic square shape, Figure 2.9. The area, H, of the stress strain diagram for the individual cycle is determined and normalized with the square of stress level, SL. For stress levels below approximately 40% of the short term strength the experimental finding is that H/SL^2 attains a constant value, hence linear viscoelasticity can be assumed in this regime. Further, it is observed that the quantity H/SL^2 is a function of waveform. The level of dissipated energy increases with waveforms arranged in the following order: periodic triangular, sinusoidal, periodic sawtooth and periodic square. This finding is modelled in an analytical form within a so called Poynting-Thompson material analogy, i.e. a spring in series with an element consisting of a parallel spring and dashpot. By use of this model and suitable material properties, Bordonné et al. (1987) are able to model the energy dissipation due to tensile load cycles of each of the four forms. The modelling shows fine agreement with the experimental finding, Figure 2.10. The analytical solutions show why larger energy dissipation per cycle is obtained for load shapes that keep large stress levels for longer times. And this finding is correlated with the finding that shorter fatigue lives are met for loading forms with larger energy dissipation per load cycle.

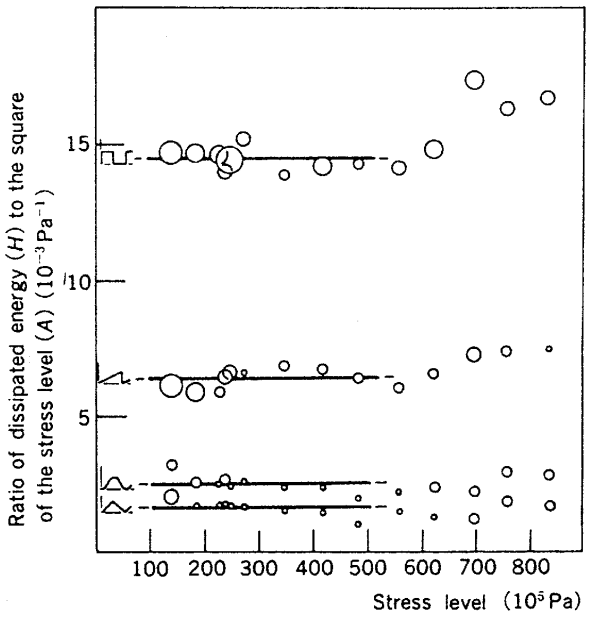

Figure 2.9: *Relation between energy dissipation and stress levels for four different wave forms from (Bordonné et al. 1987).*

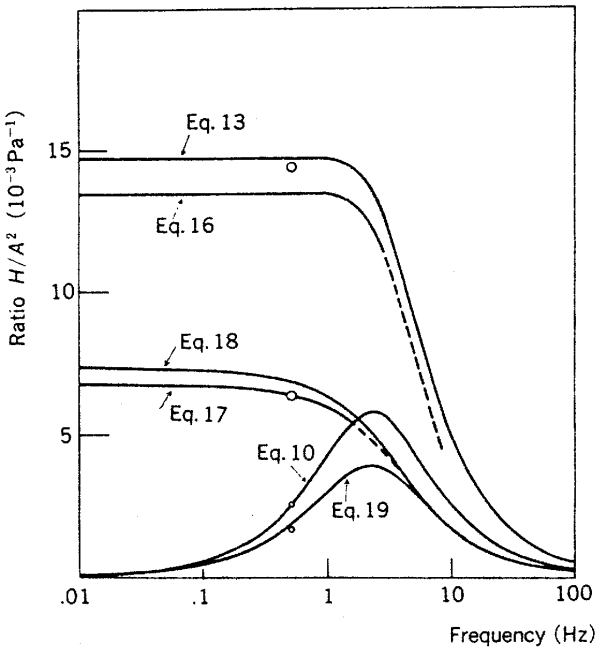

Figure 2.10: *Relation between energy dissipation and frequency for four different wave forms from: Eq. 19 triangular, Eq. 10 sinusoidal, Eqs. 13 & 16 square and Eqs. 17 & 18 sawtooth, from (Bordonné et al. 1987).*

Chapter 3

Material and specimens

3.1 Test specimen design

3.1.1 Design process

The specimen design process was governed by the aim to design a specimen to be loaded in tension perpendicular to the grain with the following characteristics:

- A relatively small specimen enabling a number of specimens to be cut from the same piece of wood. This gives specimen samples which are relatively homogeneous with respect to inherent properties.
- A specimen where failure is governed by the strength of the wood and not influenced by any notches or necking.

It was decided to let the specimens have a base of 45 x 70 mm to which metal plates were glued for load application. With this basic design decision the design process comprised numerous iterations with different orientations of the wood, different specimen heights and different annular ring orientation.

The most characteristic observation made during the design process was that the specimens preferred to fail in a radial plane. Hence, for a specimen with random orientation of the annular rings, Figure 3.1 (a), failure is most likely to occur in that end of the specimen where the angle between the radial plane and the metal plate is smallest. This failure location may be due to both the stress peak introduced in the interface as the metal plate restricts the contraction of the wood and due to the fact that the strength in the tangential direction is lower than the strength in the radial direction. An investigation of the strength in the radial and tangential direction showed the strength in the radial direction to be approximately 20% higher than the strength in the tangential direction.

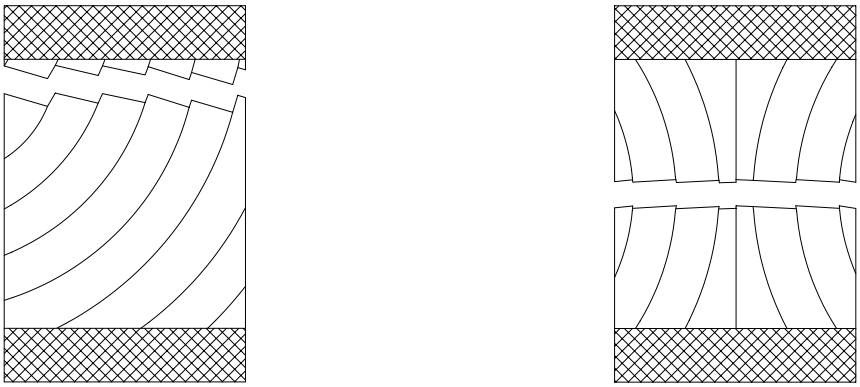

(a) Randomly oriented specimen.

(b) Double symmetrical specimen.

Figure 3.1: *Specimen with random orientation (a) and specimen with weakest plane in the center (b).*

This observation was used to design a double symmetrical specimen as shown in Figure 3.1 (b), where the location of failure is in the centre of the specimen. The failure location can be explained as the centre radial plane is the weakest plane perpendicular to the stress direction.

In the design process variations of the specimen height were made. Specimens were tested with heights of 25, 45, 70 and 130 mm as shown in Figure 3.2. This study revealed a size or height effect much larger than expected from the known size effect in tension perpendicular to the grain. It also showed that the failures were always in the central radial plane of the specimens. An analysis of the stress distribution in the specimens revealed that the difference in the radial and tangential stiffness creates an inhomogeneous stress state in the centre of the specimen for an applied homogeneous stress state. Further, the inhomogeneity of the stress state was found to increase with specimen height. These findings are reported in (Pedersen, Clorius, Damkilde & Hoffmeyer 2000) where a deterministic explanation to the observed size effect is offered. With respect to the specimens used in fatigue testing the inhomogeneity of the stress state observed corresponds to stress necking of the specimens. In other words, difference between E_R and E_T and the polar orientation of these stiffness parameters along with the double symmetrical specimens provokes a stress peak in the centre of the specimens which can explain the consistency of the failure location. Hence, though no necking due to geometrical shape is introduced, a stress necking is present.

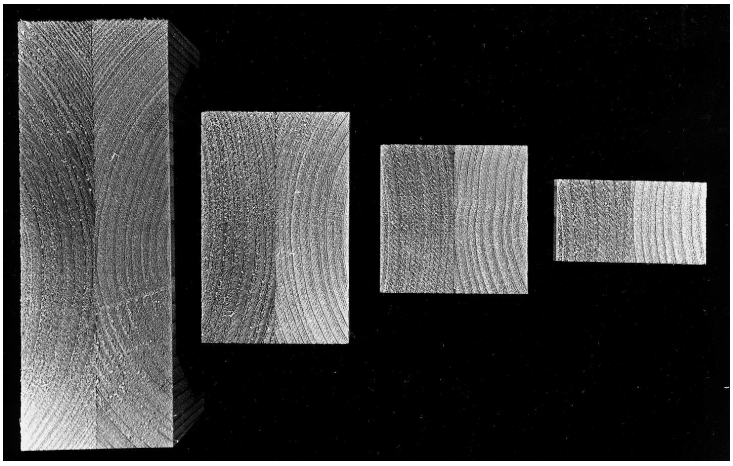

Figure 3.2: *Endview of symmetrical specimens with different heigths.*

3.1.2 Final specimen design

The final test specimen design is shown in Figure 3.4. The tensile stresses are applied via two metal plates glued to the wood. The specimens have a height of 70 mm and base dimensions 45 mm x 70 mm. Fixtures for loading were 20 mm thick metal plates glued to the specimens with epoxy glue. The wood-metal plate interface was reinforced with a thin strip of glass fibre embedded in epoxy and wrapped around the specimen at the interface, Figure 3.4. With this specimen failures were secured to be predominantly in the central radial plane as shown in Figure 3.3.

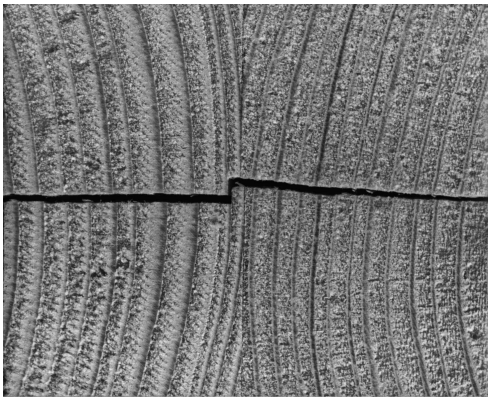

Figure 3.3: *Specimen failure in centre radial plane.*

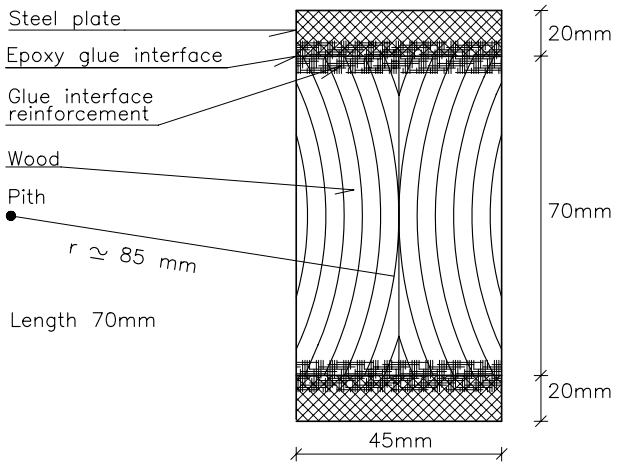

Figure 3.4: *Geometry of small specimen used in fatigue testing.*

3.2 Material and preparation

3.2.1 Wood material sample

The test material is Norwegian grown *Picea abies*. A total of 3 m^3 of 38 x 150 mm boards with an approximate length of 5 m were subdivided into three groups using an annual ring width criterion. In each group the boards were paired and glued sapwood to sapwood with the intention to from planks with symmetrical cross sections.

The emerging planks were conditioned to equilibrium with RH 65% and 20° C. A selection of 10 planks was taken to be cut for fatigue specimens, the planks were selected to cover all three annular ring width groups. The planks were planed to cross sectional dimensions of 45 x 70 mm. Subsequently, the planks were divided into 4 almost equal parts, I-IV.

Parts I and III were cut into small specimens and used for fatigue testing in equilibrium with RH 65%. Parts II and IV were conditioned in RH 85% and 20° C and first cut into specimens when at equilibrium with this higher moisture content.

The specimens were cut to avoid knots and other anomalities. Small knots with diameter less than 5 mm were allowed if they were located away from the centre of the specimen. Generally the specimens must be characterized as small clear specimens. The number of clear specimens cut from each plank varied, but as a minimum it was possible to obtain two sets of 16 specimens for fatigue testing, and 9 specimens for reference strength determination from each plank.

Figure 3.5: *Specimens kept in the climate chamber.*

3.2.2 Specimen preparation

The process of preparing specimens for fatigue testing is briefly summarized. After cutting the specimens were kept on shelves in the conditioning chambers, Figure 3.5. When preparing a test series, the specimens were cleaned of dust with high pressure air and the metal plates were sand blasted, Figure 3.6 (a). A relatively coarse sand was used as a rough surface of the metal plates enhanced the strength of the glue interface. A two component standard epoxy glue from Ciba, *Araldite Professional*, was applied to both specimen and metal plate, Figure 3.6 (b). Specimens and metal plates were placed in a teflon coated glue bench, Figure 3.6 (c). Primary glue pressure was provided in the longitudinal direction of the glue bench by an adjustment bolt, and alignment of specimens and metal plates was secured by clamps as shown in Figure 3.6 (d). After curing, the specimens were cleaned for superfluous glue and the glue interface was enhanced by gluing a strip of glass fibre mat round the specimen at the position of the glue interface, Figure 3.6 (e) and (f).

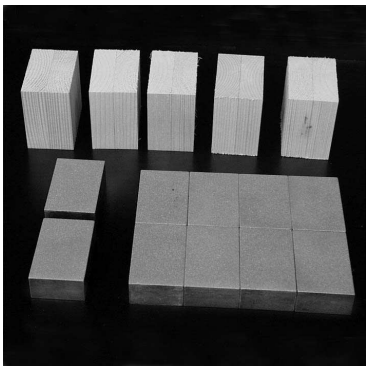

(a) Specimens and plates ready to glue

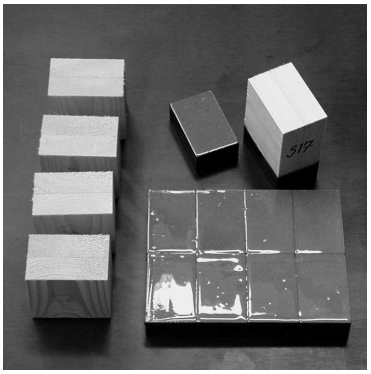

(b) Specimens and plates with glue

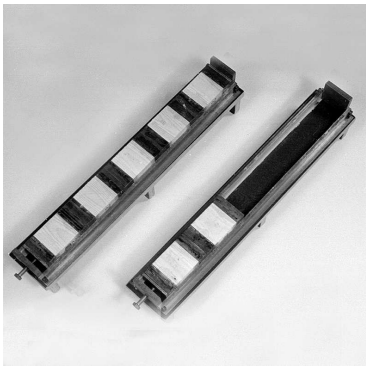

(c) Specimen and plate with glue

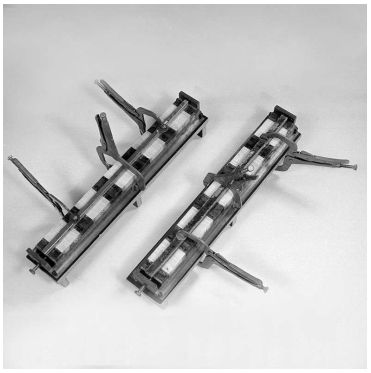

(d) Curing pressure

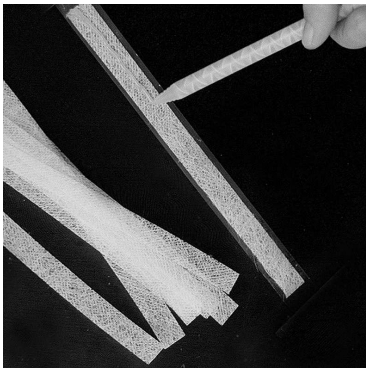

(e) Glue applied to glass fibre strip

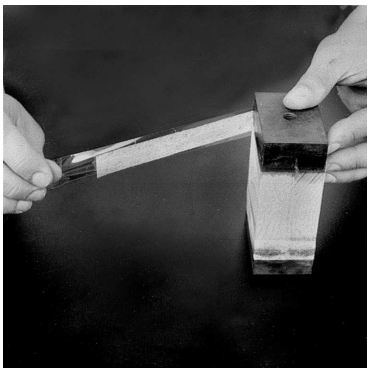

(f) Glass fibre strip wrapped round specimen

Figure 3.6: *Specimen preparation.*

Chapter 4

Test programme

4.1 Experimental Motivation

Fatigue in tension perpendicular to grain may at first glance seem to be an exclusive area with limited perspective. Though direct use of the tension strength perpendicular to the grain is preferably avoided by designers, this strength parameter is often governing the strength of the wood construction details. The list of instances where the governing strength parameter may be tension perpendicular to grain can be summarized in the following most important cases:

- The strength of notched beams is influenced by tension perpendicular to the grain. Though code rules are given in criteria in shear strength and a fracture mechanics based reduction factor, e.g. (Gustafsson 1995), the tension perpendicular strength is also governing the failure.

- The strength of connections is often governed by splitting failures due to introduction of tension perpendicular to the grain. The reduction factor to multiple dowels in a row is due to such a phenomenon, e.g. (Jorissen 1998).

- In curved beams the tension stresses perpendicular to grain can lead to failure, this is included in the code rules, and recently this kind of tension splitting has been investigated with respect to varying moisture content, e.g. (Aicher, Dill-Langer & Ranta-Maunus 1998).

- The bending strength of straight beams can due to grain angle and grain deviations round knots be governed by tension stresses perpendicular to grain, e.g. (Madsen 1992) and (Isaksson 1999).

Regular high cycle fatigue may not be interesting in all these cases. However, low cycle fatigue is certainly present in all the mentioned instances. The test programme has been designed to asses the interaction between the number of load oscillations and the duration of each load sequence, i.e. the load cycle frequency. This is of interest for the following reasons:

- From a fatigue design perspective general knowledge of the influence of the loading frequency is necessary to establish design rules for fatigue loading.
- From a duration of load perspective it is of interest to know if a low number of load cycles will accelerate influence of duration of load.

4.2 Experimental Plan

4.2.1 Reference strength

The reference strength was determined from 9 specimens from each of the 10 planks. For RH 65% testing 6 specimens in all were taken: 2 from part I, 3 from part III and 1 from part IV. The specimen from part IV were taken before this part was conditioned to RH 85%. In this way the specimens covers the whole length of the plank. The strength determination from these 60 specimens form the basis for the reference strength determination.

At RH 85% 2 specimens were taken from part II and 1 from part IV of all 10 planks. It was beforehand decided to determine the reference strength at RH 85% by means of the strength at RH 65% and a reduction factor found from the mean strength at the two moisture levels.

Reference strength was determined in a double charnier setup. The specimens were taken to failure at a constant stress rate of 0.026 MPa/s corresponding to times to failure of approximately 90 s.

4.2.2 Fatigue testing

The fatigue testing has been run in series of 10 specimens, one from each of the 10 different planks. Throughout all test series specimens from the same 10 planks have been used. Hence, each plank constitutes a block and the test plan is a block test design where the block effect is equal for all test series at all combinations of independent variables. The independent variables covers stress level, SL, frequency of the loading, FQ, and

	RH 65%				*RH* 85%			
FQ [Hz]	1	0.1	0.01	D-L	1	0.1	0.01	D-L
SL 50%	-	1	-	-	2	2	2	-
SL 65%	2	3	4	2	3	3	2	3

Table 4.1: *Test plan giving number of series tested at each set of conditions.*

equilibrium moisture content at different levels of relative humidity, RH. The independent variables take the following values:

- The frequency of the loading, FQ, is either 1 Hz, 0.1 Hz or 0.01 Hz, further tests have been made at constant load conditions, dead-load. The load shape is square wave shaped oscillation between approximately 0 load and a maximum stress level. Square wave shaped load cycles are used as this shape of the fatigue load makes it possible to separate effect of number of load cycles and effect of duration of load.

- The stress level is determined as the applied maximum stress relative to the short term strength determined in ramp load tests of short duration. In the test series SL is either 50% or 65%.

- The moisture content corresponds to equilibrium with either RH 65% ±2% or 85% ±2% at 20° C ±2° C.

In the following the test conditions for a series will be referred to by $RH/SL/FQ/$, i.e. 85/65/1 is testing at RH 85%, SL 65% and FQ 1 Hz. The combinations of test conditions used and the number of test series run at each combination are shown in Table 4.1. At RH 85% 17 test series have been tested, but at RH 65% only 12 have been run as 4 series were lost due to brake down of the test rigs occurring in the first months of the testing programme. All 1 Hz tests were performed in a servo hydraulic test equipment. The series at 0.1 Hz and 0.01 Hz were tested in a mechanical low frequency test setup except one at 85/65/0.1 which was tested in the servo hydraulic equipment in order to check reproducibility between test equipments.

Chapter 5

Methods

5.1 Fatigue rigs

5.1.1 Low frequency pneumatic fatigue rigs

Mechanical principle

The low frequency fatigue testing at 0.1 Hz and 0.01 Hz were performed in fatigue rigs constructed for this purpose. With reference to Figure 5.1 the mechanical principle of the single rig is a lever providing a 10 times gearing of the load applied in (D) relative to the specimen position (B). Unloading is accomplished by a timer controlled pneumatic actuator connected to the lever in (C). When lifted up in (C) the lever will rotate about (A) and the specimen is unloaded. The specimen is mounted in the rig in a double charnier setup as shown in Figure 5.2. Before testing each rig was individually calibrated. The load at the position of the specimen was recorded by means of a dynamometer mounted in place of a specimen and six load levels applied to the load tray. Two times 10 rigs as shown in Figure 5.1 established the whole test setup. The cyclic loading of the two series of fatigue rigs was individually controlled. A pneumatic actuator at each end of the test set up provided the possibility to lift the levers through a system of wires and wheels, Figure 5.3. Control of the load cycles was provided by magnetic switches on the pneumatic actuators connected to a timer. The actuator piston would move between two positions given by the position of the magnetic switches. The time held at top and bottom position was controlled by the timer. In order to avoid overshoot due to rapid load application the speed of the load application was controlled. This control was accomplished by valves retarding the inlet and outlet of compressed air in the piston chamber. A relatively slow load application between 0.6 s and 1.2 s was needed to avoid load overshoot.

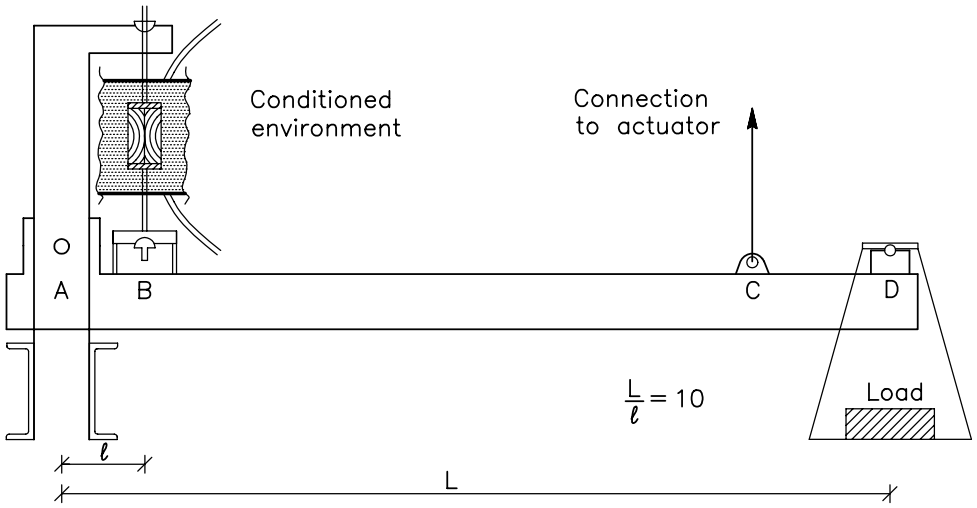

Figure 5.1: *Fatigue rigs used for fatigue testing of small specimens.*

Moisture control

PVC-disks and PVC hoses encapsulated the specimen as shown in Figure 5.2 in order to provide an air tight chamber. Humidity controlled air was generated in a climate chamber and circulated to the chamber encapsulating the specimen. Figure 5.5 shows a view of the 20 fatigue rigs including the tubes providing the humidity controlled air.

Mounting and detecting failure

Each rig in the two lines was assigned to specimens from one specific plank. That is, the lever load of a specific rig was set relative to the reference strength of a specific plank. Due to this all specimens from e.g. plank A14 was always tested in rig 12 or 7. The consequence is that any hypothetical difference in the performance between the fatigue rigs is confounded with the plank properties. To confound plank with rig was only chosen for practical reasons, alternatively the loads should have been shifted between rigs for each new series mounted, a labourious procedure which could easily have introduced fault loading of the specimens.

Mounting of a specimen in a rig was done by screwing threaded rods into the steel plates glued to each end of the specimen. In the other end of the rods a nut and counter nut kept a fixed distance between the spherical charniers in the loaded situation, Figure 5.2. This distance was important to the shape of the load cycle. When mounting a specimen it was instrumented with an extensometer and the deformation time response was recorded

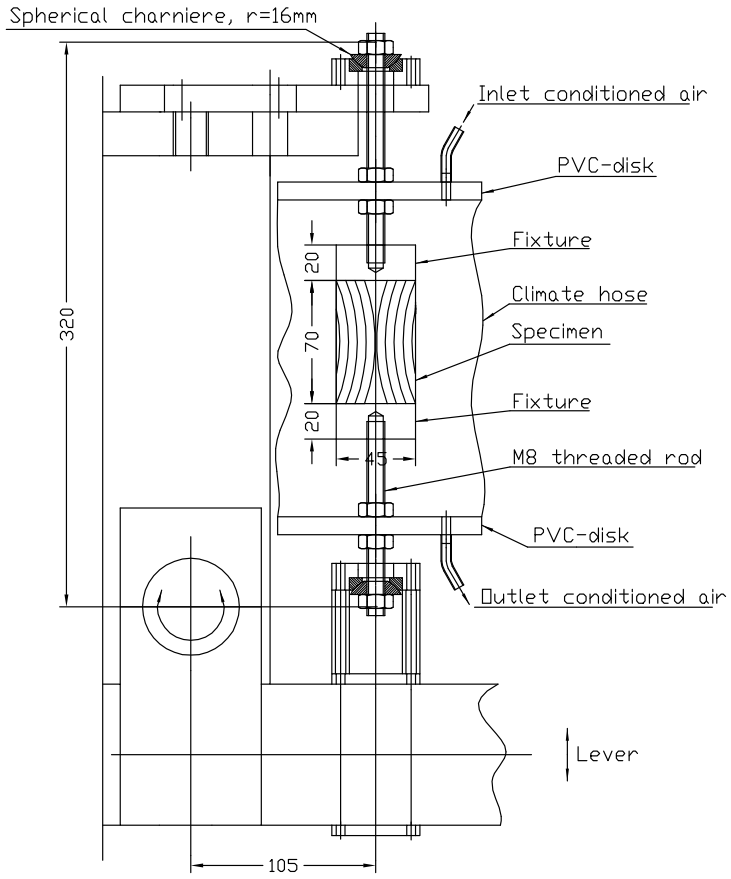

Figure 5.2: *Specimen in fatigue rig.*

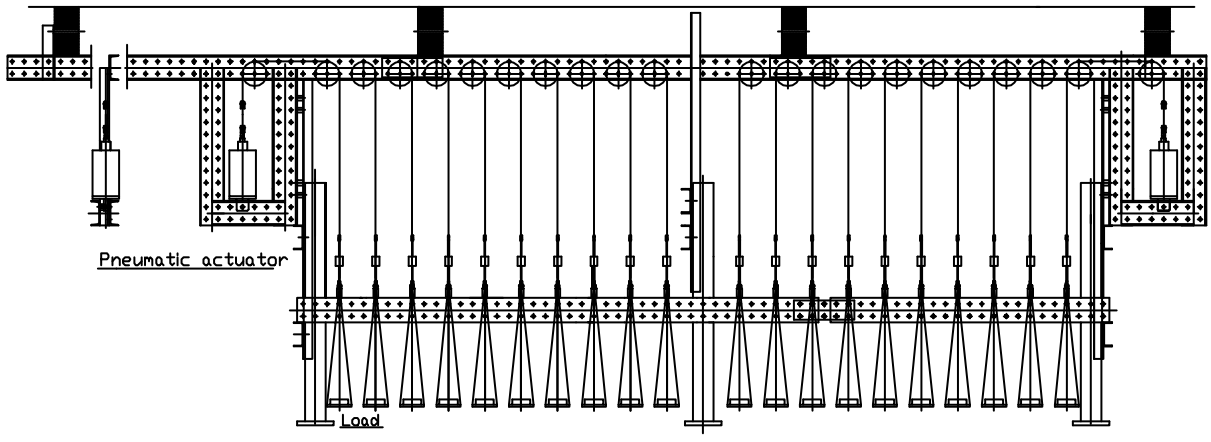

Figure 5.3: *View of fatigue rigs showing load trays and the pneumatic actuators.*

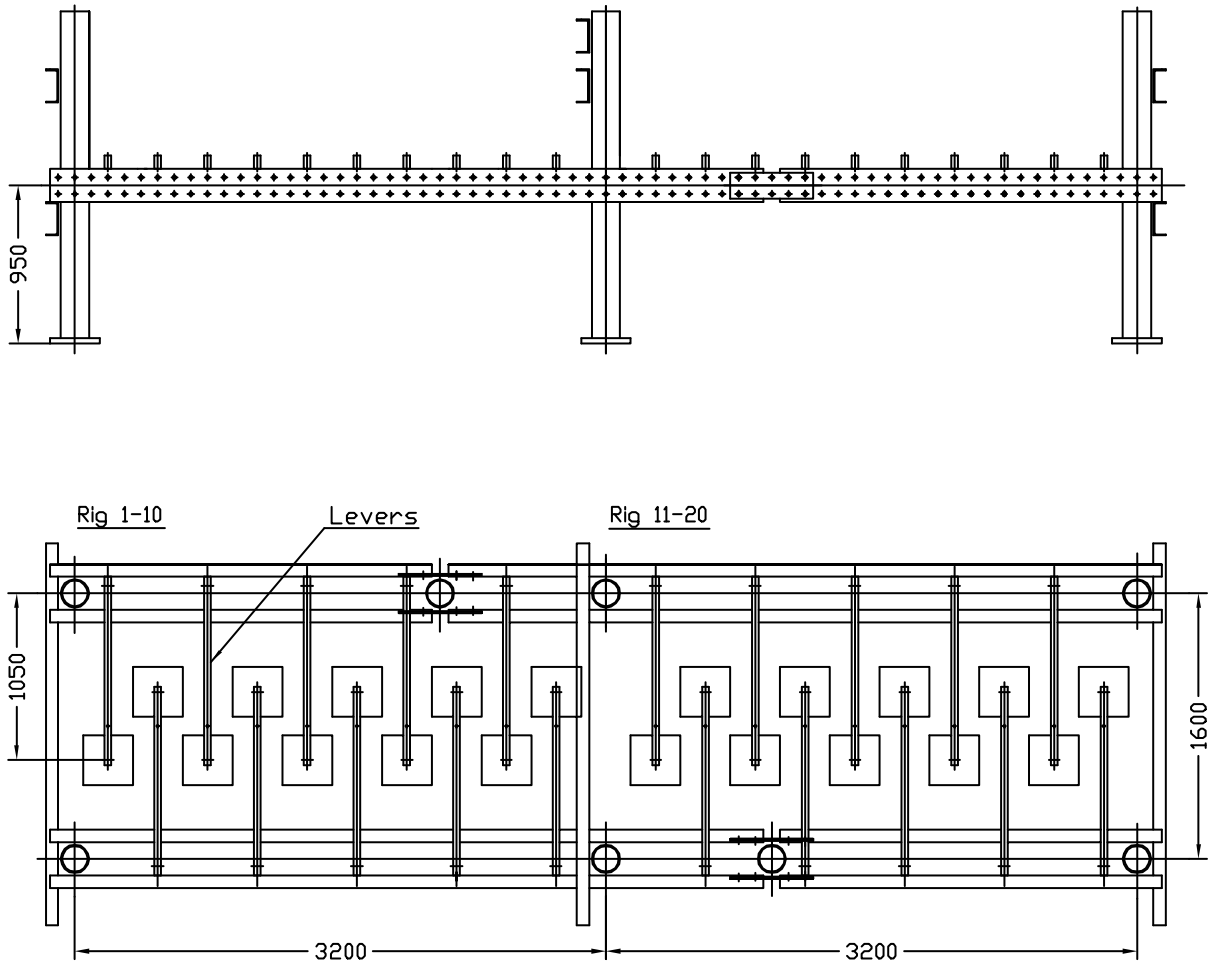

Figure 5.4: *Main measures of mechanical fatigue rigs.*

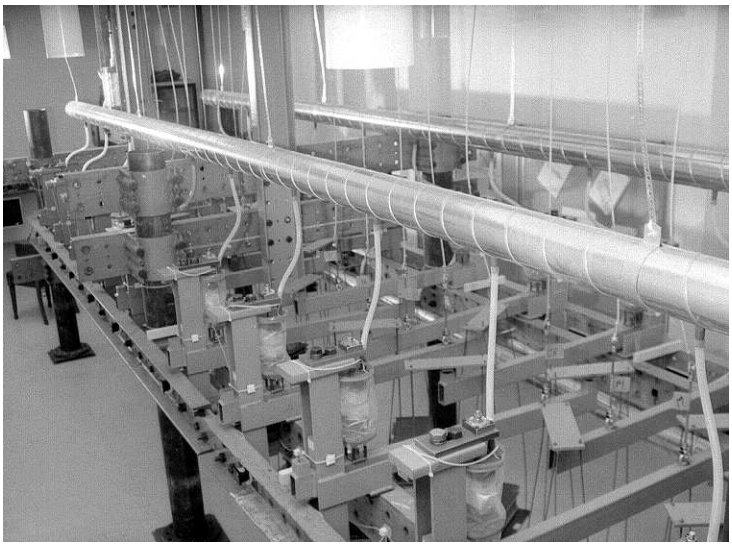

Figure 5.5: *View of the 20 fatigue rigs.*

on a storage oscilloscope and adjustments to the length between the charniers were made if necessary. In this way the load shape was checked individually for all fatigue tested specimens.

Each test rig was provided with a timer counting test duration from test start to specimen failure. The power supply for the timer was switched off at specimen failure due to a mechanical switch. Number of cycles to failure is calculated directly from the known test frequency and the test duration measured by the timer.

5.1.2 High frequency hydraulic fatigue rigs

The relatively slow load application rate needed in the mechanical fatigue rigs in order to secure well controlled load conditions did not allow for testing at frequency higher than 0.1 Hz. Hence, the tests at 1 Hz were performed in a 100 kN servo hydraulic test machine, INSTRON 8516. One series at 0.1 Hz was also performed in the INSTRON equipment in order to check the reproducibility of the tests between the mechanical rigs and the servo hydraulic equipment. The specimens were mounted in the hydraulic equipment in a double charnier setup equal to the setup used in the mechanical rigs.

The specimens in the high frequency tests in the servo hydraulic test machinery were not supplied with humidity controlled air, instead the specimens were sealed in a PVC coat to keep moisture loss at a minimum.

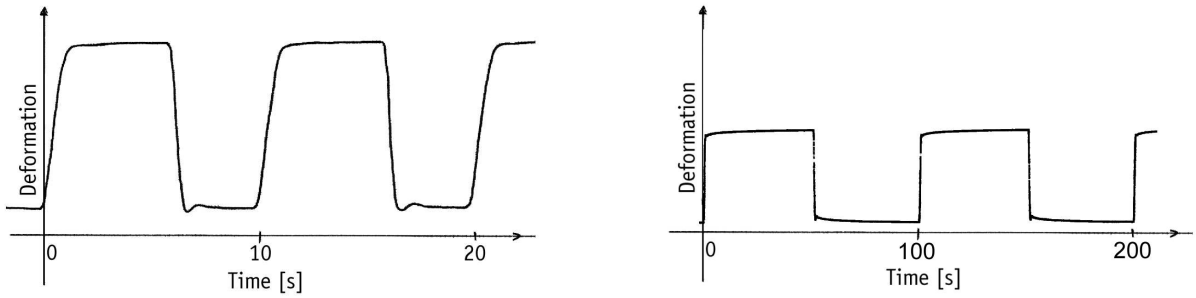

(a) 0.1 Hz test.

(b) 0.01 Hz test.

Figure 5.6: *Deformation versus time plot in mechanical rigs.*

5.2 Performance and documentation

5.2.1 Low frequency fatigue rigs

Load shape

In the mechanical low frequency fatigue rigs the load cycles were tuned to have frequencies of 0.1 Hz and 0.01 Hz. The frequency was governed by an electronic timer and the uncertainty of the period time was less than 1% on the 0.1 Hz tests. The uncertainty was determined by frequency determinations on the displacement time characteristic measured directly on the specimens with extensometers and a storage oscilloscope. This uncertainty is reflected in the calculation of number of cycles but not in the determination of total test duration. A 1% uncertainty on number of cycles due to small errors in the test frequency is negligible in this context. The period under maximum load was kept constant to half the period length, i.e. 5 s and 50 s under maximum load for the two frequencies respectively. The loading ramp from zero to maximum load was between 0.6 s to 1.2 s for both frequencies. This loading ramp was chosen on the safe side of the fastest obtainable rate that secured smooth load application without overshoot. It was not possible to obtain the same loading rate for all rigs, and in order to obtain equal time under maximum load for all specimens the loading rate varied between the rigs in the mentioned range. Unloading was made at twice the speed of the loading. The load shape obtained in the mechanical rigs is illustrated in Figure 5.6, where plots of the deformation of the specimens with an arbitrary scale is shown as function of time. The failure of one specimen was not observed to influence the failure time of the remaining specimens. At specimen failure

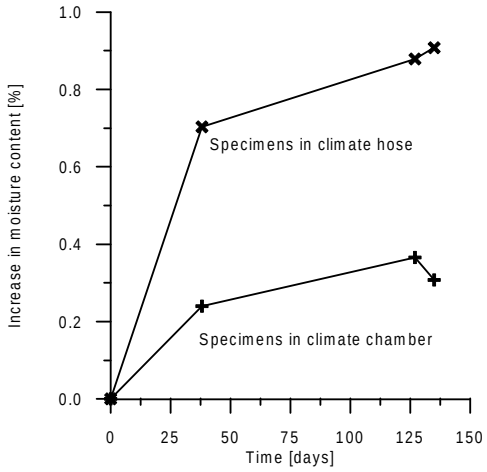

Figure 5.7: *Increase in moisture content over a period of 140 days.*

the lever falls until it is held by the wire connected to the actuator, hence the load shock imposed on the system is primarily taken by the outer frame of the system, Figure 5.3, causing small vibrations in the frames to which the levers are fixed.

Moisture control

The conditioned air provided to the climate hose encapsulating the specimens was generated in an adjacent climate chamber and the relative humidity was controlled by a hygrostat. Temperature and relative humidity was constantly recorded by a hygrothermograph. The humidity was recorded to be very constant with long term variations within ±2%. The temperature generally changed between 19° C in the winter and 23° C in the summer. For the *RH* 85% condition the development in specimen weight was observed for to series of 10 specimens during 140 days. On series was kept in the climate hoses of 10 rigs and the other in the climate chamber providing the conditioned air. The result is shown in Figure 5.7, and a significant increase in moisture content is observed. The specimens was taken directly from the *RH* 85% storage climate chamber where they had been conditioned for more than 2 years. The difference may be attributed to slight differences between the chambers. The moisture increase was round 1% for the specimens in the climate hoses and 0.4% for the specimens in the chamber over the period of 140 days, this difference between the chamber and hose is not understood.

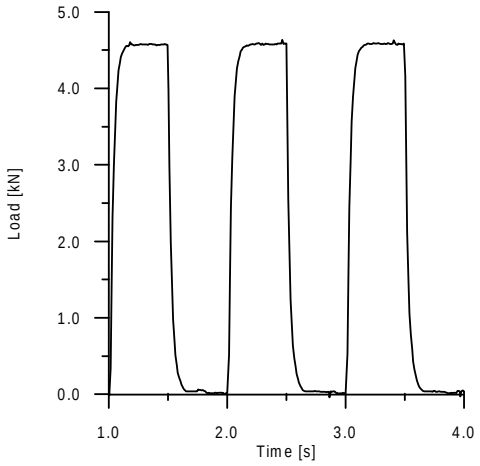

Figure 5.8: *Load time for a 1 Hz test.*

5.2.2 Hydraulic rig

Load shape

For the 1 Hz tests in the servo hydraulic equipment the loading ramp was in the order 0.05 s. This loading time was significantly shorter compared to the tests in the mechanical rigs. The uncertainty of frequency is vanishing in the servo hydraulic equipment. The load time characteristic of 1 Hz testing is shown in Figure 5.8.

Moisture control

In the testing in the servo hydraulic rig the specimens were not kept in a constant climate but only sealed and suffered hence a loss in moisture content. The losses were small; at the 85/65/1 condition the loss in moisture content was 0.2% and at the 85/50/1 condition it was 0.5%.

Chapter 6

Results

6.1 Reference strength

The mean strength, density and stiffness determined in reference strength tests of 6 specimens from each of the 10 planks is given in Table 6.1. An analysis of variance is used to analyze the strength response, F_{ij}, with respect to variation between planks and within planks, assuming the following model for the strength response:

$$F_{ijk} = \mu + p_i + E_{ijk} \tag{6.1}$$

$$\text{where:} \begin{cases} \mu & & \text{overall mean} \\ p_i & i = 1, 2, .., 10 & \text{effect of plank} \\ E_{ijk} & k = 1, 2, .., 6 & \text{random error} \end{cases}$$

The result of the analysis is shown in Table 6.2. It is seen that the effect of plank is significant at a level in excess of 99.9 %. The variation of the reference strength with specimen density and specimen stiffness is seen in Figure 6.1 (a) and (b). The strength variation between planks is not explained by the variation in plank or specimen density. The plank effect of (6.1) is significant and the mean plank strength varies from 1.8 MPa to 2.6 MPa. Hence, it was chosen determine stress level relative to the individual plank

Plank		A14	A5	A8	B9	B13	B15	B19	C1	C8	C9
$\overline{f}_{t,90}$	[MPa]	2.21	1.76	1.92	2.12	2.19	2.24	2.13	2.59	2.45	2.44
$\overline{\rho_{12}}$	[kg/m^3]	404	431	402	444	433	486	457	509	491	486
$\overline{E}$	[MPa]	360	354	339	348	386	417	398	501	467	450

Table 6.1: *Reference strength, density and E-modulus determined for 6 specimens from each plank.*

Source of Variation	Sum of Squares	Deg. of Freedom	Mean Square	F_0	P-Value
Plank	3.33	9	0.37	4.03	$> 99.94\%$
Error	4.59	50	0.09		

Table 6.2: *Analysis of the variance the specimen strength due to plank.*

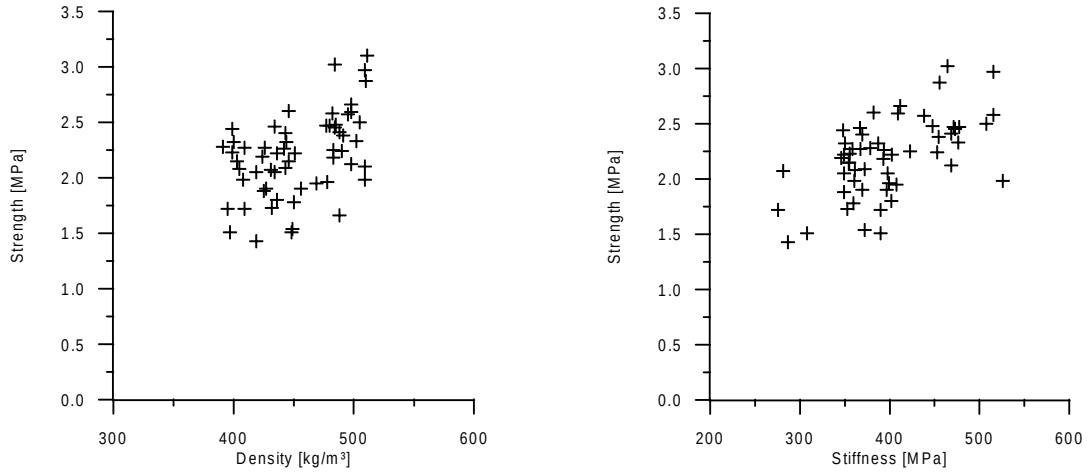

(a) Plank density and reference strength

(b) Specimen stiffness and reference strength

Figure 6.1: *Variation of reference strength with density and stiffness.*

mean strength as given in Table 6.1. This choice of using plank based means to estimate the reference strength is supported by an equally significant plank effect observed in a size effect investigation of specimens originating from three planks from the same batch of material (Pedersen et al. 2000). The reference strength for the moist specimens was determined by use of 3 specimens from each of the 10 planks. It was decided to use one common moisture adjustment factor to the strengths given in Table 6.1 in case the strength of the moist specimens deviated from the strength of the dry. The mean strength for all specimens at RH 65% was 2.20 MPa and the mean strength for all specimens at RH 85% was 2.16 MPa. Similar findings of non-significant moisture dependent strength reduction are reported in (Aicher et al. 1998) and (Gustafsson, Hoffmeyer & Valentin 1998). Aicher et al. (1998) observes no short term strength reduction with increased moisture content

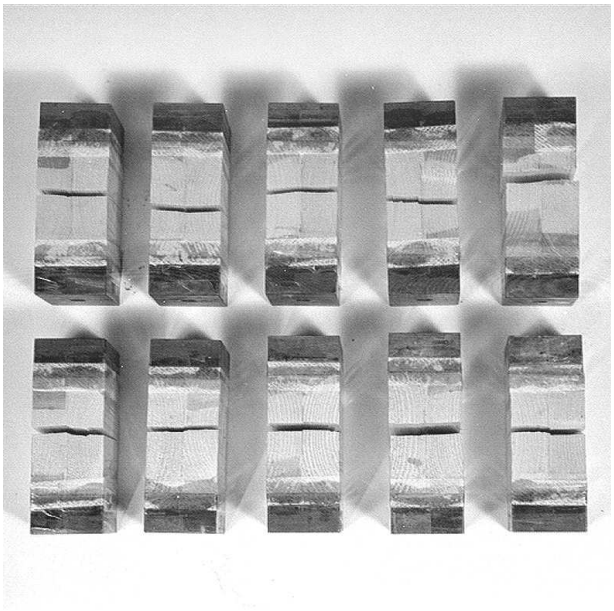

Figure 6.2: *Fatigue series failed in mid-section failure.*

for curved beams failing in tension perpendicular to the grain splitting. Gustafsson et al. (1998) finds no strength reduction of notched beams for tests in equilibrium with RH 65% and RH 85%. Hence, the specimens tested at RH 65% and at RH 85% were all loaded relative to the plank strength given in Table 6.1.

6.2 Fatigue results

6.2.1 Failure mode

The specimens were designed to yield regular wood failures in the mid section, as described in Chapter 3. The mid-section failure mode was realized in most failures and some series comprised only mid section failures as shown in Figure 6.2. However, some interface failures were present, Table 6.3. An interface failure is defined as a failure partially taking place in the glue interface between the wood and the fixture steel plates. No failures only in the glue interface was observed and only very few of the failures were not either regular mid section failures or failures interfering with the glue interface. For this reason a failure is either categorized as a regular mid section failure or an interface failure. This interpretation may be conservative as the interface failures may have been initiated in the wood. However, it is known that the mid section is the weakest section, (Pedersen

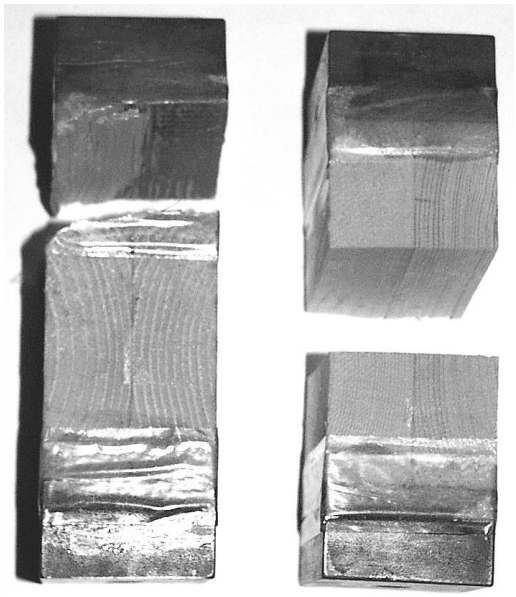

Figure 6.3: *Interface failure and regular wood failure.*

et al. 2000), hence it is assumed that when the failure does not take place in the mid section it is an interface initiated failure censoring the fatigue strength information on that specimen. In Figure 6.3 both a mid section failure and a failure categorized as an interface failure are shown.

6.2.2 Realised fatigue test series

In Appendix A the fatigue results for the individual specimens are listed in tables, one for each series. The $RH/SL/FQ$ combination for each series was generally reproduced two or more times. The resulting number of specimens at each combination is summarized in Table 6.3. The table gives test conditions, total number of specimens and the corresponding number of specimens failing in mid-section failure, interface failure, and the number of specimens not failed at the time the test was terminated. Special comments are needed for the dead load series; the 65/65/dead load yielded only 2 interface failures before it was terminated and the 85/65/dead load had relatively many interface failures. For the other series the failure majority is mid-section failure.

Conditions				Type of failure or truncation		
RH	SL	FQ	n	Mid failure	Interface failure	Stopped
65	50	0.1	10	5	3	2
65	65	1	20	15	2	3
65	65	0.1	30	21	6	3
65	65	0.01	40	27	11	2
65	65	dead-load	20	0	2	18
85	50	1	20	12	4	4
85	50	0.1	20	17	1	2
85	50	0.01	20	13	5	2
85	65	1	30	29	1	0
85	65	0.1	30	26	3	1
85	65	0.01	20	27	2	1
85	65	dead-load	30	13	14	3

Table 6.3: *Fatigue series, conditions and failure modes.*

6.2.3 Raw fatigue results

The fatigue results are presented in either time under load to failure, TUL, or in number of cycles to failure, NOC. Time under load to failure corresponds to half the test duration due to the square wave shaped load cycles, and is given in hours. The number of cycles to failure is related to TUL by the test frequency given in Hz [s^{-1}].

$$NOC = 3600 \cdot FQ \cdot 2 \cdot TUL \tag{6.2}$$

In Figures 6.4 to 6.9 TUL is given a log normal probability rank. Each graph represents a merging of data from different series at the same combination of $RH/SL/FQ$. The ranking comprises both regular mid section wood failures, interface failures and time under load corresponding to test termination. Most of the interface failures were in the upper tail. Under the assumption that the fatigue results are log normal distributed a 50-percentile estimate of the mean value is made. The standard deviation is determined on basis of the lower tail:

$$s_{50\%} = \sqrt{\frac{1}{n_{50\%} - 1} \sum_{i=1}^{i=n_{50\%}} (log(TUL_i) - log(TUL)_{50\%})^2} \tag{6.3}$$

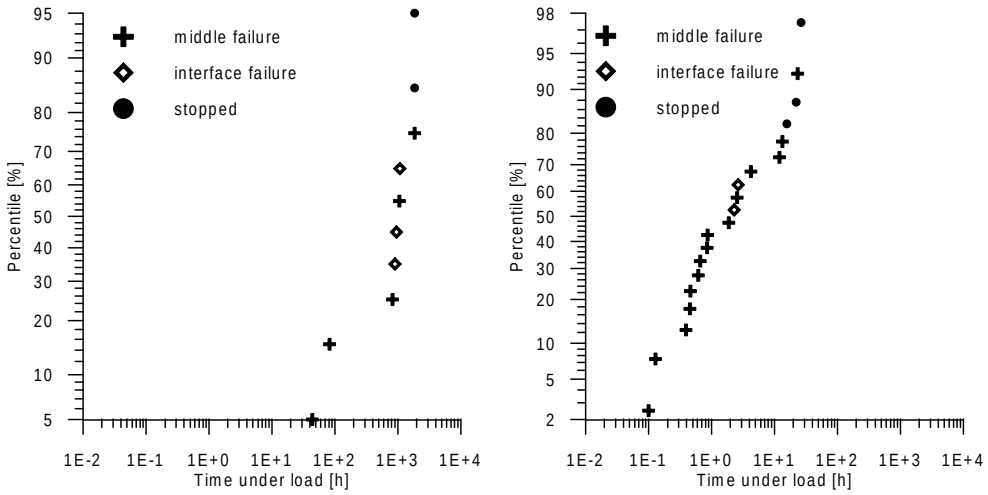

(a) 65/50/0.1

(b) 65/65/1

Figure 6.4: *Log normal probability ranking of failures.*

The values for these estimates are given in Table 6.4. The estimates are made on the logarithmically transformed data. The standard deviation, $s_{50\%}$, is invariant to shift between TUL and NOC as $log(TUL) = log(NOC) - log(7200 \cdot FQ)$. The main observations from the fatigue results given in Table 6.4 are:

- For the RH=65 % condition at 65% stress level approximately two decades in TUL are lost when FQ is raised two decades. This corresponds to constant NOC at 65/65/1-0.01 conditions.
- For the RH=85 % condition approximately one decade is lost in TUL when FQ is raised two decades. This corresponds to an increase in NOC for increased FQ.

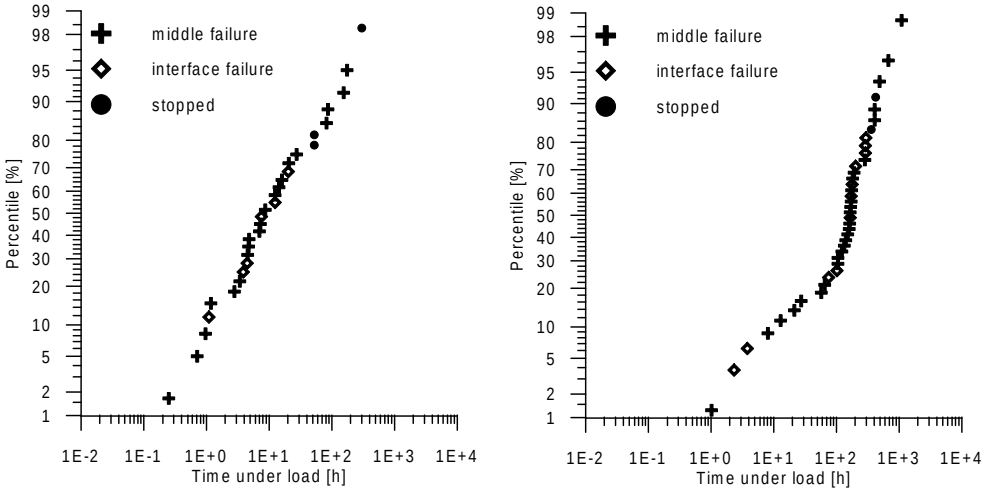

(a) 65/65/0.1 (b) 65/65/0.01

Figure 6.5: *Log normal probability ranking of failures.*

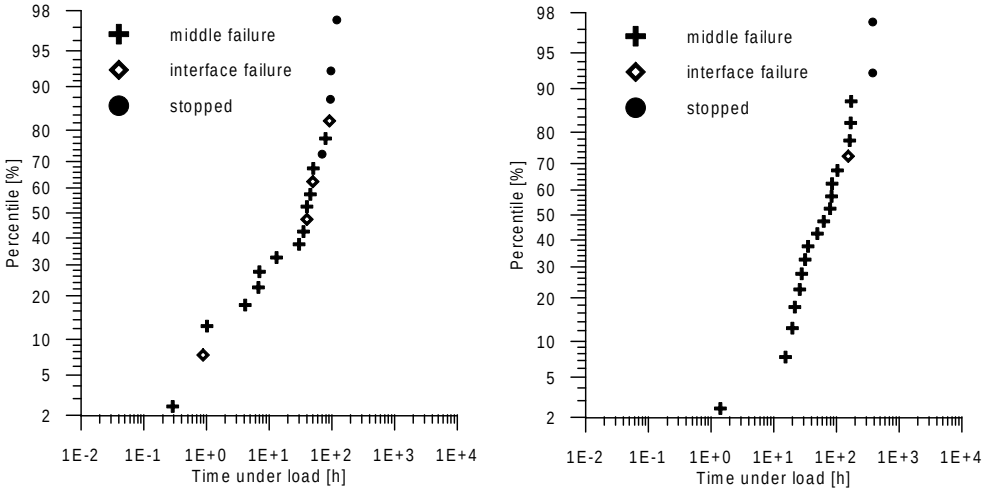

(a) 85/50/1 (b) 85/50/0.1

Figure 6.6: *Log normal probability ranking of failures.*

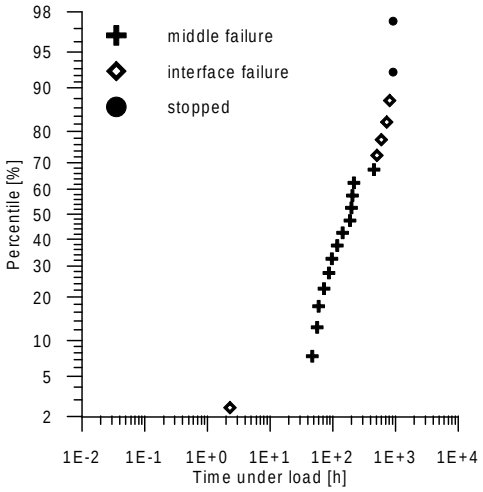

(a) 85/50/0.01

Figure 6.7: *Log normal probability ranking of failures.*

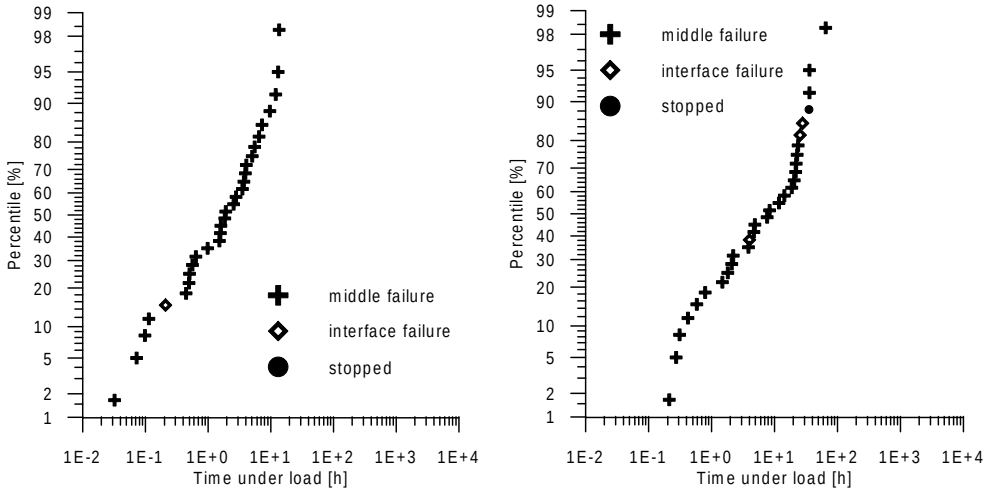

(a) 85/65/1

(b) 85/65/0.1

Figure 6.8: *Log normal probability ranking of failures.*

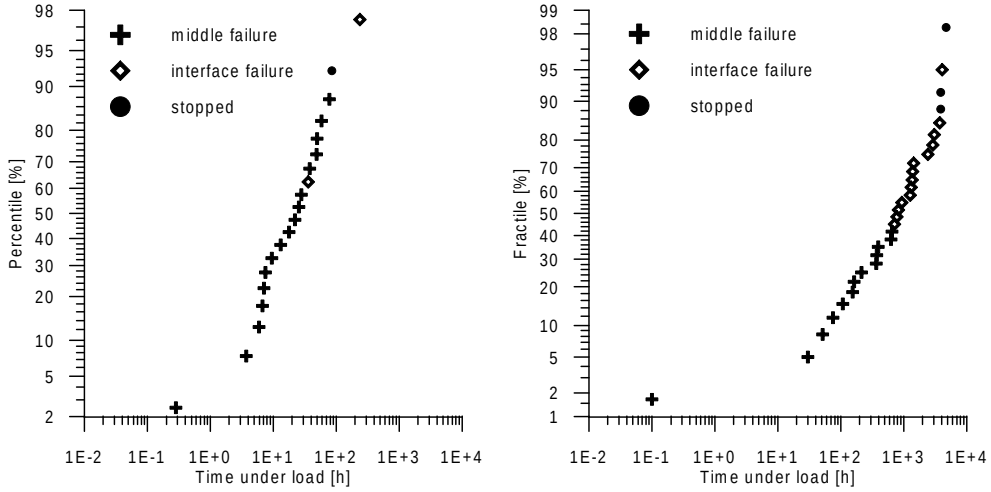

(a) 85/65/0.01

(b) 85/65/dead

Figure 6.9: *Log normal probability ranking of failures.*

Conditions				50-percentile of $log(TUL)$ and $log(NOC)$		
RH	SL	FQ	n	$log(TUL)_{50\%}$	$log(NOC)_{50\%}$	$s_{50\%}$
65	50	0.1	10	3.00	5.86	0.87
65	65	1	20	0.32	4.18	0.77
65	65	0.1	30	0.91	3.77	0.68
65	65	0.01	40	2.22	4.08	0.92
65	65	dead-load	20	-	-	-
85	50	1	20	1.60	5.46	1.17
85	50	0.1	20	1.85	4.71	0.71
85	50	0.01	20	2.29	4.15	0.75
85	65	1	30	0.27	4.13	0.88
85	65	0.1	30	0.90	3.76	0.94
85	65	0.01	20	1.37	3.23	0.80
85	65	dead-load	30	2.90	-	1.26

Table 6.4: *50-percentile of log(TUL) and log(NOC) and corresponding standard deviations.*

Chapter 7

Discussion

7.1 Basic tools and assumptions used in fatigue analysis

7.1.1 Fatigue life distribution

As a basic assumption it is chosen to assume that the fatigue lives obtained are log normal distributed. This distribution is chosen among other distributions as it is operational in interpretation. The adequacy of fitting the data to a log normal probability distribution is verified in Figure 7.1(a) where a log normal probability plot of the random distributed residuals is given. The residuals r_{ij} are calculated as:

$$r_{ij} = log(TUL_{ij}) - \overline{log(TUL_j)}_{SAS}, \tag{7.1}$$

where $log(TUL_{ij})$ is the i'th observation in the j'th group of conditions and $\overline{log(TUL_j)}_{SAS}$ is the mean in the j'th group of conditions estimated by a SAS procedure taking the censored data into account. The SAS procedure is described in a later section. The assumption of log normal distribution is verified as the central part of the randomly distributed error terms in Figure 7.1(a) form a straight line in the normal probability plot. It should be observed that the ranking of residuals in Figure 7.1(a) include the censored data. The logarithmic transformation of the data has the benefit of stabilizing the variation between series so one common normal distributed error term can be fitted to all data. This is seen in Figure 7.1(b) where the standard deviation of $log(TUL)$ is given as function of the mean of $log(TUL)$. It is seen that the standard deviation is about 0.8 decade for means spanning three decades.

7.1.2 Reproducibility

The variation between series at identical conditions is exemplified in Figure 7.2. As seen the reproductivity between series at identical conditions is relatively poor. Series 17 in

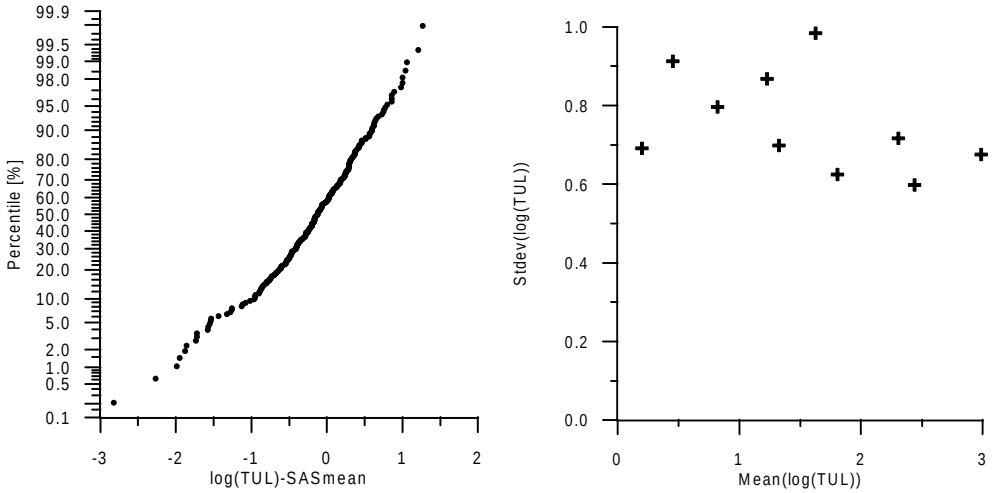

(a) Log normal probability plot of residuals

(b) Standard deviation as function of mean

Figure 7.1: *Adequacy of the logarithmical transformation of data.*

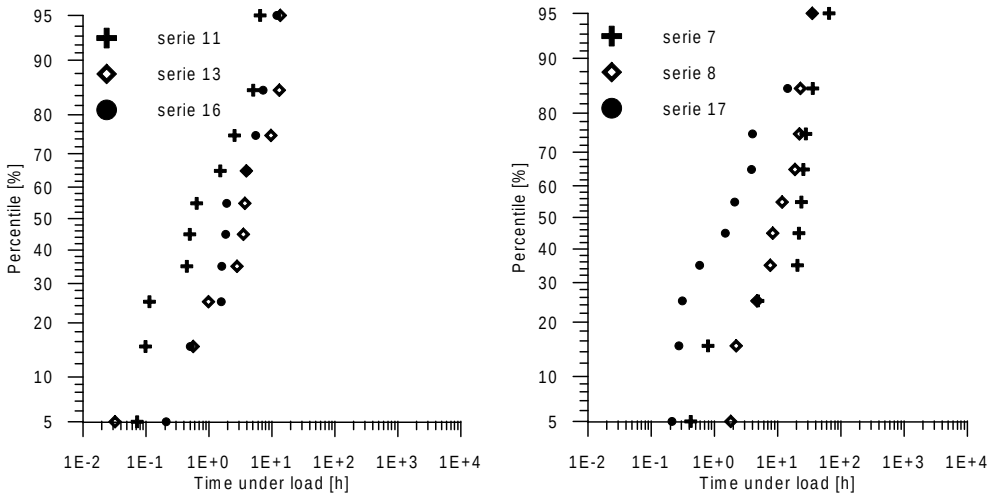

(a) Three series at 85/65/1

(b) Three series at 85/65/0.1

Figure 7.2: *Variation between series at identical conditions.*

Figure 7.2 (b) was run at 0.1 Hz in a servo hydraulic equipment to compare it with series run in the mechanical test rigs. Though series 17 was run so that the failure of one specimen could never influence the failure of another the mean survival time for series 17 is shorter than for the other series at 0.1 Hz in Figure 7.2 (b). There is no evidence that the conditions in the servo hydraulic equipment was less controlled than in the mechanical rigs. Large scatter is also seen between series run in the same equipment, e.g. Figure 7.2 (a) showing three 1 Hz tests series tested in the servo hydraulic equipment.

The number of specimens taken to failure at each set of test conditions is limited by the total number of specimens in the whole test block. Prior to testing it was assumed that 10 specimens at each set of test conditions was sufficient, however it was from an early stage clear that more than one series was needed. The statistical strength of tests on the data will show if the number of specimens has been sufficient to discriminate differences in survival times for the different set of test conditions.

7.1.3 Censoring

The fatigue results presented are inflicted with two kinds of censoring, namely:

- Interface failure prior to regular mid section wood failure.
- Truncation of test series due to test stop.

In Chapter 6 mean and standard deviation are given based on the 50-percentiles of the obtained data. In all cases most of the failures below the 50-percentile were regular wood failures. Hence, the basis for the estimates of mean and standard deviation in Chapter 6 is good provided the data are logarithmically normal distributed and the number of data observed is sufficiently high. However, in order to benefit from all obtained data a maximum likelihood procedure including censored data must be employed.

The censoring by the interface failures is due to the fatigue strength of the glue line. The distribution of this strength is unknown. A similar problem of regular wood failures interfered by failures from another failure distribution is treated by e.g. Källsner & Ditlevsen (1994); it is assumed that the strength of the wood and interface are stochastic variables, X_W and X_I. The strength of a specimen, X, follows the extreme value distribution corresponding to the minimum of these:

$$X = min\{X_W, X_I\} \tag{7.2}$$

If X_W has the distribution $F_W(x)$ and X_I has the distribution $F_I(x)$ the probability of encountering a strength larger than x is determined by:

$$1 - F(x) = (1 - F_W(x))(1 - F_I(x)) \tag{7.3}$$

If the failure distribution is the outcome of a process of the form (7.3), the distribution for the wood fatigue failures $F_W(x)$ may in principle be determined using a maximum likelihood procedure and a suitable restriction based on the observed probability of encountering interface failure. The outcome of such a procedure would be an estimate of the wood failure distribution with a somewhat higher mean value than estimated by use of only wood failures. However, this method requires an assumption on the distribution of the interface failures. A distribution for the interface failures cannot be selected on a rational basis due to the limited number of occurring interface failures in each series, Table 6.3.

The censoring due to both interface failures and test termination can however be treated as one phenomenon without any assumption on the distribution of the interface failures. This can be done by treating the results as right censored data and by use of a maximum likelihood method to analyse the data. Similar censoring due to two independent factors are often met in medical statistics. Here the censoring factors may be test termination or the death of a test participant due to other reasons than the disease within the test. The first censoring factor is equal to the test stop in the fatigue test runs and the second to the interface failures. Though the censoring factors are different they are treated as one and the same right censoring phenomenon.

In (Cox & Oakes 1984) a procedure is given for statistical analysis of censored data by use of a maximum likelihood method. The likelihood function for a single sample is determined as:

$$lik = \prod_u f(t_i) \prod_c F(c_i), \tag{7.4}$$

where the two products are taken over censored and uncensored observations respectively. The density function evaluations, $f(t_i)$, are made for all uncensored failure times, t_i, and the censoring at c_i contributes to the likelihood function by survival function evaluations at all censor times. The survival function $F(c_i)$ is defined as:

$$F(c_i) = \int_{c_i}^{\infty} f(u)du \tag{7.5}$$

In the maximum likelihood procedure the density function of the distribution is varied seeking a maximum of the likelihood function (7.4) by maximizing the log likelihood

function:

$$l = \sum_u log(f(t_i)) + \sum_c log(F(c_i)) \tag{7.6}$$

Treating censored data

In the following discussion interface failure and test termination are treated alike as one right censoring of the data. In the statistics program SAS, the standard procedure LIFEREG is available for means estimation and regression of censored data, the procedure is described in (SAS Institute 1994). With this procedure it is possible to make log likelihood estimates of the mean and standard variation of the data at each set of conditions including the censored data. Further, it is possible to make linear regressions to the data variation with the independent variables, e.g. the test conditions FQ and SL, while at the same time including the censored data in a procedure such as (7.4). The additive linear model does not allow interaction between the effects and takes the general form:

$$\mathbf{y} = \mathbf{X}\beta + \sigma\epsilon \tag{7.7}$$

In the present context the response $\mathbf{y}$ is the modelled response given as $log(TUL)$ or $log(NOC)$, the vector $\mathbf{X}$ contains the independent variables, e.g. SL or $log(FQ)$, and β is a vector of the unknown regression parameters. As a log transformation of the data is used the error term contains a vector of the errors from a standard normal distribution, $\epsilon \in \mathbf{N}(\mathbf{0}, \mathbf{1})$, scaled in the regression by the factor σ.

7.2 Fatigue analysis

7.2.1 The influence of conditions

In an initial analysis of the data it is the objective to asses the log likelihood estimates of mean and standard deviation of $log(TUL)$ and to compare them with mean and standard deviation determined on basis of the lower 50-percentile of the distribution. As a log normal distribution of the data is assumed and as the data in the lover 50-percentile of the data is less inflicted by censoring than the whole set of data it is anticipated that the SAS-estimates based on all data is relatively close to the 50-percentile estimates. The comparison is shown in Table 7.1. The SAS estimated mean is generally close to the 50-percentile estimates, only for tests highly influenced by censoring such as the 85/65/dead-load case, where more than 50% of the results are censored, the SAS estimate is substantially higher than the 50-percentile estimate.

Conditions			50-percentile		SAS-LIFEREG	
RH	SL	FQ	$log(TUL)_{50\%}$	$s_{log(TUL)_{50\%}}$	$\overline{log(TUL)}$	$s_{log(TUL)}$
65	50	0.1	3.00	0.87	3.20	0.88
65	65	1	0.32	0.77	0.45	0.91
65	65	0.1	0.91	0.68	1.23	0.87
65	65	0.01	2.22	0.92	2.31	0.72
85	50	1	1.60	1.17	1.63	0.98
85	50	0.1	1.85	0.71	1.81	0.62
85	50	0.01	2.29	0.75	2.44	0.60
85	65	1	0.27	0.88	0.20	0.69
85	65	0.1	0.90	0.94	0.82	0.80
85	65	0.01	1.37	0.80	1.33	0.70
85	65	dead-load	2.90	1.26	3.57	1.71

Table 7.1: *Mean and standard deviation of log(TUL).*

In the following discussion of the results, where simple regression models are made to seek a correlation with test conditions, the SAS estimates of mean $log(TUL)$ and $s_{log(TUL)}$ are used as reference points of the modelling. The Figures 7.3 to 7.5 shows the variation with frequency of NOC and TUL for constant moisture and stress condition. The log normal probability plots show all data including censored data. From Table 7.1 it is seen that for the tests at 65/65/1-0.01 conditions almost a decade is gained in TUL when FQ is lowered one decade, corresponding to constant NOC independent of frequency. This is reflected in Figure 7.3 (a) where the curves for the three frequencies are coinciding. For the tests at RH 85% the distributions for both NOC and TUL lies distinct for the different frequencies as seen in Figures 7.4 and 7.5. The corresponding observation from Table 7.1 is that less than a decade in TUL is gained when the frequencies are lowered a decade.

7.2.2 Regression models

By use of the general linear additive model (7.7) regressions have been made with the SAS procedure LIFEREG in search of simple correlation between $log(TUL)$ and the different test conditions. The more variables fitted at a time the more coarse a model is anticipated. The independent variables have been included in the regression step by step by use of the

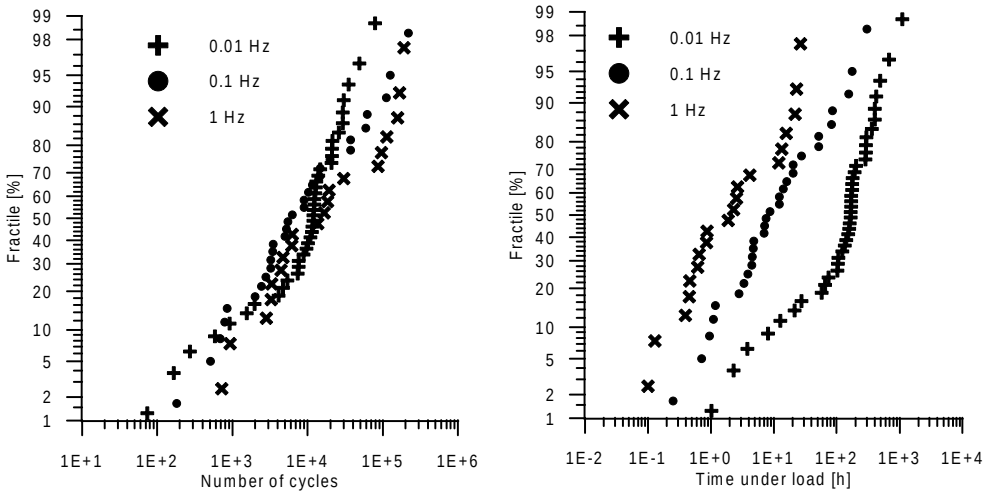

(a) 65/65/all frequencies (b) 65/65/all frequencies

Figure 7.3: *Log-normal probability ranking of failures for both TUL and NOC.*

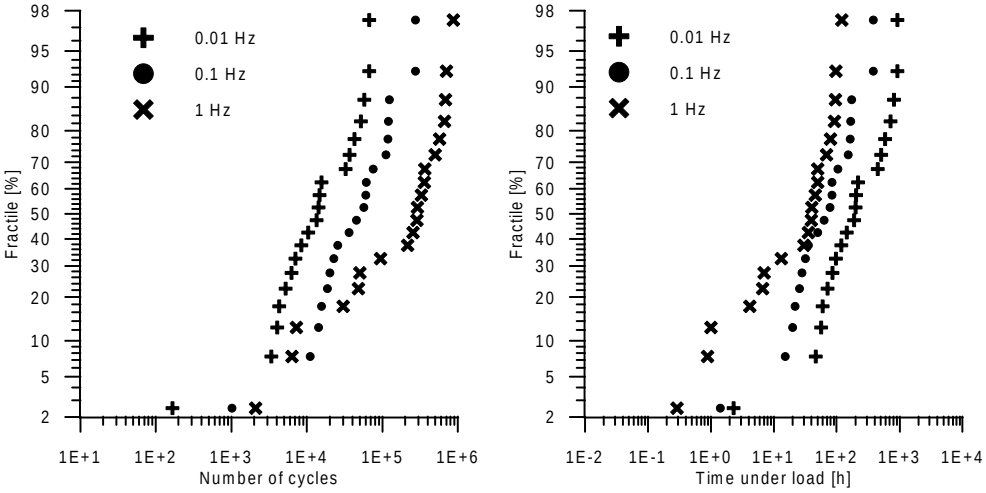

(a) 85/50/all frequencies (b) 85/50/all frequencies

Figure 7.4: *Log-normal probability ranking of failures for both TUL and NOC.*

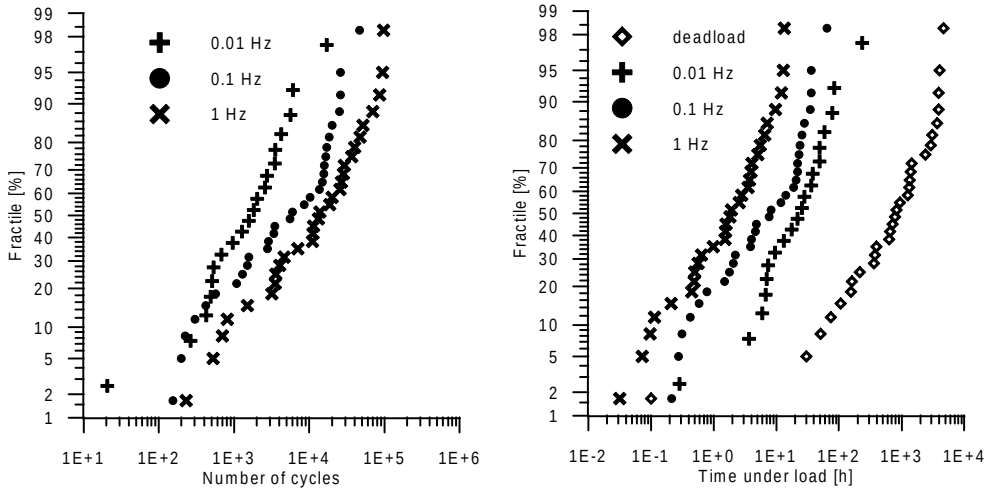

(a) 85/65/all frequencies

(b) 85/65/all frequencies

Figure 7.5: *Log-normal probability ranking of failures for both TUL and NOC.*

following three types of regressions where the response is made dependent on an increasing number of independent variables:

- Type 1: $log(FQ)$
- Type 2: $log(FQ)$ and SL
- Type 3: $log(FQ)$ and SL and RH

The regression including all independent variables takes the form:

$$log(TUL) = \mu + \alpha log(FQ) + \beta SL + \gamma RH + \sigma\epsilon \tag{7.8}$$

For the specimens at RH 65% only one FQ is tested at SL 50% and the difference in the regression parameters between regression type 1 and 2 is only an insignificant difference in the scale parameter, σ. The regression result is:

$$log(TUL) = 8.34 - 0.97log(FQ) - 0.12SL + 0.83\epsilon \tag{7.9}$$

For the specimens at RH 85% the regression models of type 1 reads for SL 50%:

$$log(TUL) = 1.48 - 0.47log(FQ) + 0.74\epsilon, \tag{7.10}$$

and for SL 65%:

$$log(TUL) = 0.22 - 0.57log(FQ) + 0.73\epsilon \tag{7.11}$$

It is seen that $log(TUL)$ has almost the same dependence on $log(FQ)$ for the two stress levels and the difference is attributed statistical uncertainty. When using both stress levels, i.e. regression type 2, the result is:

$$log(TUL) = 5.29 - 0.53log(FQ) - 0.078SL + 0.73\epsilon \tag{7.12}$$

Comparing (7.9) and (7.12) it is seen that the difference between the $log(FQ)$ regression parameters cannot be due just to statistical uncertainty, i.e. a regression of type 3 is too coarse and the effect of RH on $log(TUL)$ cannot be considered as additive.

The regressions can also be made on the data in NOC. As TUL is given in hours and FQ is given in Hz the following relations exist between $log(NOC)$ and $log(TUL)$:

$$log(NOC) = log(2 \cdot 3600 \cdot FQ \cdot TUL) = log(7200) + log(FQ) + log(TUL) \tag{7.13}$$

Hence, the regressions in $log(NOC)$ moves the intercept $log(7200)$ and the regression parameter with $log(FQ)$ is increased by 1. Figures 7.6 and 7.7 show the regressions (7.9) and (7.12) for both $log(TUL)$ and $log(NOC)$ with the individual SAS estimate for each set of conditions. In Table 7.2 SAS etimates of mean $log(TUL)$ for each set of test conditions are compared to the SAS regression estimates of mean $log(TUL)$.

7.3 Reference strength

In the treatment of the fatigue results the stress level, SL, is determined as the load relative to the plank reference strength. The argument for the procedure is that the reference strength is better determined within a plank than as a mean of all planks. However, it may be argued that the stress level should have been determined based on mean strength for all planks and the scatter hereby introduced should have been removed by including a plank specific variation in the modelling. The effect of plank strength, PS, could then be included as an extra term ΔPS in (7.8), either as a regression in the plank strength variation about a common mean or as a class variable taking a plank specific value independent of the strength variation.

The regression for the RH 85% takes the following form when the plank specific stress level, SL, is replaced with a stress level relative to the mean strength of all planks, SL_{mean}:

$$log(TUL) = 4.15 - 0.55log(FQ) - 0.059SL_{mean} + 0.74\epsilon \tag{7.14}$$

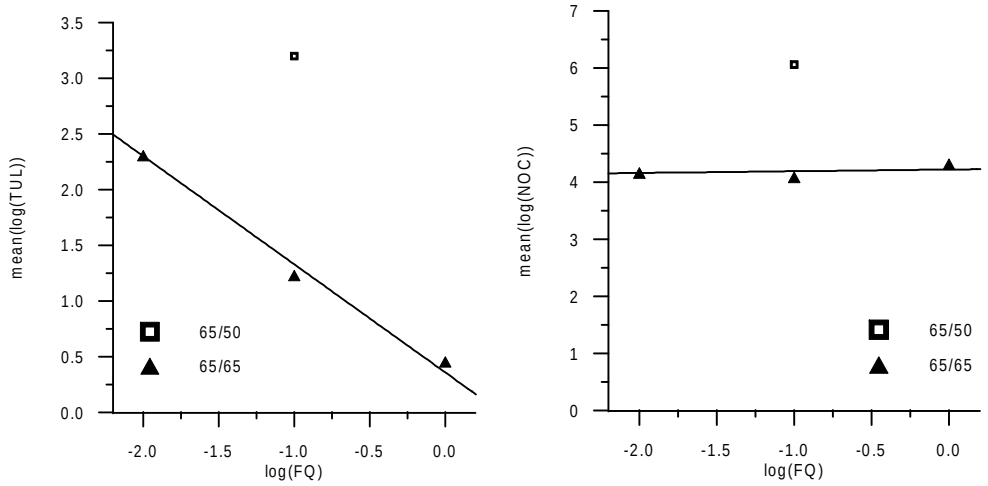

(a) Time under load (b) Number of cycles

Figure 7.6: *Regression for all RH 65% specimens.*

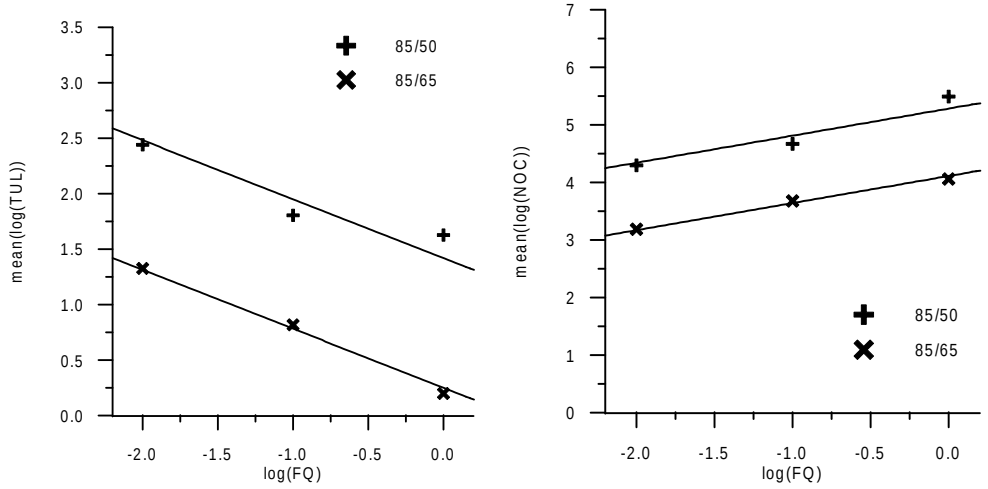

(a) Time under load (b) Number of cycles

Figure 7.7: *Regression for all RH 85% specimens.*

Conditions			Individual estimate		Regression 1		Regression 2	
RH	SL	FQ	$\overline{log(TUL)}$	$s_{log(TUL)}$	$\overline{log(TUL)}$	$s_{log(TUL)}$	$\overline{log(TUL)}$	$s_{log(TUL)}$
65	50	0.1	3.20	0.88			3.17	0.83
65	65	1	0.45	0.91			0.36	0.83
65	65	0.1	1.23	0.87			1.33	0.83
65	65	0.01	2.31	0.72			2.30	0.83
85	50	1	1.63	0.98	1.48	0.74	1.42	0.73
85	50	0.1	1.81	0.62	1.94	0.74	1.94	0.73
85	50	0.01	2.44	0.60	2.41	0.74	2.47	0.73
85	65	1	0.20	0.69	0.22	0.73	0.25	0.73
85	65	0.1	0.82	0.80	0.78	0.73	0.78	0.73
85	65	0.01	1.33	0.70	1.35	0.73	1.30	0.73

Table 7.2: *Mean and standard deviation of log(TUL) determined from regression 1 and 2 in SAS-LIFEREG.*

When further the plank strength variation about the common mean, $(PS - PS_{mean})$ is included as a regression factor, the form is:

$$log(TUL) = 5.27 - 0.53log(FQ) - 0.077SL_{mean} + 1.2(PS - PS_{mean}) + 0.70\epsilon \quad (7.15)$$

These two regressions are to be compared with the original regression in SL given in (7.12):

$$log(TUL) = 5.29 - 0.53log(FQ) - 0.078SL + 0.73\epsilon, \quad (7.16)$$

and its counterpart including $(PS - PS_{mean})$:

$$log(TUL) = 5.27 - 0.53log(FQ) - 0.077SL - 0.83(PS - PS_{mean}) + 0.70\epsilon \quad (7.17)$$

The whole idea of loading with a plank specific stress level, SL, is to minimize the variation with plank. In both regressions including $(PS-PS_{mean})$ the factor is significant, i.e. plank variation has not been completely eliminated by the chosen procedure. When comparing (7.17) and (7.16) it is observed that the inclusion of the plank strength variation does not affect the regression parameters for $log(FQ)$ and SL. The main effect of the inclusion is that the error term is reduced. When comparing (7.14) and (7.15) the inclusion of variation with plank is seen to have a large effect on the regression parameter for SL. In conclusion the variation with plank is reduced sufficiently by determining the stress level relative to the plank reference strength.

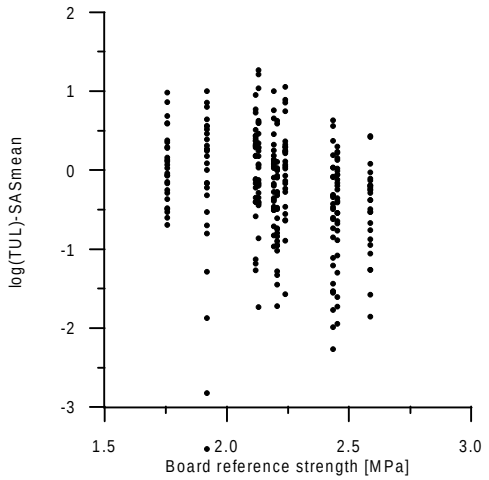

Figure 7.8: *The influence of the absolute stress level on the fatigue resistance.*

The regression in (7.17) shows specimens with high reference strength to survive shorter than specimens with lower reference strength. The reference strength is confounded with plank, i.e. density and other inherent properties of each of the 10 planks. Hence, if the fatigue life is a function of the absolute strength level it may reflect either that the reference strength for each plank is not determined accurately enough or that the fatigue life is also a function of some of the factors confounded with strength. It may for instance be the case that dense wood is more brittle and hence survive fewer cycles than less dense wood. The influence of the absolute stress level is reflected in Figure 7.8, where the residuals r_{ij} as defined in (7.1) are shown as function of the reference strength.

Chapter 8

Fatigue Modelling

In Chapter 2 a simple heuristic failure surface in stress level, time under load and number of cycles is suggested and in Figure 8.1 it is reprinted. The failure surface is divided into schematic regimes. At high stress levels a regime is suggested where an effect of number of cycles interact with the duration of load. This interaction makes it impossible to determine number of cycles to failure independent of the frequency. At intermediate stress levels, below a stipulated duration of load threshold, failure is only governed by number of cycles. Below a stipulated fatigue threshold failure is never encountered.

In Chapter 7 regressions (7.9) and (7.12) were given in $log(TUL)$ for all combinations of SL and FQ at the two levels of RH. The same regressions may be given in $log(NOC)$, for RH 65%:

$$log(NOC) = 12.20 + 0.03log(FQ) - 0.12SL + 0.83\epsilon, \tag{8.1}$$

and for RH 85%:

$$log(NOC) = 9.15 + 0.47log(FQ) - 0.078SL + 0.73\epsilon \tag{8.2}$$

It is observed that:

- At RH 65%, NOC is invariant to FQ and number of cycles to failure depends only on stress level. This corresponds to the II. regime of Figure 8.1.
- At RH 85%, NOC is highly influenced by FQ corresponding to interaction between NOC and TUL as in the I. regime of Figure 8.1. The frequency dependency of NOC is equal at SL 65% and 50%.

The damage accumulation laws referred to in Section 2.1.1 take only the time dependent damage into account. As the RH 65% tests show no variation with time the damage

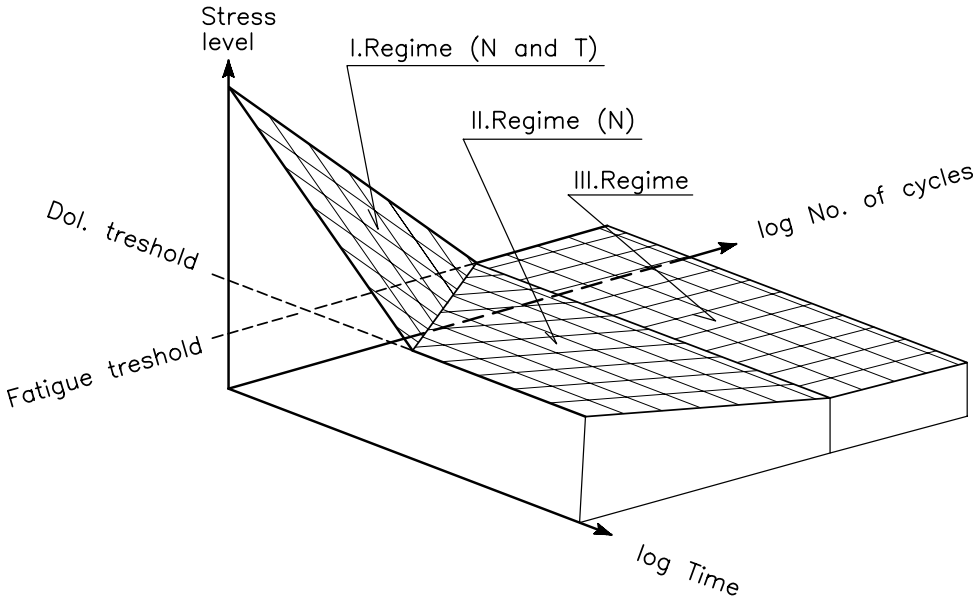

Figure 8.1: *Combined fatigue and duration of load failure surface divided into three possible failure regimes.*

accumulation laws are an inadequate tool in describing the fatigue failures. The same comment applies to the wood fatigue model resting on polymer debonding referred to in Section 2.1.2. Since collection of deformation during the fatigue tests has not been made, energy based failure models cannot be tested by use of the results presented. The modified work density model by Philpot et al. (1994) referred to in Section 2.1.3 has however been applied to parallel to grain fatigue data in (Clorius et al. 2000). The modified work density at failure was found to be of the same order of magnitude for tests at different frequencies and different levels of moisture content. Though a failure criterion stated only in number of cycles to failure such as the traditional Wöhler approach referred to in Section 2.1.4 is applicable to the RH 65% tests it is clearly inadequate for the RH 85% tests.

The DVM theory described in Section 2.1.5 incorporates a time dependent effect in a fracture mechanics based number of cycles approach. With respect to the observations at RH 85% the DVM theory is a priori interesting as the theory allows for an interaction between frequency and number of cycles of the kind observed. In the following the failure predictions of the DVM theory are tested against the test results.

8.1 DVM lifetime prediction

In (Fuglsang Nielsen 2000*b*) equations and values are given for all material parameters in the DVM theory. The equations and values are the result of an investigation of a number of tests on wood fatigue reported in literature. An algorithm to solve the differential equation (2.43) is given in (Fuglsang Nielsen 2000*b*). In the following the result of using this algorithm with the material parameters in (Fuglsang Nielsen 2000*b*) is presented for the different test conditions in the tension perpendicular to grain investigation. The strength of the DVM theory in this context is its ability to take into account both energy dissipation in the crack due to creep, i.e. duration of load, and energy dissipation due to load oscillations, i.e. number of cycles. This is reflected in the critical strain energy release rate, (8.3), where the first term corresponds to creep energy dissipation and the second to energy dissipation due to number of load oscillations.

$$\Gamma_{cr} = \sigma_l \delta_{max} \left[C_{cl} \left(\frac{\Omega}{q} \right) + Z \frac{\Omega}{T} \right] \tag{8.3}$$

8.1.1 Parameters from literature

Table 8.1 lists equations and values for the material parameters needed, τ, b, FL, C and M. The parameter values corresponds to the recommended values given in (Fuglsang Nielsen 2000*b*).

8.1.2 DVM versus experiments

The Figures 8.2, 8.3, and 8.4 show SL as function of either $log(TUL)$ or $log(NOC)$ as predicted by the DVM theory with the material parameters given in Table 8.1. In general it is observed that lifetime predicted by DVM is of the same order of magnitude as the experimental results. The fine correspondence between experimental results and predictions is impressive considering that only one assumption was made in choice of model parameters, namely that the wood was clear with an initial crack length $l_0 = 1.5$ mm. The model parameters p, β, f and SL are determined explicitly from the load conditions, and the remaining model parameters C, M, τ and b have the values recommended by Fuglsang Nielsen (2000*b*). Hence, the DVM theory predicts the order of magnitude of $log(TUL)$ or $log(NOC)$ without parameter fitting. A further strength of the theory will be its ability to predict correctly the interaction between NOC and TUL.

Parameter		Equation	Value
Creep doubling time	τ	$log_{10}(\tau) \approx log_{10}(\tau_b) - 4.5 + d_u + d_T$ $log_{10}(\tau_b) = 4,$ $d_u \approx \frac{12\%-u\%}{10},$ $d_{u=12\%} = 0,\ d_{u=18\%} = -0.6$ $d_T \approx \frac{20\%-T^\circ C}{15} = 0$	$\tau_{u=12\%} = 0.32$ $\tau_{u=18\%} = 0.08$
Creep power	b		$b = 1/3$
Strength level	FL	$FL \approx \sqrt{1 - \exp\left(-\frac{d}{l_0}\right)} \approx \sqrt{\frac{d}{l_0}}$	$FL = 0.45$
Damage rate constant	C		$C = 3$
Damage rate power	M		$M = 9$

Table 8.1: *Material parameters from (Nielsen 2000b), (τ in days).*

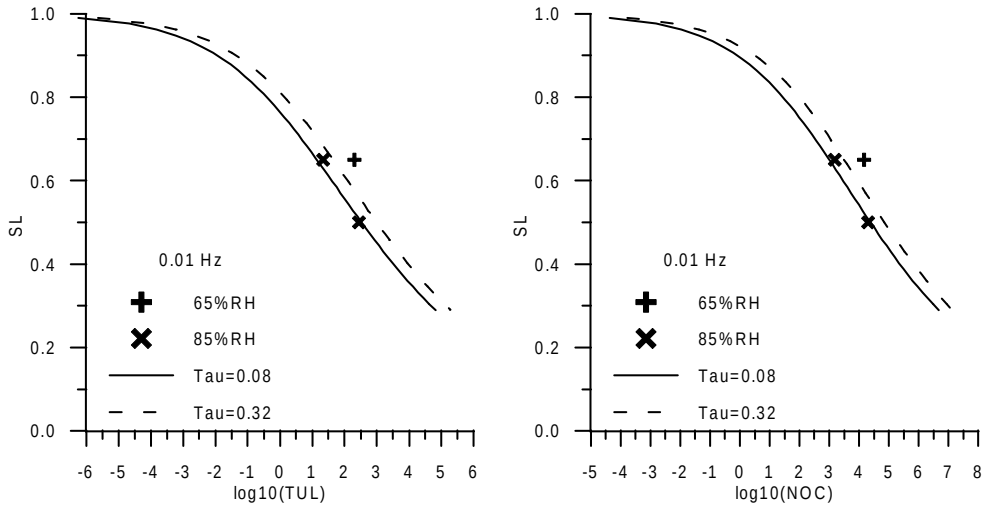

(a) Time under load

(b) Number of cycles

Figure 8.2: *DVM lifetime prediction at 0.01 Hz with experimental results.*

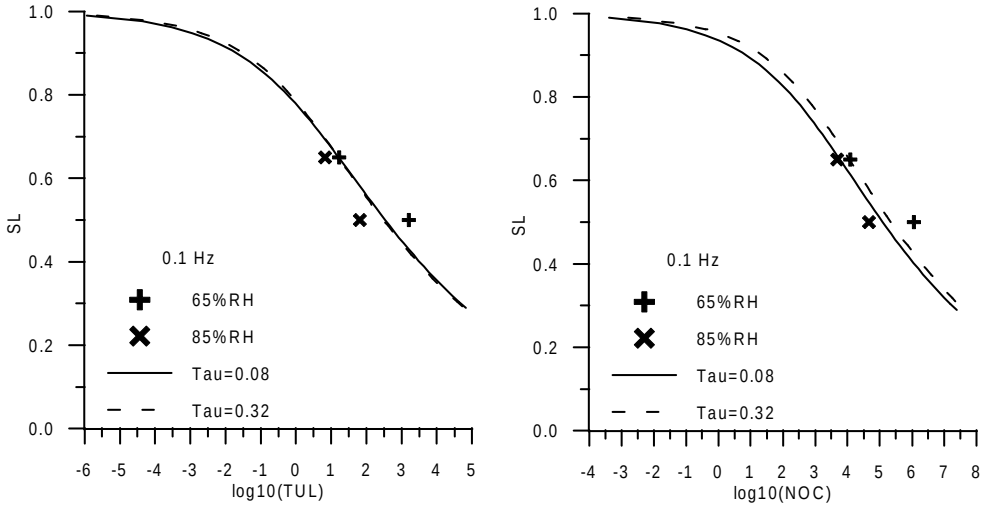

(a) Time under load (b) Number of cycles

Figure 8.3: *DVM lifetime prediction at 0.1 Hz with experimental results.*

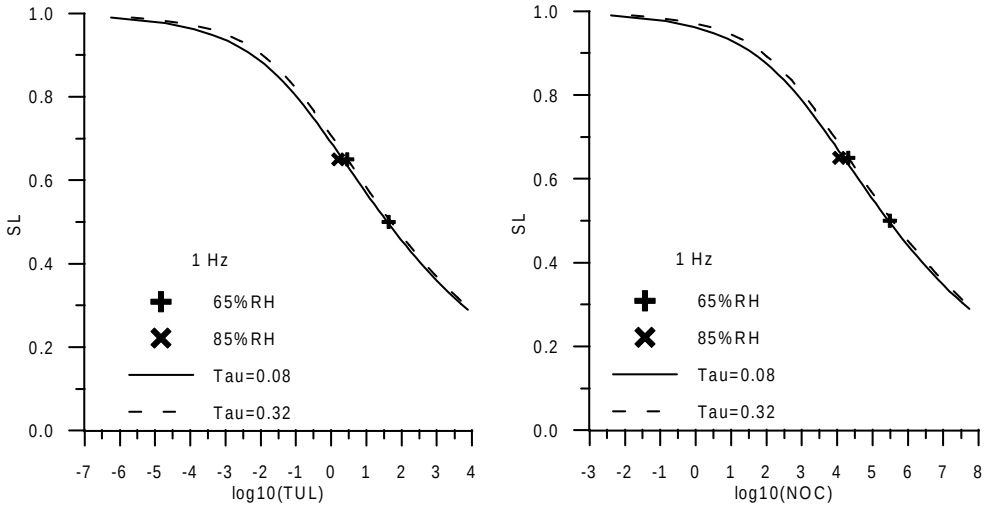

(a) Time under load (b) Number of cycles

Figure 8.4: *DVM lifetime prediction at 1 Hz with experimental results.*

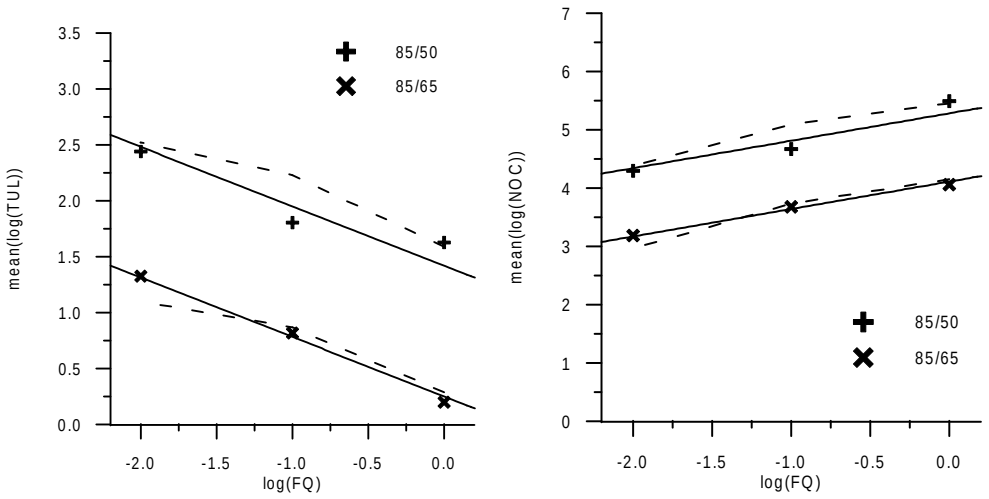

(a) Time under load (b) Number of cycles

Figure 8.5: *DVM lifetime prediction (dashed line) and SAS regression (full line) for 85% RH.*

8.1.3 DVM versus regression

In Figure 8.5 the DVM lifetime predictions are shown along with experimental results and the SAS regressions for the RH 85% tests. The general trend of the experimental results, namely decrease in NOC for decreased FQ, is predicted by the DVM theory. The order of magnitude of NOC at both SL 50% and 65% is correct. However, the DVM theory predicts a not experimentalle observable increased influence of time when FQ is lower than 0.1 Hz.

In Figure 8.6 the DVM lifetime predictions are shown along with experimental results and the SAS regressions for the RH 65% tests. The prediction of NOC for the 65/50/0.1 tests is too low, but it may be a reflection of the experimental uncertainty as these tests only comprise one series. The tests at SL 65% show no influence of time in the failure explanation, the DVM predictions however include an influence of time and the prediction of the 0.01 Hz tests is too conservative.

8.1.4 Improved DVM prediction

By use of the parameter values recommended in (Fuglsang Nielsen 2000*b*) it is possible to model the interaction between TUL and NOC for tests at RH 85%. The model is however not able to model the RH 65% tests adequately as it overestimates the time

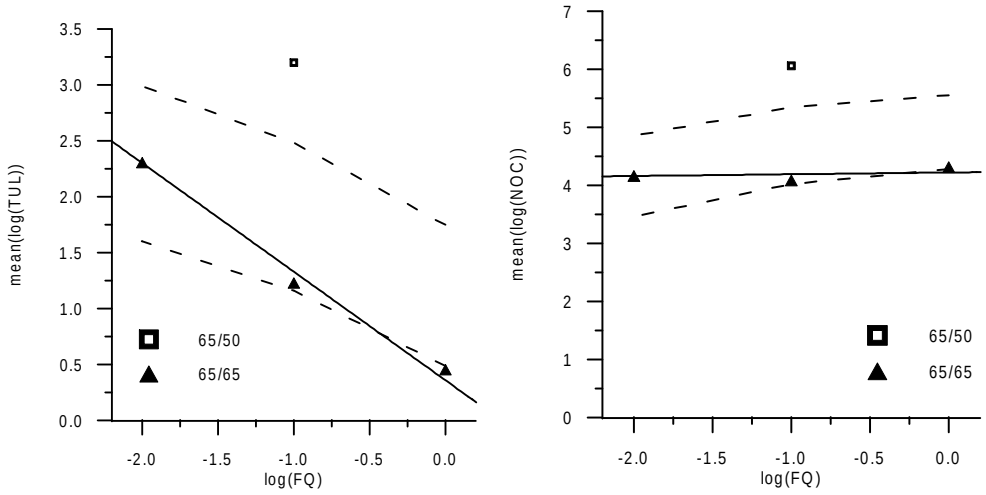

(a) Time under load

(b) Number of cycles

Figure 8.6: *DVM lifetime prediction (dashed line) and SAS regression (full line) for 65% RH.*

influence for these tests. The parameters which governs the time dependent properties are τ and b, of these only τ is a function of RH. To improve the RH 65% predictions a larger value for τ is used, i.e the term corresponding to creep energy dissipation in the crack is suppressed for the RH 65% tests. In Figure 8.7 DVM predictions for increased values of τ are shown. It is seen that $\tau = 4$ days almost cancels the effect of time and the predictions fit the experiments. The parameter study of the influence of τ shows how NOC is dominating at high FQ as the predictions are almost invariant to change of τ at high FQ, this is so as τ does not modify the NOC term in (8.3).

8.2 Failure surface

The heuristic failure surface in Figure 8.1 assumes an area with interaction between NOC and TUL for high stress levels and a regime where failure is dominated by NOC for lower stress levels and the assumption is that these regimes are independent of FQ. The DVM theory is more refined as it allows a shift between NOC and TUL dominated failure at all stress levels. Figure 8.8 shows DVM lifetime predictions in both $log(NOC)$ and $log(TUL)$ at 65% SL for four different values of τ. The observations with respect to NOC and TUL failure domination are:

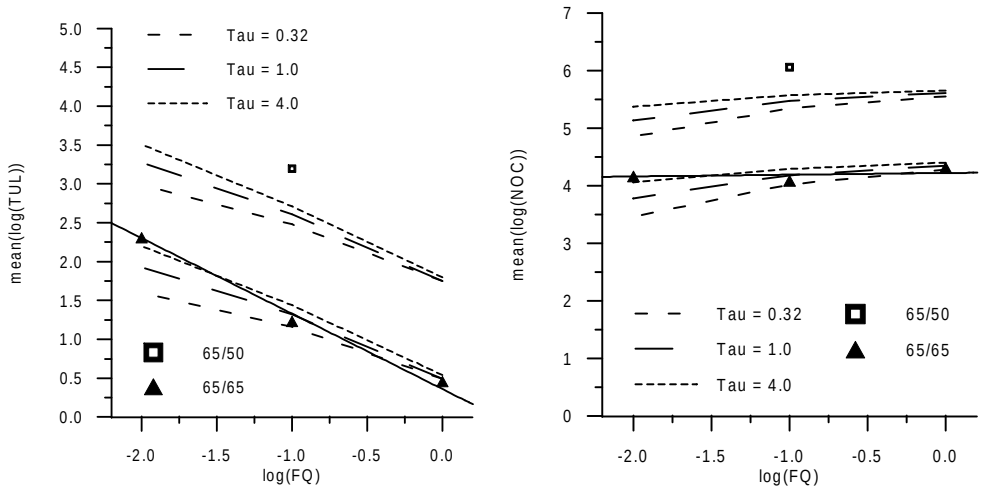

(a) Time under load (b) Number of cycles

Figure 8.7: *DVM lifetime prediction for different values of τ [days] for 65% RH, (full line: SAS regression).*

- For low frequencies, failures are dominated by TUL only, corresponding to zero slope in Figure 8.8 (a) and slope one in Figure 8.8 (b). The fatigue life increases for increased value of τ.
- For high frequencies, failures are dominated by NOC only, corresponding to a negative slope of one in Figure 8.8 (a) and zero slope in Figure 8.8 (b). The fatigue life becomes invariant to the value of τ for high frequencies.
- The shift between NOC and TUL dominated failure takes place at lower frequencies for increased values of τ.

The structure of the DVM theory allows for time independent failures for the RH 65% tests and failures due to a combination of time and number of cycles at RH 85%. As argued in the preceding section the principal trend for the RH 85% tests and RH 65% tests can be modelled by values of τ of 0.08 and 4 respectively.

In Figure 8.9 a failure surface based on the DVM theory is given in a space spanned by SL, $log(TUL)$ and $log(NOC)$. The surface is constructed by DVM predictions of TUL and NOC for FQ ranging from 10^{10} Hz to 10^{-10} Hz and is drawn for SL between 1 and 0.3. The iso-SL lines of the surface have a part with constant TUL and a part with constant NOC, and a part corresponding to interaction between TUL and NOC.

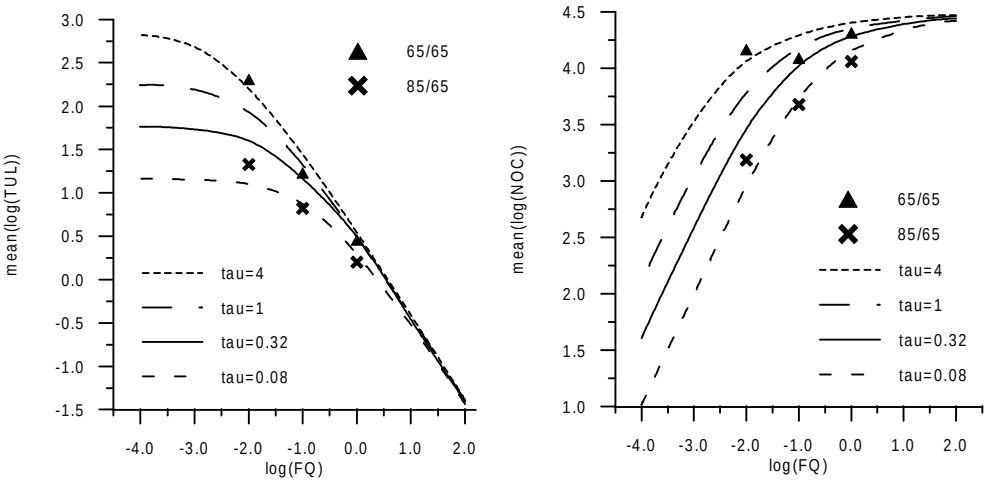

(a) Time under load (b) Number of cycles

Figure 8.8: *Shift between TUL and NOC dominated failures according to the DVM theory for SL 65%.*

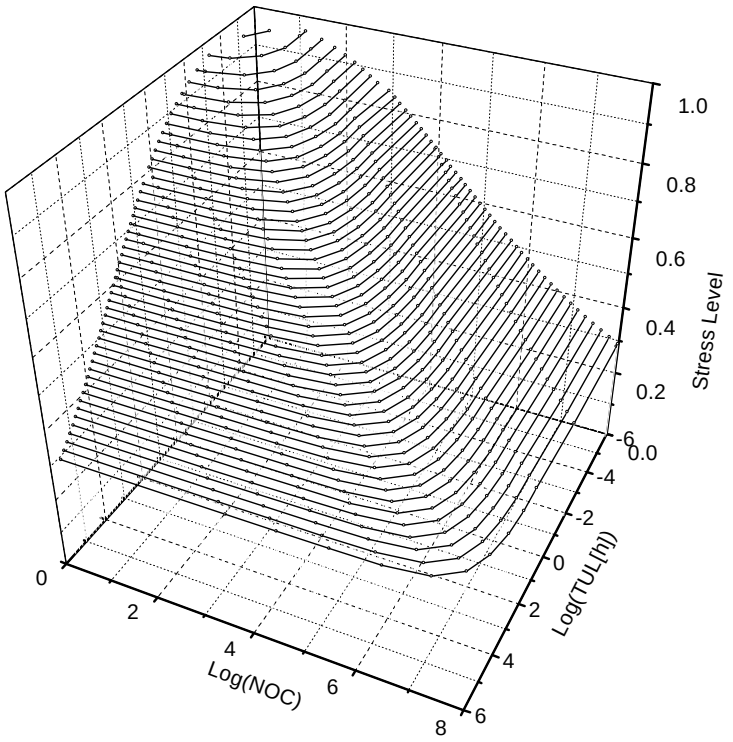

Figure 8.9: *Failure surface according to DVM theory without threshold, determined for τ=0.32 days.*

The surface is given for τ=0.32, for this choice of the creep doubling time the interaction area centres at an FQ corresponding to 0.1 Hz, for higher FQ the failures take place at a constant value of NOC and for lower FQ the failures take place at a constant value of TUL.

The experimental results shown in Figure 8.8 (b) do to some degree support the existence of a NOC threshold at high frequencies as NOC for 85/65 and 65/65 tests approach a common value for increased frequency. The TUL threshold is more problematic. The tests lie in the frequency range from 1 Hz to 0.01 Hz, but may be attempted used to predict the time to failure at dead load. If the SAS regression (8.2) is used to predict time to failure in the first cycle for the 85/65 tests $log(TUL) = 4.8$ is obtained. The DVM prediction in Figure 8.8 (a) gives directly the $log(TUL)$ threshold, it is seen to be approximately 1.2 for the RH 85% tests. Neither extrapolation of the SAS regression nor the DVM prediction corresponds to the SAS estimate $log(TUL) = 3.6$ for the 85/65/dead-load tests given in Table 7.1. The SAS regression is only a local fit in the tested frequency range and it is not expected to be able to predict dead load failure. The DVM theory on the other hand is expected to be able to predict dead load failure and the severe discrepancy between DVM prediction and empirical dead load time to failure points at a limitation of the parameter calibration in (Fuglsang Nielsen 2000*b*). The experimental dead load time to failure is confirmed by a fit to duration of load testing in tension perpendicular to the grain in (Aicher et al. 1998), wherefrom $log(TUL) = 3.4$ for SL 65% is predicted.

Chapter 9

Fatigue in Connections

This chapter reports fatigue in small double shear connections taken to failure in bending. The connections were designed and loaded so that they always failed in tension splitting perpendicular to the grain. The intension of the tests is to seek for similarities in the fatigue behaviour between the connection tests and the small clear specimens, making it possible to use the results from the small specimens in the modelling of more complex design details.

9.1 Method and specimens

9.1.1 Specimen design

The material used for the specimens was taken from the same batch of material used for fatigue testing of small clear specimens, i.e. 5 m long planks consisting of two boards glued sapwood to sapwood as described in Chapter 3.

The specimens containing a joint were designed with tension perpendicular to grain as limiting strength factor independent of the embedment strength. A specimen has a length of 900 mm with a joint in one end. A joint consists of an 8 mm slotted in steel plate fitting tightly in the groove in the wood. Two tightly fitting dowels of diameter d=12 mm connect wood with steel plate. The distances between dowels and from dowel to edge are 7d. The joint geometry is shown in Figure 9.1 (a).

Test plan

Each plank yielded 5 specimens of length 900 mm, of these the central specimen was used for reference strength determination and the remaining 4 were used for fatigue testing. A test series consists of 16 specimens from 8 different planks. Tests were made at two

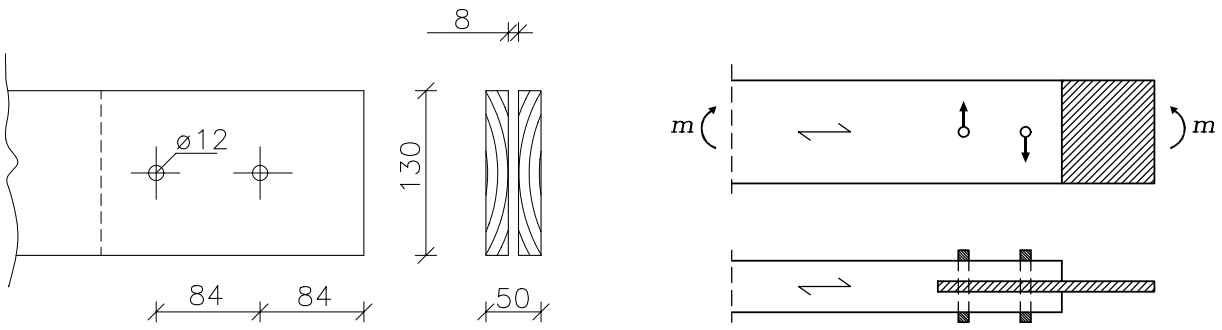

(a) Joint geometry (b) Loading mode

Figure 9.1: *Geometry and load application of fatigue tested dowel type joint.*

	RH 65%		*RH* 85%	
FQ [Hz]	0.1	0.01	0.1	0.01
SL 75%	2 x 16	2 x 16	16	16

Table 9.1: *Test plan giving number of specimens tested at each set of conditions.*

frequencies, two moisture levels and one stress level. Specimens from each plank were tested at the two frequencies but between the two levels of relative humidity the specimens originated from different planks. Hence, the planks are confounded with relative humidity but not with frequency. The test plan is given in Table 9.1. The test series were all terminated between the failure corresponding to the 50-percentile and failure of the last specimen.

Test set-up

A specimen was connected with a twin specimen to form a 1.8 m long member with a central connection. When one of the specimens failed the surviving was connected to a steel dummy. This means that for half of the specimens the fatigue testing was interrupted for shorter or longer time. The members were tested in four point bending rigs giving tension perpendicular to the grain stresses in the wood, Figure 9.1 (b). The eight fatigue rigs had individual load control and they were placed in a climate chamber. For each rig load application was provided by a pneumatic actuator in a feed back load controlled

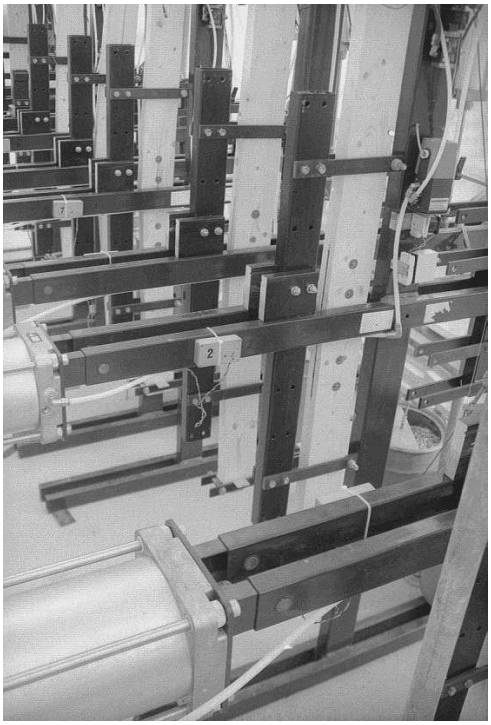

Figure 9.2: *View of four-point bending fatigue rigs.*

loop, Figure 9.2. Square wave shaped load cycles were used with a characteristic as shown in Figure 9.3 for a 0.01 Hz test. The period length of the 0.1 Hz tests was only correct as a mean over several cycles, computer updating of the feed back control loops resulted in retardation of the load application. The load oscillated between zero and maximum load with occasional overshoots of about 2-5% of the maximum stress.

9.2 Results

9.2.1 Reference strength

The reference strength was determined individually for each plank, and the loading was relative to this plank strength. This procedure was chosen because a study reported in (Clorius, Pedersen, Hoffmeyer & Damkilde 1999) showed the variation between planks to be larger than the variation within planks. In Table 9.2 the mean strengths per shear plane for the dowel type connections are given at the two levels of RH. As were the case for the small specimens increased moisture content does not entail any significant strength reduction. Failures obtained were all tension splitting failures perpendicular to the grain.

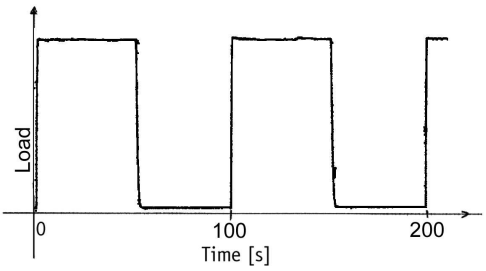

Figure 9.3: *Load versus time plot for a 0.01 Hz joint specimen.*

		Density, ρ_{12}		F_{ult}	
	n	mean	stdev	mean	stdev
65 % RH	16	473	32	3.86	0.44
85 % RH	8	457	23	3.68	0.34

Table 9.2: *Density, [kg/m^3], ultimate strength pr. shear plane, [kN], of specimens taken to failure in 4-point bending at 65% RH or 85% RH.*

9.2.2 Fatigue results

The splitting failures developed gradually during the fatigue life, in Figure 9.4 a typical tension splitting failure is shown. In Figures 9.5 and 9.6 log normal probability ranking of the test results at the four test conditions are shown. In Table 9.3 the 50-percentile estimates of $log(TUL)$ and $log(NOC)$ and standard deviation determined by use of the lower tail of the distributions are given.

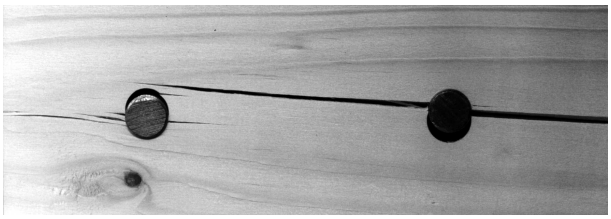

Figure 9.4: *Tension splitting failure perpendicular to the grain in joint.*

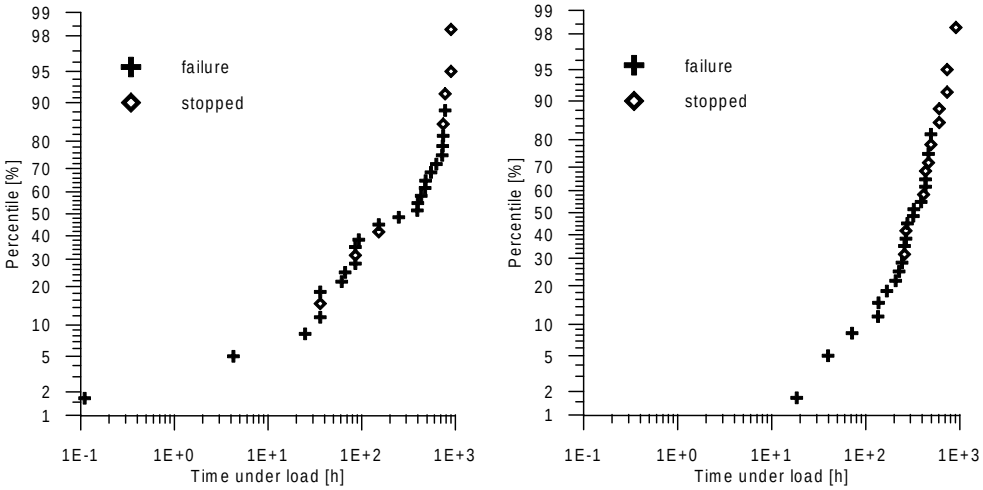

(a) 65/75/0.1 (b) 65/75/0.01

Figure 9.5: *Log normal probability ranking of failures.*

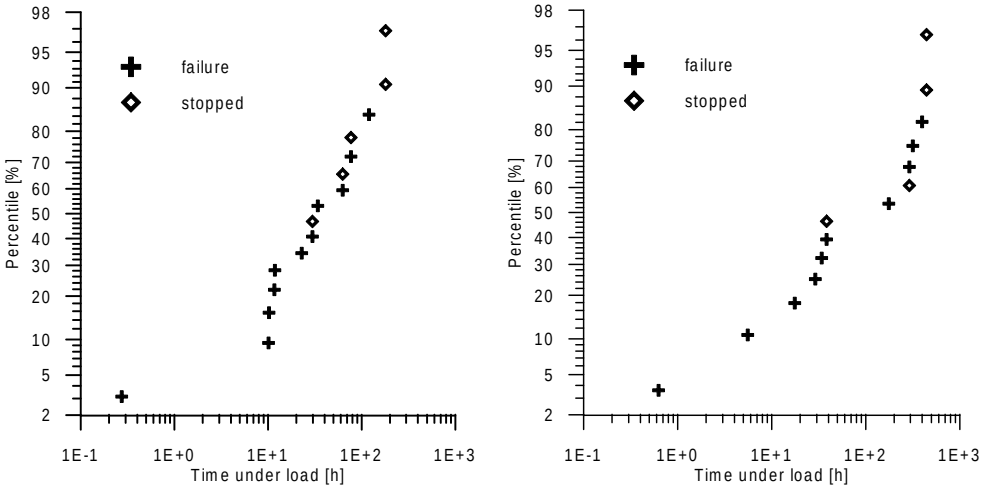

(a) 85/75/0.1 (b) 85/75/0.01

Figure 9.6: *Log normal probability ranking of failures.*

Conditions				50-percentile of $log(TUL)$ and $log(NOC)$		
RH	SL	FQ	n	$log(TUL)_{50\%}$	$log(NOC)_{50\%}$	$s_{50\%}$
65	75	0.1	32	2.19	5.05	1.24
65	75	0.01	32	2.45	4.31	0.36
85	75	0.1	16	1.46	4.32	0.86
85	75	0.01	16	1.82	3.68	1.07

Table 9.3: *50-percentile of log(TUL) and log(NOC) and corresponding standard deviations.*

Conditions			50-percentile		SAS-LIFEREG	
RH	SL	FQ	$log(TUL)_{50\%}$	$s_{log(TUL)_{50\%}}$	$\overline{log(TUL)}$	$s_{log(TUL)}$
65	75	0.1	2.19	1.24	2.37	0.96
65	75	0.01	2.45	0.36	2.59	0.51
85	75	0.1	1.46	0.86	1.65	0.87
85	75	0.01	1.82	1.07	2.03	1.03

Table 9.4: *Mean and standard deviation of log(TUL).*

9.3 Discussion

Due to the test termination prior to failure of all tested specimens the fatigue data are treated as right censored data and estimates of mean $log(TUL)$ are made by use of the SAS-LIFEREG procedure described in Chapter 7. The SAS estimates are made for each set of conditions individually. In Table 9.4 the SAS estimates are given along with 50-percentile estimates. In Figure 9.7 the individual SAS estimates of mean $log(TUL)$ and $log(NOC)$ are given as function of test frequency, and SAS regressions at both levels of RH are shown. For tests at 65% RH the regression in TUL is:

$$log(TUL) = 1.99 - 0.34log(FQ) + 0.79\epsilon \tag{9.1}$$

The corresponding regression for tests at 85% RH is:

$$log(TUL) = 1.33 - 0.34log(FQ) + 0.95\epsilon \tag{9.2}$$

It is observed that the influence of FQ is the same at both levels of RH, this is not the case when comparing the individual estimates at the two levels of RH in Table 9.4.

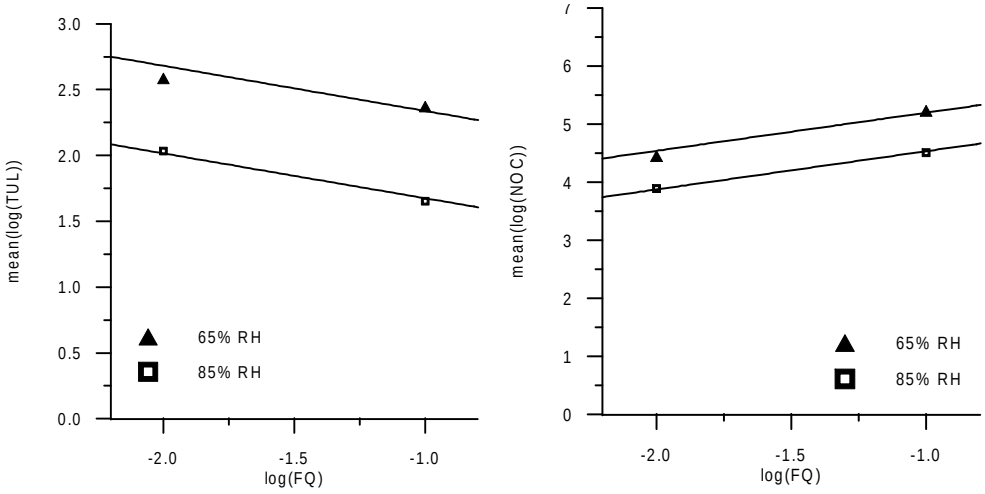

(a) Time under load (b) Number of cycles

Figure 9.7: *$log(NOC)$ and $log(TUL)$ estimates in dependency of $log(FQ)$.*

However, the regression in SAS assumes a common standard deviation at both frequencies and this moves the centre of the distribution. For increased RH a decrease in $log(TUL)$ is observed. The fatigue behaviour of the connectors does not follow the trends observed for the small tension specimens:

- At both levels of RH interaction between NOC and TUL is observed, for the small specimens the RH 65% tests were only governed by NOC.
- The influence of TUL is more pronounced for the connector specimens than for the small specimens.
- The connector specimens survive longer even though they are loaded at a higher stress level than the small specimens, SL 75% compared to SL 65%.

The connector specimens differ from the small tension specimens as the former have stress singularities close to the dowel holes. If the material is able to redistribute the stresses over time this may explain the longer lives met. The larger influence of TUL in the failure explanation of the connector specimens compared to the small clear specimens and the equal influence at both levels of RH is however not explained by stress redistribution. The observed difference in fatigue behaviour between the small clear specimens and the

connector specimens does not make it possible to extrapolate directly from the small clear tests to the tested connectors.

Chapter 10

Conclusion

Small clear specimens have been taken to failure in fatigue loading perpendicular to the grain at stress levels of 50% and 65% of the short term strength and at frequencies of loading ranging from 1 Hz to 0.01 Hz and at dead load condition. Square wave load shape was used. The specimens were tested with a moisture content in equilibrium with either 65% or 85% relative humidity. The test was designed as a block test using material from 10 different planks in test series of 10 specimens. In total approximately 300 small specimens were tested.

A special test specimen was designed to ensure failure at the free length of the specimen. The specimens were cut from planks consisting of two boards glued together sapwood to sapwood forming a symmetrical cross section with the weak radial section in the centre. In the fatigue testing most failures were regular wood failures but some specimens failed in interface failures and some were terminated prior to failure. Statistically interface failures and test termination are treated as right censored data.

Mean value of number of cycles and time under load to failure could be estimated from the 50-percentile of the failure distribution. However, in order to utilize all data obtained a likelihood procedure was used to estimate means by use of all data including the right censored data. It was assumed that the failure distribution was log normal and the assumption was confirmed by an analysis of residuals.

The objective of the investigation was to search for an interaction between number of cycles and time under load to failure. Such an interaction corresponds to frequency dependent fatigue. The trends of the logarithmically transformed data were investigated by use of linear regressions including the above mentioned likelihood procedure. With respect to the specimens tested at RH 65% it is observed that:

- Number of cycles to failure depends only on stress level and is invariant to frequency.

- At a stress level of 50% of the short term strength the mean number of cycles to failure is in the order 1 10^6 at a frequency of 0.1 Hz.

- At a stress level of 65% of the short term strength the mean number of cycles to failure is in the order 2 10^4 at frequencies ranging from 1 Hz to 0.01 Hz.

With respect to the specimens tested at RH 85% it is observed that:

- Number of cycles to failure is highly influenced by frequency corresponding to interaction between number of cycles and time under load to failure.

- At a stress level of 50% of the short term strength the mean number of cycles to failure is in the order:

  - 3 10^5 at 1 Hz
  - 5 10^4 at 0.1 Hz
  - 2 10^4 at 0.01 Hz

- At a stress level of 65% of the short term strength the mean number of cycles to failure is in the order:

  - 1 10^4 at 1 Hz
  - 5 10^3 at 0.1 Hz
  - 2 10^3 at 0.01 Hz

In the literature wood fatigue has been attempted modelled by either number of cycles or by duration of load, the experimental observations laid forward have the following consequences for fatigue modelling:

- Wöhler curves, i.e. design diagrams giving number of cycles to failure at a given stress level, cannot be used to quantify wood fatigue independent of the loading frequency.

- Damage accumulation laws, which assumes the damage rate to be only time dependent, cannot adequately model wood fatigue as fatigue damage is also a function of the number of cycles.

A model comprising both a time dependent term and a term related to the number of load oscillations is offered by the theory of wood as a damaged viscoelastic material, the DVM theory. A brief summary of the theory is given in Chapter 2. Essentially the DVM theory predicts a frequency range where failure is governed by interaction between number of cycles and time under load. Above the frequency range failure is due to number of cycles and below due to time under load. By use of model parameters suggested by Fuglsang Nielsen (2000*b*) the model predicts the same order of magnitude of number of cycles to failure as found from the tests. Further it is observed that:

- The tests at RH 85% are correctly predicted to be in the frequency range with interaction.
- The model prediction at RH 65% gives too much weight to the time dependent damage, this can partially be overcomed by increasing the creep doubling time in the model, hereby suppressing the time dependency in the failure explanation.

Double shear dowel type connections have been tested in fatigue bending. The failure mode was tension splitting perpendicular to the grain. A total of 96 specimens were tested at a stress level of 75%, at RH 65% and 85% and at frequencies of 0.01 Hz and 0.1 Hz. The connector specimens exhibit a larger influence of time under load than observed for the small specimens, and the influence of time under load is present at both levels of RH. Though fatigue tested at a higher stress level the connector specimens survive longer than the small specimens. Due to these differences it is not possible to use the results from the small specimens to predict the behaviour of the connector specimens. As the test conditions were better controlled for the small specimens than for the connector specimens the former yields the most reliable results. It is therefore still the hope to be able to predict the tension perpendicular to grain fatigue behaviour of complex design details by knowledge of stress level, load frequency, moisture content and basic knowledge from uniaxial fatigue testing.

Bibliography

Aicher, S., Dill-Langer, G. & Ranta-Maunus, A. (1998), 'Duration of load effect in tension perpendicular to the grain of glulam in different climates', *Holz als Roh- und Werkstoff* **56**, 295–305.

Ansell, M. P. (1987), Laymans guide to fatigue, *in* J. M. Galt, ed., 'Wind Energy Conversion 1987', Mechanical Engineering Publications Ltd., pp. 39–54.

Ansell, M. P. (1995), Fatigue design for timber and wood-based materials, step lecture E22, *in* H. J. Blass et al., ed., 'Timber Engineering STEP 2', Centrum Hout, pp. E22/1–E22/8.

Bach, L. (1967), Static fatigue of wood under constant strain, Information Report VP-X-24, Canadian Forest Prod. Lab., Vancouver B.C., Canada.

Bach, L. (1973), 'Reiner-Weisenberg's theory applied to time-dependent fracture of wood subjected to various modes of mechanical loading', *Wood Science* **5**(3), 161–171.

Bach, L. (1975), Frequency-Dependent Fracture in Wood under Pulsating Loading, *in* 'FPRS-Annual meeting Proceedings, June 15, 1975', Portland, Oregon, USA.

Barrett, J. O. & Foschi, R. O. (1978*a*), 'Duration of load and probability of failure in wood. PartI. Modelling creep rupture.', *Canadian Journal of Civil Engineering* **5**(4), 505–514.

Barrett, J. O. & Foschi, R. O. (1978*b*), 'Duration of load and probability of failure in wood. PartII. Constant, ramp and cyclic loadings', *Canadian Journal of Civil Engineering* **5**(4), 515–532.

Bohannan, B. & Kanvik, K. (1969), Fatigue Strength of Finger Joints, Research Paper FPL 114, U.S.D.A. Forest Service, U.S. Department of Agriculture, Forest Service, Madison, Wis., USA.

Bonfield, P. W. (1991), Fatigue evaluation of wood laminates for the design of wind turbine blades, PhD thesis, University of Bath.

Bonfield, P. W. & Ansell, M. P. (1991), 'The fatigue properties of wood in tension, compression and shear', *Journal of Materials Science* **26**, 4765–4773.

Bonfield, P. W., Ansell, M. P. & Dinwoodie, J. M. (1994), Fatigue testing of wood, A detailed guide for the development of life prediction formulae from fatigue data, *in* 'Proceedings of IUFRO S5.02, International Timber Engineering Conference', Sidney, Australia, pp. 163–174.

Bordonné, P.-A., Okuyama, T. & Marsoem, S. N. (1987), 'Mechanical Responses of Wood to Repeated Loading III', *Mokuzai Gakkaishi, Journal of the Japan Wood Research Society* **33**(8), 623–629.

Cai, Z., Bradtmueller, J. P., Hunt, M. O., Fridley, K. J. & Rosowsky, D. V. (1996), 'Fatigue Behaviour of OSB in Shear', *Forest Products Journal* **46**(10), 81–86.

Chaplain, M., Fournely, E. & Vergne, A. (1996), Prévision de la durée de vie d'assemblagees boulonnées de structures en bois sous chargements sévères, Annales GC Bois, Vol 1 1.

Chaplain, M., Valentin, G. & Fournely, E. (1999), Lifetime of Wood Joints: Fracture Mechanics and Damage Modelling, *in* B. Walford, ed., 'Pacific Timber Engineering Conference, Rotorua, New Zealand March 1999', pp. 414–421.

Clorius, C. O., Pedersen, M. U., Hoffmeyer, P. & Damkilde, L. (1999), Fatigue, Research Report Wooden Bridges – Phase 2, Subproject 2.3 Fatigue, Nordic Wood, Nordic Timber Council AB, Stockholm.

Clorius, C. O., Pedersen, M. U., Hoffmeyer, P. & Damkilde, L. (2000), 'Compressive Fatigue in Wood.', *Wood Science and Technology* **34**, 21–37.

Cox, D. R. & Oakes, D. (1984), *Analysis of survival data*, Chapman and Hall, London, England.

Dugdale, D. S. (1960), 'Yielding of steel sheets containing slits', *J. Mechanical Physics Solids* **8**(11), 100–104.

EC5-2 (1997), Eurocode 5 – Design of timber structures – Part 2: Bridges, Preliminary building code prENV 1995-2, European Committee for Standardization.

Foschi, R. O. & Yao, Z. C. (1986), Another look at three duration of load models, *in* '19th. CIB/W18 meeting Florence, Italy', pp. CIB–W18/19–9–1.

Fuglsang Nielsen, L. (2000*a*), 'Lifetime and residual strength of wood subjected to static and variable load. part i: Introduction and analysis', *Holz als Roh- und Werkstof* **58**, 81–90.

Fuglsang Nielsen, L. (2000*b*), 'Lifetime and residual strength of wood subjected to static and variable load. part ii: Applications and design', *Holz als Roh- und Werkstof* **58**(3), 141–152.

Gerhards, C. C. & Link, C. L. (1986), 'Effect of loading rate on bending strength of Douglas-fir 2 by 4's', *Forest Products Journal* **36**(2), 63–66.

Gustafsson, P. J. (1995), Notched beams and holes in glulam beams B5, *in* H. J. Blass et al., ed., 'Timber Engineering STEP 1', Centrum Hout, pp. B5/1–B5/9.

Gustafsson, P. J., Hoffmeyer, P. & Valentin, G. (1998), 'Dol behaviour of end-notched beams', *Holz als Roh- und Werkstoff* **56**, 307–317.

Imayama, N. & Matsumuto, T. (1970), 'Studies on the Fatigue of Wood I. Phenomenal Study on the Fatigue Process', *Mokuzai Gakkaishi, Journal of the Japan Wood Research Society* **16**, 319–325.

Imayama, N. & Matsumuto, T. (1974), 'Studies on the Fatigue of Wood II. On the Temperature-rise Generated with Fatigue', *Mokuzai Gakkaishi, Journal of the Japan Wood Research Society* **20**, 53–62.

Isaksson, T. (1999), Modelling the Variability of Bending Strength in Structural Timber, Length and Load Configuration Effects, PhD thesis, Lund Institute of Technology.

Jorissen, A. (1998), Double shear timber connections with dowel type fasteners, PhD thesis, Delft University.

Källsner, B. & Ditlevsen, O. (1994), Lengthwise bending strength variation of structural timber, *in* P. Hoffmeyer, ed., 'IUFRO/S5.02 Timber Engineering Meeting, Sydney, Australia July 1994', Building Materials Laboratory, DTU, Denmark, pp. 333–352.

Kitahara, R., Tsutsumi, J. & Matsumoto, T. (1981), 'Observations on Cell Wall Response and Mechanical Behaviour in Wood Subjected to Repeated Static Bending Load', *Mokuzai Gakkaishi, Journal of the Japan Wood Research Society* **27**(1), 1–7.

Kohara, M., Kanayama, K., Nakai, A., Nagata, K. & Okuyama, T. (1997), 'Damages in Wood Beams Caused by Fatigue under Pulsating Loads', *Mokuzai Gakkaishi, Journal of the Japan Wood Research Society* **43**(11), 909–915.

Küch, W. (1939), 'Untersuchungen an Holz, Sperrholz und Schichthölzern im Hinblick auf ihre Verwendung im Flugzeugbau', *Holz als Roh- und Werkstoff* **2**(7/8), 257–272.

Küch, W. (1942), 'Zeit- und Dauerfestigkeit von Lagernhölzern', *Holz als Roh- und Werkstof* **5**(2/3), 69–73.

Liu, J. Y. & Ross, R. J. (1995), Energy criterion for fatigue strength of wood structural members, *in* 'Proceedings of the 1995 ASME meeting, Mechanics of Cellulosic Materials, Los Angeles', Vol. AMD 209/MD 60, pp. 125–133.

Liu, J. Y., Zahn, J. J. & Schaffer, E. L. (1994), 'Reaction rate model for the fatigue strength of wood', *Wood and Fiber Science* **26**(1), 3–10.

Madsen, B. (1992), *Structural Behaviour of Timber*, 1th edn, Timber Engineering ltd., Vancouver, Canada.

Mohr, B. (1996), Fatigue of Structural Timber, *in* S. Aicher, ed., 'Proceedings of the 1996 International Conference on Wood Mechanics, Stuttgart, Germany, May 14–16, 1996', pp. 217–225.

Nielsen, L. F. (1979), Crack Failure of Dead-, Ramp-, and Combined Loaded Viscoelastic Materials, *in* 'Proc. First Int. Conf. on Wood Fracture, Banff, Alberta, Canada, august 1978', pp. 187–200.

Nielsen, L. F. (1986), Elastic fatigue of wood and other building materials, Technical Report 170A, Building Mat. Lab., Technical University of Denmark.

Nielsen, L. F. (1996), Lifetime and residual strength of wood subjected to static and variable load, Technical Report R-6, Department of Structural Engineering and Materials, Technical University of Denmark.

Norlin, L. P., Norlin, C. M. & Lam, F. (1999), 'Shear behaviour of laminated Douglas fir veneer', *Wood Science and Technology* **33**, 199–208.

Okuyama, T., Itoh, A. & Marsoem, S. N. (1984), 'Mechanical Response of Wood to Repeated Loading I. Tensile and compressive fatigue fractures', *Mokuzai Gakkaishi, Journal of the Japan Wood Research Society* **30**(10), 791–798.

Pedersen, M. U., Clorius, C. O., Damkilde, L. & Hoffmeyer, P. (1999), 'Strength of Glued-In Bolts after Full-Scale Loading', *ASCE, Journal of Performance of Constructed Facilities* **13**(3), 107–113.

Pedersen, M. U., Clorius, C. O., Damkilde, L. & Hoffmeyer, P. (2000), 'A Simple Size Effect Model for Tension Perpendicular to the Grain', *Accepted for publication in: Wood Science and Technology.*

Philpot, T. A., Fridley, K. J. & Rosowsky, D. V. (1994), 'Energy-based failure criterion for wood', *Journal of Materials in Civil Engineering, ASCE* **6**(4), 578–594.

Reiner, M. & Weisenberg, K. (1939), 'A thermodynamic theory of the strength of materials', *Rheological leaflet.*

Rice, J. R. (1967), 'Mechanics of crack tip deformation and extension by fatigue, fatigue crack propagation', *ASTM STP* (415), 247–311.

Rose, G. (1965), 'Das mechanishe Verhalten des Kiefernholzes bei dynamisher Dauerbeanspruchung in abhngigkeit von Belastungsart, Belastungsgrösse, Feuchtigkeit und Temperatur', *Holz als Roh- und Werkstof* **23**(7), 271–284.

SAS Institute (1994), *SAS/STAT User's Guide, Vol. 2, GLM-VARCOM*, SAS Institute, Cary, NC, USA.

Thompson, R. J., Bonfield, P. W., Dinwoodie, J. M. & Ansell, M. P. (1996), 'Fatigue and creep in chipboard. Part 3. The effect of frequency', *Wood Science and Technology* **30**, 293–305.

Appendix A

Fatigue results

Series S13 RH=65 % SL=65 % FQ=1 Hz			
Specimen [id]	Time under load [h]	Number of cycles	Failure mode
b9iii9	0.10	722	m
a14iii8	0.13	924	m
a8i4	0.39	2824	m
b13i7	0.46	3317	m
c9iii8	0.65	4703	m
c1iii6	0.85	6113	m
b15i10	2.29	16511	i
a5iii10	2.56	18435	m
c8i6	2.65	19079	i
b19iii8	21.88	157562	s

Table A.1: *Fatigue results S13, 65/65/1*

Series S14 RH=65 % SL=65 % FQ=1 Hz			
Specimen [id]	Time under load [h]	Number of cycles	Failure mode
c8iii9	0.45	3266	m
c1iii4	0.62	4443	m
a14iii7	0.87	6272	m
b15iii4	1.87	13494	m
b9iii10	4.20	30228	m
b19iii9	12.00	86411	m
a8iii8	13.37	96268	m
b13i8	15.62	112471	s
c9i6	23.12	166441	m
a5iii19	26.37	189850	s

Table A.2: *Fatigue results S14, 65/65/1*

Series S1 RH=65 % SL=65 % FQ=0.1 Hz			
Specimen [id]	Time under load [h]	Number of cycles	Failure mode
C1III10	0.71	511	m
A14III4	2.79	2009	m
A8III9	3.87	2783	i
B15III3	4.52	3251	m
A5III4	4.80	3452	m
B13III9	12.34	8881	i
B19III7	12.34	8881	m
C8III4	20.17	14522	i
C9III5	51.89	37361	s
B9III7	51.90	37364	s

Table A.3: *Fatigue results S1, 65/65/0.1*

Series S4 RH=65 % SL=65 % FQ=0.1 Hz			
Specimen [id]	Time under load [h]	Number of cycles	Failure mode
c9i7	0.25	180	m
a14iii9	0.95	688	m
b15iii12	1.10	792	i
b19iii5	1.18	846	m
b9i7	3.38	2430	m
c1i6	4.45	3200	i
c8iii3	7.53	5425	i
a8iii7	16.06	11560	m
a5i10	82.46	59368	m
b13iii6	86.18	62046	m

Table A.4: *Fatigue results S4, 65/65/0.1*

Series S5	RH=65 %	SL=65 %	FQ=0.1 Hz
Specimen [id]	Time under load [h]	Number of cycles	Failure mode
c8iii2	4.74	3409	m
c9i3	6.96	5011	m
b9iii5	7.20	5188	m
b13iii12	8.65	6228	m
a5i11	14.23	10246	m
c1iii9	20.43	14713	m
a14iii3	27.63	19894	m
b15iii8	154.66	111355	m
a8i3	174.97	125978	m
b19i6	302.07	217490	s

Table A.5: *Fatigue results S5, 65/65/0.1*

Series S6	RH=65 %	SL=65 %	FQ=0.01 Hz
Specimen [id]	Time under load [h]	Number of cycles	Failure mode
a14iii10	8.08	581	m
c9iii4	101.98	7342	i
c8i5	165.37	11907	i
b19iii3	168.46	12129	m
c1i9	176.78	12728	i
b13iii10	179.40	12917	m
b9iii8	191.70	13802	m
b15iii5	291.17	20965	i
a8i8	291.37	20979	i
a5i9	359.04	25851	s

Table A.6: *Fatigue results S6, 65/65/0.01*

Series S8	RH=65 %	SL=65 %	FQ=0.01 Hz
Specimen [id]	Time under load [h]	Number of cycles	Failure mode
c8iii7	2.32	167	i
b19i7	3.78	273	i
c1iii8	27.42	1974	m
b15i12	57.33	4127	m
a14i10	65.61	4724	m
b13iii4	166.18	11965	m
c9i4	170.66	12288	i
a5i13	488.33	35160	m
a8iii2	672.90	48449	m
b9iii11	1099.67	79176	m

Table A.7: *Fatigue results S8, 65/65/0.01*

Series S9	RH=65 %	SL=65 %	FQ=0.01 Hz
Specimen [id]	Time under load [h]	Number of cycles	Failure mode
c1i10	12.76	918	m
c9i5	74.66	5376	i
b13iii8	122.81	8842	m
a8iii4	158.79	11433	m
b19iii2	161.03	11594	m
b15i13	170.51	12276	m
b9iii4	175.66	12648	m
c8i4	203.78	14672	i
a14i11	296.14	21322	i
a5iii7	898.88	64719	s

Table A.8: *Fatigue results S9, 65/65/0.01*

Series S12 RH=65 % SL=65 % FQ=0.01 Hz			
Specimen [id]	Time under load [h]	Number of cycles	Failure mode
c9iii10	1.02	73	m
c1i8	21.44	1544	m
b15iii10	104.94	7555	m
b13iii5	106.20	7646	m
a5iii5	134.28	9668	m
c8iii8	140.89	10144	m
b9i5	151.75	10926	m
a8iii3	286.35	20617	m
b19i10	402.99	29015	m
a14i14	420.94	30308	s

Table A.9: *Fatigue results S12, 65/65/0.01*

Series S15 RH=65 % SL=65 % FQ=deadload			
Specimen [id]	Time under load [h]	Number of cycles	Failure mode
a14i8	701.04	-	i
c8i2	1155.20	-	i
b13i9	1506.23	-	s
a5i4	1506.22	-	s
b9i9	1506.21	-	s
c1iii5	1506.20	-	s
b19i4	1506.19	-	s
c1i3	1506.20	-	s
a8i5	1506.18	-	s
b15iii67	1506.18	-	s

Table A.10: *Fatigue results S15, 65/65/deadload*

Series S16 RH=65 % SL=65 % FQ=deadload			
Specimen [id]	Time under load [h]	Number of cycles	Failure mode
B19i11	432	-	s
C1iii12	432	-	s
A5i3	432	-	s
B15i11	432	-	s
C8iii10	432	-	s
A5i6	432	-	s
A14i7	432	-	s
B13iii11	432	-	s
B15i7	432	-	s
B9i2	432	-	s

Table A.11: *Fatigue results S16, 65/65/deadload*

Series S7 RH=65 % SL=50 % FQ=0.1 Hz			
Specimen [id]	Time under load [h]	Number of cycles	Failure mode
c9iii9	43.76	31511	m
a14i15	82.81	59623	m
b19iii10	814.09	586141	m
c1iii3	892.47	642578	i
a8iii11	941.34	677761	i
b9iii3	1060.18	763330	m
c8iii5	1081.74	778853	i
b13iii3	1828.44	1316473	m
a5iii8	1828.44	1316477	s
b15iii2	1828.44	1316477	s

Table A.12: *Fatigue results S7, 65/50/0.1*

Series S14 RH=85 % SL=50 % FQ=1 Hz			
Specimen [id]	Time under load [h]	Number of cycles	Failure mode
C9iv7	0.29	2079	m
C8iv10	1.01	7248	m
A5iv9	29.96	215699	m
B19ii7	40.05	288389	m
A14ii14	45.41	326919	m
C1iv11	49.95	359617	i
B13iv7	69.44	499983	s
b9iv8	79.69	573792	m
B15iv4*	92.17	663624	i
A8iv8	97.04	698682	s

Table A.13: *Fatigue results S14, 85/50/1*

Series S15 RH=85 % SL=50 % FQ=1 Hz			
Specimen [id]	Time under load [h]	Number of cycles	Failure mode
B15ii13	0.89	6383	i
A14iv3	4.18	30119	m
A5ii9	6.70	48219	m
C8iv9	7.00	50397	m
B9ii12	13.15	94688	m
C9iv8	35.37	254679	m
C1iv7	39.83	286758	i
B13iv8	50.33	362362	m
B19ii12	95.10	684690	s
A8ii1	120.11	864760	s

Table A.14: *Fatigue results S15, 85/50/1*

Series S1 RH=85 % SL=50 % FQ=0.1 Hz			
Specimen [id]	Time under load [h]	Number of cycles	Failure mode
a5ii4	25.82	18590	m
c8ii6	31.53	22702	m
c1ii8	49.79	35849	m
a14ii1	62.87	45266	m
a8ii6	78.81	56740	m
c9ii8	83.58	60178	m
b19ii4	84.37	60743	m
b15ii3	153.84	110768	i
b13ii7	164.35	118332	m
b9ii5	167.11	120319	m

Table A.15: *Fatigue results S1, 85/50/0.1*

Series S3 RH=85 % SL=50 % FQ=0.1 Hz			
Specimen [id]	Time under load [h]	Number of cycles	Failure mode
c1ii9	1.41	1015	m
c8ii3	15.34	11048	m
c9ii3	19.88	14317	m
b13ii12	21.66	15592	m
a14ii11	27.89	20081	m
b19ii5	35.24	25376	m
a5ii6	104.08	74941	m
b9ii3	172.56	124243	m
a8ii8	380.98	274306	s
b15ii1	380.99	274309	s

Table A.16: *Fatigue results S3, 85/50/0.1*

Series S2	RH=85 %	SL=50 %	FQ=0.01 Hz
Specimen [id]	Time under load [h]	Number of cycles	Failure mode
b13ii6	46.90	3377	m
a14ii5	56.44	4064	m
c1ii7	59.66	4296	m
c9ii4	86.37	6219	m
a5ii2	97.31	7006	m
b15ii9	117.76	8479	m
c8ii11	143.74	10349	m
b19ii3	187.07	13469	m
b9ii11	204.31	14710	m
a8ii4	216.61	15596	m

Table A.17: *Fatigue results S2, 85/50/0.01*

Series S4	RH=85 %	SL=50 %	FQ=0.01 Hz
Specimen [id]	Time under load [h]	Number of cycles	Failure mode
a8iv11	2.29	165	i
a14iv8	72.08	5190	m
c8iv6	199.26	14347	m
a5iv4	452.96	32613	m
b13iv2	505.55	36400	i
b19iv9	591.43	42583	i
c9iv1	721.04	51915	i
b15iv7	803.45	57848	i
c1iv10	922.15	66395	s
b9iv3	922.16	66395	s

Table A.18: *Fatigue results S4, 85/50/0.01*

Series S11 RH=85 % SL=65 % FQ=1 Hz			
Specimen [id]	Time under load [h]	Number of cycles	Failure mode
A14iv4	0.07	525	m
B13ii1	0.10	701	m
C1iv4	0.11	813	m
A5iv3	0.44	3190	m
b9ii7	0.49	3549	m
C8iv2	0.64	4596	m
C9iv4	1.52	10974	m
B19iv6	2.57	18527	m
B15ii7	5.06	36417	m
A8ii3	6.54	47100	m

Table A.19: *Fatigue results S11, 85/65/1*

Series S13 RH=85 % SL=65 % FQ=1 Hz			
Specimen [id]	Time under load [h]	Number of cycles	Failure mode
C1ii6	0.03	230	m
A14ii6	0.56	4067	m
A5iv8	0.98	7054	m
A8ii11	2.79	20084	m
C9ii6	3.54	25466	m
B15iv8	3.74	26946	m
C8ii8	3.93	28277	m
B19ii8	9.69	69772	m
B13ii4	13.05	93982	m
b9iv7	13.55	97590	m

Table A.20: *Fatigue results S13, 85/65/1*

Series S16 RH=85 % SL=65 % FQ=1 Hz			
Specimen [id]	Time under load [h]	Number of cycles	Failure mode
C9ii5	0.21	1511	i
A14iv2	0.50	3599	m
C8iv3	1.56	11199	m
B15ii8	1.59	11450	m
B13ii11	1.83	13195	m
A5iv7	1.92	13837	m
B19iv1	4.08	29395	m
B9ii8	5.52	39742	m
C1ii5	7.18	51688	m
A8ii5	11.99	86312	m

Table A.21: *Fatigue results S16, 85/65/1*

Series S17 RH=85 % SL=65 % FQ=0.1 Hz			
Specimen [id]	Time under load [h]	Number of cycles	Failure mode
B13ii9	0.21	153	m
C8ii1	0.28	198	m
A8ii7	0.31	224	m
C1ii1	0.58	418	m
C8iv7	1.49	1073	m
A14iv9	2.08	1500	m
B15ii12	3.85	2773	m
B9ii9	4.00	2878	i
A5iv1	14.19	10216	m
B19ii9	36.20	26066	m

Table A.22: *Fatigue results S17, 85/65/0.1*

Series S7 RH=85 % SL=65 % FQ=0.1 Hz			
Specimen [id]	Time under load [h]	Number of cycles	Failure mode
c9iv6	0.42	302	m
c1ii11	0.78	565	m
a14iv6	4.84	3485	m
a5ii3	20.59	14821	m
a8ii12	21.74	15653	m
c8ii9	23.88	17194	m
b15iv9	25.66	18475	i
b19iv11	27.92	20102	i
b9iv2	36.11	25999	m
b13iv10	64.61	46519	m

Table A.23: *Fatigue results S7, 85/65/0.1*

Series S8 RH=85 % SL=65 % FQ=0.1 Hz			
Specimen [id]	Time under load [h]	Number of cycles	Failure mode
c9ii1	1.80	1292	m
c8ii1	2.20	1584	m
a14ii12	4.68	3370	m
c1iv2	7.65	5512	m
b15iv10	8.27	5954	m
b13ii8	11.86	8539	m
b19iv10	18.95	13644	m
a5iv8	21.92	15786	m
b9ii4	22.95	16528	m
a8ii6	35.02	25214	s

Table A.24: *Fatigue results S8, 85/65/0.1*

Series S5 RH=85 % SL=65 % FQ=0.01 Hz			
Specimen [id]	Time under load [h]	Number of cycles	Failure mode
a14iv1	3.68	265	m
c8ii5	5.95	428	m
c9iv2	7.03	507	m
b19ii1	7.43	535	m
c1iv3	13.18	949	m
a5ii11	17.72	1276	m
b13iv11	28.09	2022	m
a8ii5	35.92	2586	i
b9iv9	48.51	3493	m
b15iv3	235.17	16933	i

Table A.25: *Fatigue results S5, 85/65/0.01*

Series S6 RH=85 % SL=65 % FQ=0.01 Hz			
Specimen [id]	Time under load [h]	Number of cycles	Failure mode
a8iv6	0.28	21	m
c1ii3	6.80	490	m
c8ii4	9.46	681	m
a14iv10	22.01	1585	m
b19ii6	25.47	1834	m
b13iv1	38.05	2739	m
b15ii5	49.26	3546	m
b9ii1	58.45	4208	m
c9ii9	77.84	5604	m
a5ii8	84.63	6093	s

Table A.26: *Fatigue results S6, 85/65/0.01*

Series S9 RH=85 % SL=65 % FQ=deadload			
Specimen [id]	Time under load [h]	Number of cycles	Failure mode
c9iv3	51.11	-	m
c8iv4	74.64	-	m
a14ii8	106.90	-	m
b9ii13	162.19	-	m
b13iv3	931.35	-	i
c1iv1	1253.61	-	i
b19iv2	1355.32	-	i
a8iv7	1442.05	-	i
a5iv6	3883.14	-	s
b15ii11	3883.14	-	s

Table A.27: *Fatigue results S9, 85/65/deadload*

Series S10 RH=85 % SL=65 % FQ=deadload			
Specimen [id]	Time under load [h]	Number of cycles	Failure mode
a8iv3	0.10	-	m
c1iv6	29.93	-	m
c9ii7	155.76	-	m
c8iv1	215.10	-	m
a5ii5	363.54	-	m
b13ii5	374.74	-	m
b9iv11	391.84	-	m
b15ii4	712.69	-	i
a14ii4	1318.60	-	i
b19i4	3055.46	-	i

Table A.28: *Fatigue results S10, 85/65/deadload*

Series S12 RH=85 % SL=65 % FQ=deadload			
Specimen [id]	Time under load [h]	Number of cycles	Failure mode
C8ii7	628.29	-	m
A8iv4	650.62	-	m
C9iv5	779.37	-	i
B9iv1	825.05	-	i
A14ii9	1391.73	-	i
B13ii8	2416.57	-	i
B15iv2	2888.61	-	i
C1ii4	3693.01	-	i
A5ii7	4040.21	-	i
B19iv8	4679.58	-	s

Table A.29: *Fatigue results S12, 85/65/deadload*

Appendix B

SAS LIFEREG

The regression analysis are made by use of the SAS LIFEREG procedure. An input exsample is given in Part B.1. The input contains a card on all relevant information on the specimens, i.e. series, board, SL, RH, FQ and $log(FQ)$, as well as TUL and NOC. A $ indicates if the variable is a class or regression parameter. Failure mode is given and the censor status is indicated with a 0 for all right censored data, i.e. all specimens failed in interface failures and all specimens not failed at test termination, and 1 for non censored data corresponding to failures in the middle of the specimens. The example includes various model commands such as:

```
model TUL*censor(0)= logFQ SL /dist=lnormal
```

This command invokes a regression analysis of TUL as function of $log(FQ)$ and SL. The censored data are included by means of the likelihood procedure and the data are assumed log normal distributed. The example also includes models where the plank reference strength, `Plankstrength`, is included as a regression variable.

Resulting regressions are shown for the core analysis in Part B.2 to B.6, for models with dependent variable TUL and independent variables $log(FQ)$ and SL. SAS uses the natural logarithm in the logarithmic transformation of the data. In all examples given the resulting model is shown both in ln and in $log = log_{10}$ as it is the latter form which is used throughout the fatigue discussion.

B.1 SAS input example

```
data fatigue;
input
Serie $ Board $ Specimen $ SL RH logFQ NOC TUL Failure$
Censor Plankstrength FQ;

cards;
 s1   c8   c8ii6   50  85  -1  22702   31.53   m  1  2.45  0.1
 s1   a14  a14ii1  50  85  -1  45266   62.87   m  1  2.21  0.1
 .
 .
 s15  a8   A8ii1   50  85  0   864760  120.11  s  0  1.92  1
 .
 .
 .
 s17  a8   A8ii7   65  85  -1  224     0.31    m  1  1.92  0.1
 s17  b9   B9ii9   65  85  -1  2878    4.00    i  0  2.12  0.1
;
run;

proc lifereg outest=fit;
model NOC*censor(0)= logFQ SL /dist=lnormal;
model TUL*censor(0)= logFQ SL /dist=lnormal;
model NOC*censor(0)= logFQ SL Plankstrength/dist=lnormal;
model TUL*censor(0)= logFQ SL Plankstrength/dist=lnormal;
run;
proc print data=fit;
title 'Regression RH85 SL50 and SL65';
run;
```

B.2 65/65/1-0.01

The SAS System

The LIFEREG Procedure

Model Information

Data Set	WORK.FATIGUE
Dependent Variable	Log(TUL)
Censoring Variable	censor
Censoring Value(s)	0
Number of Observations	90
Noncensored Values	62
Right Censored Values	28
Left Censored Values	0
Interval Censored Values	0
Name of Distribution	LNORMAL
Log Likelihood	-146.9403491
Algorithm converged.	

```
model TUL*censor(0)= logFQ /dist=lnormal;
```

Analysis of Parameter Estimates

Variable	DF	Estimate	Std. Error	Chi-Square	Pr > ChiSq	Label
Intercept	1	0.82780	0.38706	4.5739	< 0.0325	Intercept
logFQ	1	-2.22756	0.26898	68.5830	< .0001	
Scale	1	1.89662	0.17513			Normal scale

B.2.1 Resulting model

$$ln(TUL) = 0.82780 - 2.22756log(FQ) + 1.89662\epsilon,$$

or

$$log(TUL) = 0.35951 - 0.96742log(FQ) + 0.82369\epsilon$$

B.3 65/65,50/1-0.01

The SAS System

The LIFEREG Procedure

Model Information

Data Set	WORK.FATIGUE
Dependent Variable	Log(TUL)
Censoring Variable	Censor
Censoring Value(s)	0
Number of Observations	100
Noncensored Values	67
Right Censored Values	33
Left Censored Values	0
Interval Censored Values	0
Name of Distribution	LNORMAL
Log Likelihood	-160.8485647

Algorithm converged.

```
model TUL*censor(0)= logFQ SL /dist=lnormal;
```

Analysis of Parameter Estimates

Variable	DF	Estimate	Std. Error	Chi-Square	Pr > ChiSq	Label
Intercept	1	19.20044	3.00261	40.8908	< .0001	Intercept
logFQ	1	-2.22800	0.27035	67.9181	< .0001	
SL	1	-0.28263	0.04716	35.9102	< .0001	
Scale	1	1.90622	0.17001			Normal scale

B.3.1 Resulting model

$$ln(TUL) = 19.20044 - 2.22800log(FQ) - 0.28263SL + 1.90622\epsilon,$$

or

$$log(TUL) = 8.33865 - 0.96761log(FQ) - 0.12274SL + 0.82786\epsilon$$

B.4 85/50/1-0.01

The SAS System

The LIFEREG Procedure

Model Information

Data Set	WORK.FATIGUE
Dependent Variable	Log(TUL)
Censoring Variable	Censor
Censoring Value(s)	0
Number of Observations	60
Noncensored Values	42
Right Censored Values	18
Left Censored Values	0
Interval Censored Values	0
Name of Distribution	LNORMAL
Log Likelihood	-96.77744906
Algorithm converged.	

```
model TUL*censor(0)= logFQ /dist=lnormal;
```

Analysis of Parameter Estimates

Variable	DF	Estimate	Std. Error	Chi-Square	Pr > ChiSq	Label
Intercept	1	3.39723	0.37403	82.4973	< .0001	Intercept
logFQ	1	-1.07577	0.28820	13.9333	< 0.0002	
Scale	1	1.69901	0.19680			Normal scale

B.4.1 Resulting model

$$ln(TUL) = 3.39723 - 1.07577log(FQ) + 1.69901\epsilon,$$

or

$$log(TUL) = 1.4754 - 0.4672log(FQ) + 0.73787\epsilon$$

B.5 85/65/1-0.01

The SAS System

The LIFEREG Procedure

Model Information

Data Set	WORK.FATIGUE
Dependent Variable	Log(TUL)
Censoring Variable	Censor
Censoring Value(s)	0
Number of Observations	80
Noncensored Values	72
Right Censored Values	8
Left Censored Values	0
Interval Censored Values	0
Name of Distribution	LNORMAL
Log Likelihood	-146.7836116

Algorithm converged.

```
model TUL*censor(0)= logFQ /dist=lnormal;
```

Analysis of Parameter Estimates

Variable	DF	Estimate	Std. Error	Chi-Square	Pr > ChiSq	Label
Intercept	1	0.49696	0.28674	3.0038	< 0.0831	Intercept
logFQ	1	-1.30828	0.24515	28.4804	< .0001	
Scale	1	1.68573	0.14218			Normal scale

B.5.1 Resulting model

$$ln(TUL) = 0.49696 - 1.30828log(FQ) + 1.68573\epsilon,$$

or

$$log(TUL) = 0.21583 - 0.56818log(FQ) + 0.73210\epsilon$$

B.6 85/65,50/1-0.01

The SAS System

The LIFEREG Procedure

Model Information

Data Set	WORK.FATIGUE
Dependent Variable	Log(TUL)
Censoring Variable	Censor
Censoring Value(s)	0
Number of Observations	140
Noncensored Values	114
Right Censored Values	26
Left Censored Values	0
Interval Censored Values	0
Name of Distribution	LNORMAL
Log Likelihood	-243.7521307
Algorithm converged.	

```
model TUL*censor(0)= logFQ SL /dist=lnormal;
```

Analysis of Parameter Estimates

Variable	DF	Estimate	Std. Error	Chi-Square	Pr > ChiSq	Label
Intercept	1	12.18686	1.21755	100.1863	< .0001	Intercept
logFQ	1	-1.21005	0.18665	42.0272	< .0001	
SL	1	-0.17852	0.02008	79.0446	< .0001	
Scale	1	1.69162	0.11537			Normal scale

B.6.1 Resulting model

$$ln(TUL) = 12.18686 - 1.21005log(FQ) - 0.17852SL + 1.69162\epsilon,$$

or

$$log(TUL) = 5.29269 - 0.52552log(FQ) - 0.07753SL + 0.73466\epsilon$$

List of Symbols

Symbols used only locally in the text e.g. in summaries of theories are not included in the list.

β Time under load relative to total time

Γ_{cr} Critical strain energy release rate

δ Crack front opening

$\Delta\delta$ Crack front opening amplitude

ρ Density. Subscript indicates nominal level of moisture content

κ Damage ratio, $\kappa = l/l_0$

σ_{cr} Strength of material with initial damage according to DVM theory

σ_l Theoretical strength of undamaged material according to DVM theory

τ Creep doubling time

ω Specific energy

C Damage rate constant

d Dowel diameter

l Crack length

l_0 Initial crack length

M Damage rate power

R Width of crack front zone

s Standard Deviation

T Period time

Z Contact parameter according to DVM theory

List of Abbreviations

DOL	Duration of load
DVM	Damaged cracked viscoelastic theory
FL	Strength level relating strength of damaged material to strength of material with initial damage
FQ	Frequency of load application
NOC	Number of cycles to failure
RH	Relative humidity
SL	Stress level relative to ultimate strength
TUL	Time under load

Wood Science and Technology 34 (2000) 21–37 © Springer-Verlag 2000

Compressive fatigue in wood

C. O. Clorius, M. U. Pedersen, P. Hoffmeyer, L. Damkilde

Summary An investigation of fatigue failure in wood subjected to load cycles in compression parallel to grain is presented. Small clear specimens of spruce are taken to failure in square wave formed fatigue loading at a stress excitation level corresponding to 80% of the short term strength. Four frequencies ranging from 0.01 Hz to 10 Hz are used. The number of cycles to failure is found to be a poor measure of the fatigue performance of wood. Creep, maximum strain, stiffness and work are monitored throughout the fatigue tests. Accumulated creep is suggested identified with damage and a correlation is observed between stiffness reduction and accumulated creep. A failure model based on the total work during the fatigue life is rejected, and a modified work model based on elastic, viscous and non-recovered viscoelastic work is experimentally supported, and an explanation at a microstructural level is attempted. The outline of a model explaining the interaction of the effect of load duration and the effect of the loading sequences is presented.

1
Introduction

Three fundamentally different types of models have been used to describe wood fatigue. Wöhler curves states fatigue resistance in number of cycles, N, and stress level, whereas duration of load models explain failure by the total accumulated time under load, T, and denies any effect of the oscillations of the load counted by N. Finally, energy criteria have been suggested in various forms, formalised as critical values of energy stored in one or more elements of rheological models.

1.1
Wöhler curves

Wöhler curves, or S–N diagrams, describe fatigue resistance by a critical value of load cycles, N, leading to failure at a given stress level, S, e.g.:

$$\log(N) = A + B \cdot \log(S) \quad , \tag{1}$$

where the coefficients A and B depend on the factor R, which is determined as $R = S_{min}/S_{max}$, where S_{min} and S_{max} are the minimum and maximum stress level in a cycle, respectively. The number of cycles to failure is determined in constant

Received 8 December 1997

C. O. Clorius (✉), M. U. Pedersen, P. Hoffmeyer, L. Damkilde
Department of Structural Engineering and Materials,
Technical University of Denmark, DK-2800 Lyngby

amplitude tests at a number of different stress levels with varying R values as done by Bonfield (1991) in an extensive experimental work. This leads to empirical relations of the form given in (1). In order to verify the Palmgren–Miner summation rule Bonfield carried out tests where each specimen was subjected to different stress levels. The main results from (Bonfield, 1991) are presented in (Bonfield and Ansell, 1991). Based on these results a life prediction analysis is presented in (Bonfield et al., 1994).

The nature of Bonfield's life prediction analysis based on Wöhler curves is presented in (Ansell, 1995). An explanation of the fatigue phenomena is not established, but the underlying theory for the empirical fits is a Paris law relation, placing all emphasis on N according to the fracture mechanical approach presented in (Ansell, 1987).

1.2 Duration of load

In an investigation by Bach (1975) wood fatigue is suggested reduced to a duration of load phenomenon. Bach investigated the influence of frequency, f, on fatigue failure. Compressive square wave shaped load cycles were imposed parallel to grain on small clear specimens at frequencies ranging from 0.1 Hz to 10^{-6} Hz spaced by one decade. The number of cycles to failure was reduced from several hundred to one in the frequency range investigated. It was concluded that failure is best predicted by T determined as:

$$T = \frac{N}{2f} \quad , \tag{2}$$

where 1/2f is the time under load in each cycle.

1.3 Energy criteria

Energy based failure criteria are expressed as a critical value of a specific energy quantity, w, which is calculated as an integral of a stress component times the corresponding strain increment:

$$w = \int \sigma \, d\varepsilon \quad . \tag{3}$$

The stress component can be identified with the stress in an element of a rheological model. Due to the time dependent properties of wood, energy based failure criteria can be expressed in rates of stress, $\dot{\sigma}$, and strain, $\dot{\varepsilon}$, or generally stress work rate, $\dot{w}$:

$$w(t_f) = \int_0^{t_f} \dot{\sigma}\varepsilon + \sigma\dot{\varepsilon} \, dt = \int_0^{t_f} \dot{w} \, dt \quad . \tag{4}$$

A simple theoretical basis can be a four element viscoelastic rheological material model, Fig. 1, representing the three strain components: elastic strain, ε_E, viscoelastic strain, ε_{VE} and viscous strain, ε_V. Integrating all stress and strain components of the model in Fig. 1 yields the total stress work (4).

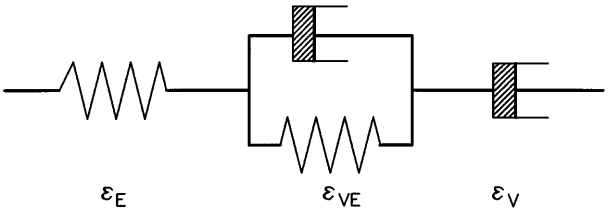

Fig. 1. Four element viscoelastic model, the Burger model

An elaborate energy failure criterion was put forward by Reiner and Weisenberg (1939). This criterion has recently been theoretically exploited by Liu and Ross (1995). According to the Reiner–Weisenberg theory failure will occur when the strain work, w_c, due to the recoverable part of the deformation attains a critical value. Hence, the dissipation rate of non-elastic energy, $\dot{D}$, is subtracted from the work integral:

$$w_c(t_f) = \int_0^{t_f} (\dot{w} - \dot{D})dt \ . \tag{5}$$

The Reiner–Weisenberg theory as expressed by Eq. (5) states failure at a critical value of the energy stored due to ε_E and ε_{VE}. However, the Reiner–Weisenberg theory does not include stress relaxation failure as observed by Bach (1967). Stress relaxation failure occurs at constant strain condition due to redistribution of the strain components. To include stress relaxation failure Bach (1973) proposed a modification of (5). The modified criterion includes only the energy stored due to ε_{VE}, hence the instantaneuosly recoverable elastic energy at failure, $w_c^E(t_f)$, is excluded. The criterion takes the form:

$$w_c^{VE}(t_f) = -w_c^E(t_f) + \int_0^{t_f} (\dot{w} - \dot{D})dt \ . \tag{6}$$

Bach (1975) attempted to verify the criterion (6) experimentally. However, Bach found that failure was best expressed by a time under load criterion.

Philpot et al. (1994) discuss energy based failure models. In a work density model failure is suggested identified with a critical value of the total work, Eq. (4), due to all strain components in Fig. 1. However, this model has the theoretical obstacle of rupture at almost any magnitude of load under repeated loading due to creep recovery, i.e. regain of ε_{VE} in periods without load. Hence, a modification is suggested which omits the work corresponding to creep recovery, i.e. the energy corresponding to the closed part of the hysteresis loop in a load cycle. The modification takes an empirical form and essentially the modified work density model Philpot et al. (1994) is a stress level dependent criterion on the maximum strain.

2
Test outline and data acquisition

The aim of the present study is to explore the interaction of N and T in a series of wood fatigue experiments. The study assesses the validity of the three types of

failure criteria put forward in Sect. 1 and suggests a damage mechanical approach, i.e. an approach that takes into consideration the influence of 2nd order phenomena such as stiffness reduction on the accumulation of damage leading to failure. The following quantities have been measured throughout the tests:

- Number of cycles and time to failure
- E-moduli from loading and unloading sequences
- Maximum and minimum strain in each cycle
- Dissipated energy

2.1 Test plan

Small clear prismatic ($25 \times 25 \times 75$ mm) specimens of spruce (*Picea abies*) were taken to failure in compressive square wave shaped fatigue loading parallel to grain. The stress excitation level oscillated between 80% and 0.8% of the short term strength. Four frequencies ranging from 0.01 Hz to 10 Hz were used. The tests have been performed on two samples in equilibrium with 65% RH and 85% RH respectively. A fatigue specimen was the mid specimen of three in the fiber direction consecutive clear specimens. The reference short term strength of the fatigue specimen was determined on the basis of the two neighbouring specimens taken to failure in approximately 90 s. Specimens were used in fatigue testing only if the two reference short term strength values deviated less than 4% interpreted as an uncertainty of $\pm 2\%$ on the short term strength. The density range was from 377 kg/m^3 to 437 kg/m^3.

2.2 Experimental set-up and machine performance

The specimens were placed centrically between stiff compression planes of the test machine and equipped with two extensometers with a gauge length of 50 mm. The specimens were taken directly from the conditioning chambers to the test machine where they were immediately sealed off from the environment by a polyethylene tubing. The specimens suffered a mean reduction in moisture content of 0.5% during testing. The machine used for the testing is an 250 kN 8502 INSTRON actuator. The actuator can apply load to the specimens with a rate of approximately 2900 kN/s with overshoots of no more than 2% of the load amplitude. In the tests the fatigue load ranged between approximately 0.1 kN and a maximum load between 15 and 24 kN leading to load rise and load fall times from 5 to 8 ms.

2.3 Data acquisition

It is possible to collect a set of data every 0.4 ms, leading to 15–17 sets of data for each loading or unloading sequence when data for time, load, deformation, strain and cycle number are collected simultaneously. In the constant load sequences the acquisition is restricted to 25 sets of data. The number of cycles stored is restricted by a criterion set on amplitude of strain supplemented by a linear sampling criterion. Figure 2 shows the load time and load strain history for a cycle at 10 Hz.

Data points for the regression analysis of the E-moduli are restricted to those in the interval with maximum load application rate, that is, between two successive data points the difference in load must be greater than 0.4 kN and the

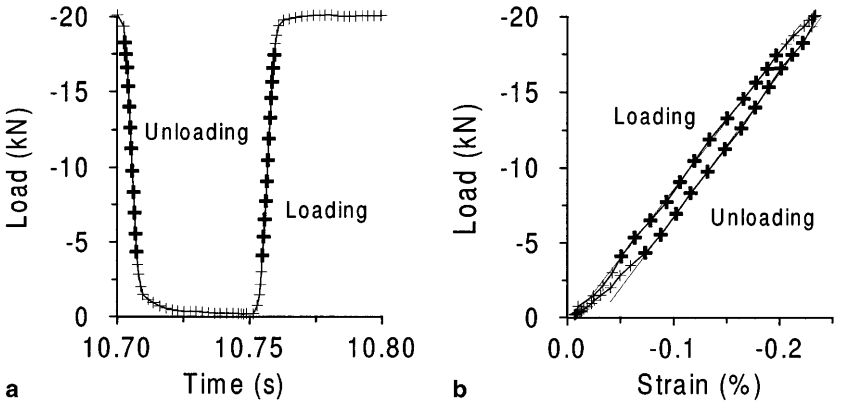

Fig. 2. Load-time and corresponding Load-strain diagram for a 10 Hz test

difference in time must be no more than 0.6 ms. The highlighted data at the linear flanges of the time load history in Fig. 2 are used for the determination of the E-modulus in loading, E_L, and unloading, E_U.

The energy represented by the area under the stress strain curve of each load cycle is determined. Fig. 3a shows area or work density for three separate load cycles. The total work density is calculated as the sum of work density for all load cycles. As the hysteresis loops overlap, the area below the envelope of all load cycles is covered several times. An interpolation is used to estimate the value of the work density of the cycles not recorded. The energy represented by the area below the envelope of all hysteresis loops, Fig. 3b, corresponds to the modified work density introduced by (Philpot et al., 1994).

As adiabatic heating may be present, especially in the high frequency tests, additional specimens were equipped with thermo-elements glued into the specimens to monitor any temperature development during testing.

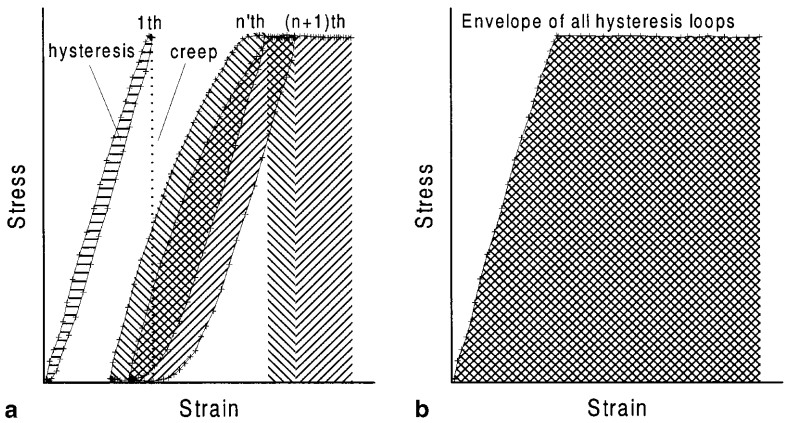

Fig. 3a, b. Calculation of work density. **a** Total work as sum of work in all cycles. **b** Modified work corresponding to envelope of all cycles

3
Results

3.1
Number of cycles and time to failure

The mean number of load cycles to failure, $\bar{N}$, is given in Table 1 for all specimens tested. Obviously, $\bar{N}$ increases with the frequency. Though the scatter is substantial, the four frequencies result in significantly different values of $\bar{N}$.

The substantial standard deviation s_N probably reflects a logarithmic relation between N and stress level. By using data from Bach (1975) the uncertainty of N due to the known uncertainty of ±2% on the reference strength can be estimated to ±0.3 decade. As $s_{\log(N)}$ is less than 0.6 decade, Table 1, the bulk part of the scatter can be explained by the uncertainty of the reference strength.

The values of mean time under load to failure, $\bar{T}$, in Table 1 present no new information, as T = N/2f due to the square wave load cycles. However, $\bar{T}$ accentuates that the survival time decreases with increasing frequency.

The shorter fatigue lives met in the high frequency tests may reflect a temperature related strength reduction. The result of the temperature monitoring of 8 specimens is shown in Fig. 4. The adiabatic heating is found to be insignificant for testing at frequencies up to 1 Hz. At 10 Hz the temperature rise from test start to failure is of the order of 10 °C. According to Gerhards (1982) this is equivalent to a strength reduction of the order 5–10%. The temperature increase was not followed by a corresponding loss of moisture.

3.2
Failure modes

The visual failure was seen either as a fine-meshed pattern of compression zones scattered over a large section of the specimen or as localised failure restricted to one compression band. The visible failure developed during the last few load cycles. The two categories of failure modes are shown in Fig. 5. The proportion of fine-meshed failures increases with decreasing frequency and increasing moisture content as seen in Table 2. A similar dependency of failure mode and time under load is reported in (Madsen, 1992).

3.3
Stiffness development

The stiffness decreases during the fatigue life; this gives a fatigue life dependent E-modulus, E(t). The stiffness, $E_U(t)$, recorded in the unloading sequences develops somewhat differently from the stiffness, $E_L(t)$, in the loading sequences. Generally, the stiffness reduction obtained in the unloading sequence is smaller than the reduction obtained in the loading sequence.

Figure 6 exemplifies the development of stiffness obtained from loading and unloading sequences. The reduction of the stiffness obtained in loading is determined as function of the fatigue life:

$$\text{Stiffness reduction} = \frac{E_L(t)}{E_L(0)} \quad , \tag{7}$$

where the initial stiffness, $E_L(0)$, is defined as the stiffness recorded in the loading sequence of the 2nd load cycle. The specimens failing within the gauge length of the extensometers all exhibit reduction of stiffness during the fatigue life, whereas

Table 1. Number of cycles to failure and time under load to failure

Frequency [Hz]	No. of specimens		Mean no. of cycles to failure $\bar{N}$		Standard deviation s_N		Mean log(N)		Standard deviation $s_{log(N)}$		Mean time under load $\bar{T}$ [sec]		Mean log(T)	
RH [%]	65	85	65	85	65	85	65	85	65	85	65	85	65	85
0.01	12	12	48	26	35	41	1.60	1.10	0.29	0.56	2421	1308	3.29	2.80
0.1	14	12	284	98	262	81	2.32	1.82	0.34	0.42	1420	490	3.02	2.52
1	12	11	3048	367	3569	213	3.27	2.47	0.44	0.34	1524	183	2.97	2.17
10	11	11	21749	4431	29905	7529	4.09	3.38	0.46	0.43	1087	222	2.79	2.08

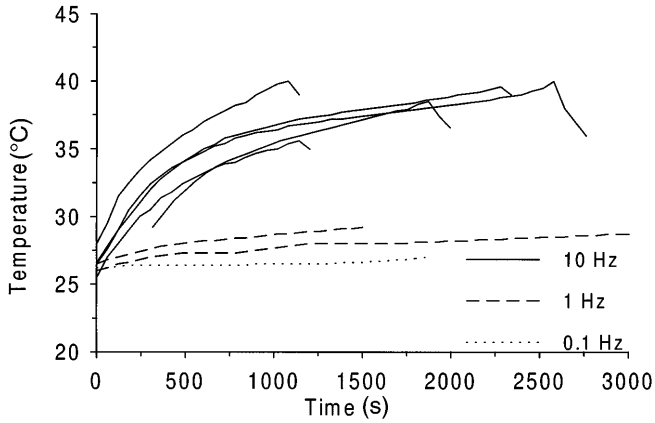

Fig. 4. Temperature development during testing

the stiffness reduction for the specimens failing outside the gauge length of the extensometers is less characteristic. Hence, values for specimens failed outside the extensometer gauges are excluded from Table 3. The table lists stiffness reductions at 0.1 and 0.9 fatigue life.

In order to quantify the different developments of E_U and E_L, the ratio between the stiffness recorded in unloading and loading sequences at any given time of the fatigue life is defined in Eq. (8). Table 3 gives the ratio determined at 0.1 and 0.9 of the fatigue life.

$$\text{Stiffness ratio} = \frac{E_U(t)}{E_L(t)} \tag{8}$$

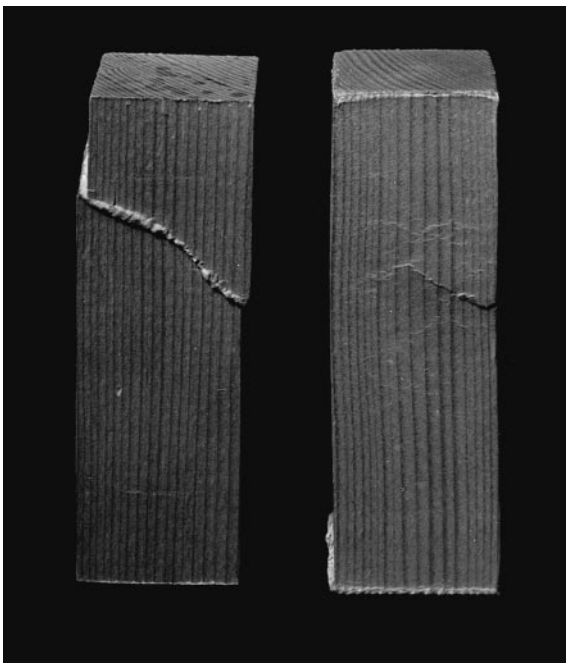

Fig. 5. A specimen failed in localised failure (left) and one failed in fine–meshed pattern (right)

Table 2. The ratio (in %) of specimens failed in a fine-meshed pattern to total number of specimens

Freq. [Hz]	0.01	0.1	1	10
65% RH	17	21	8	0
85% RH	33	25	18	9

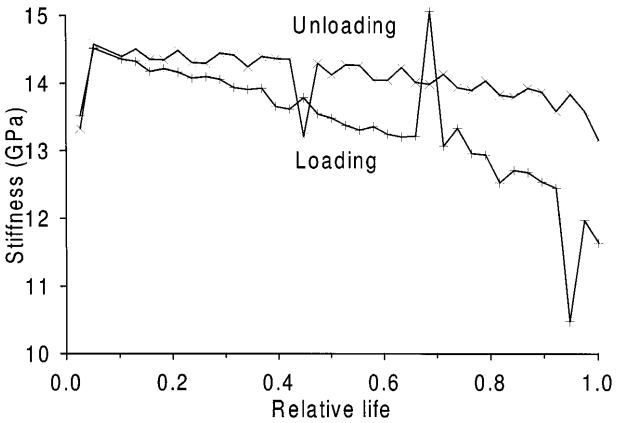

Fig. 6. Development of E_U and E_L, 85% RH, 0.01 Hz

3.4 Strain development

Residual strain is defined as the strain measured at the end of an unloaded sequence at any given time of the fatigue life. Figure 7 exemplifies the development of residual strain for specimens at 85% RH. The development is seen to be highly frequency dependent; the higher the frequency the more rapid the development of final failure when a critical residual strain level is met. The magnitude of the residual strain is moisture dependent. The 85% RH specimens have twice the residual strain of the 65% RH specimens at 0.95 fatigue life as seen from Table 4. The maximum strain at 0.0 and 0.95 fatigue life is seen in Table 4. At 0.0 fatigue life the maximum strain of the moist specimens is less than the maximum strain of the dry specimens. This reflects that going from dry to moist condition yielded a 25% strength reduction not followed by a significant stiffness reduction.

Table 3. Mean stiffness reductions and ratios at 0.1 and 0.9 fatigue life

Freq [Hz]	Stiffness reduction				Stiffness ratio			
	0.1 fatigue life		0.9 fatigue life		0.1 fatigue life		0.9 fatigue life	
	65% RH	85% RH	65% RH	85% RH	65% RH	85% RH	65% RH	85% RH
0.01	1.01	0.99	0.96	0.89	1.00	1.03	1.01	1.09
0.1	1.01	0.99	0.97	0.86	1.00	1.03	1.02	1.10
1	1.01	1.01	0.97	0.89	1.00	1.01	1.01	1.08
10	1.01	1.02	0.97	0.94	1.00	1.01	1.01	1.06

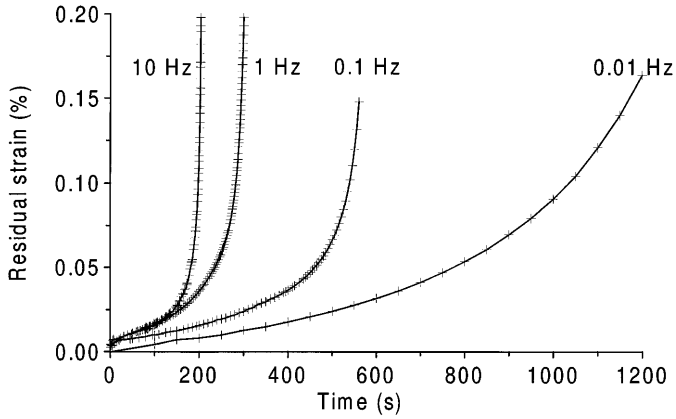

Fig. 7. Development of residual strain for four 85% RH specimens

Table 4. Maximum and residual strain at various stages of the fatigue life

RH [%]	Maximum strain				Residual strain 0.95 fatigue life	
	0.0 fatigue life		0.95 fatigue life			
	$\bar{\varepsilon}_{max}$ [%]	$s_{\varepsilon_{max}}$ [%]	$\bar{\varepsilon}_{max}$ [%]	$s_{\varepsilon_{max}}$ [%]	$\bar{\varepsilon}_{res}$[%]	$s_{\varepsilon_{res}}$ [%]
65	0.27	0.02	0.35	0.07	0.06	0.04
85	0.22	0.02	0.41	0.06	0.11	0.03

However, at 0.95 fatigue life the maximum strain of the moist specimens exceeds the maximum strain of the dry specimens. This corresponds to the observation that more residual strain is accumulated in the moist specimens.

3.5
Energy development

The total work density of the specimens, Eq. (4), has been calculated at 0.5 and 0.9 fatigue life for all specimens, Table 5. The values of the total work density is highly dependent on frequency. Though more energy is dissipated per cycle in low frequency tests this is outweighed by the higher number of cycles met in high frequency tests. The modified work density does not show this frequency dependency. Mean values of the modified work density at 0.1 and 0.9 fatigue life are given in Table 5.

4
Discussion

4.1
Effect of frequency and moisture

In a statistical analysis the number of cycles to failure, N_{ijk}, is the random response of a process with two fixed effects: frequency, f_i, and moisture content, m_j and k replicants. A variance stabilizing transformation, $Y_{ijk} = \log(N_{ijk})$, is used in order to perform an analysis of variance. The transformation implies that the data

Table 5. Mean values of total and modified work density

Freq [Hz]	Total work density [kPa]				Modified work density [kPa]			
	0.5 fatigue life		0.9 fatigue life		0.1 fatigue life		0.9 fatigue life	
	65% RH	85% RH	65% RH	85% RH	65% RH	85% RH	65% RH	85% RH
0.01	360	320	680	740	62.9	38.0	92.7	100.7
0.1	1350	480	3250	1310	57.5	34.8	81.3	63.2
1	18950	1490	35800	3260	50.2	38.5	64.7	75.3
10	39300	25650	73200	49900	55.7	37.4	73.0	60.7

are logarithmically normal distributed. This assumption is confirmed by a normal probability test on the residuals from the final analysis. The statistical analysis is performed according to Montgomery (1997). The following linear two-factor statistical model including interaction is used:

$$Y_{ijk} = \mu + f_i + m_j + fm_{ij} + E_{ijk} \quad \begin{cases} i = 1,2 & \text{two moisture levels} \\ j = 1,2,3,4 & \text{four frequencies} \\ k = 1,2,\ldots,n & \text{number of replicates} \end{cases}, \tag{9}$$

where μ is the mean, fm_{ij} is the interaction term between the effects of frequency, f_i, and moisture, m_j, and E_{ijk} is the random error. Both the effect of frequency f_i and the effect of moisture m_j are highly significant with levels of confidence in excess of 99.9%. The analysis show the interaction fm_{ij} to be non-significant which means that the reduction of log N when going from low to high moisture content is independent of the frequency. The consequence on the non-transformed data is a moisture effect proportional to the frequency. A Newman–Keuls test on the differences between the effects of frequencies shows that: $f_1 \neq f_2 \neq f_3 \neq f_4$ at a level of confidence higher than 99%.

As N is logarithmically normal distributed and as the frequencies range three decades, a double logarithmic diagram is used to present the data of Table 1. Figure 8 shows the log(N)–log(f) relations with linear regression lines, both with and without tests performed at 10 Hz. When the whole frequency range is used

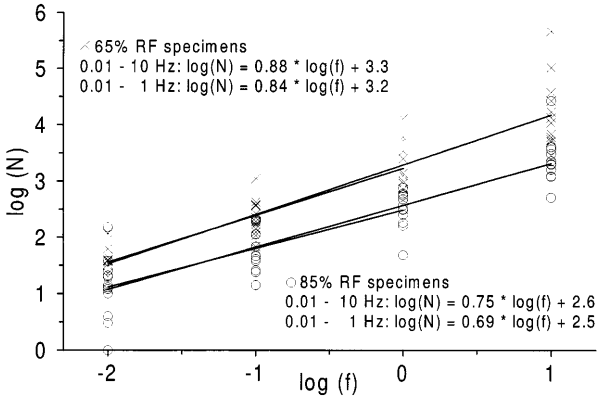

Fig. 8. Log(N) versus log(f)

the coefficients of determination are $r^2 = 0.84$ and $r^2 = 0.79$ for the dry and moist specimens respectively. These values are acceptable considering both the large scatter of N obtained for each frequency and the narrow log(f) range. The values of the standard error of regression, s_{yx}, are within the bounds of the standard deviations, $s_{\log(N)}$, observed for all groups individually, Table 1.

The linear fits in Fig. 8 express the relation between N and f in the following form:

$$\log(N) = a \cdot \log(f) + b \Rightarrow N = cf^a \qquad (10)$$

The sensitivity of the fatigue life to number of loading sequences, the "cycle effect", is reflected in the exponent a; the smaller the exponent, the greater the influence of the mere number of loading sequences. For a = 0 a failure criterion can be expressed solely in terms of N, see Eq. (1), whereas a = 1 leads to a duration of load criterion, see Eq. (2). As a is less than 1 for the regression lines in Fig. 8, time under load does not fully explain the relation between N and f. Due to the smaller exponent the moist specimens seem to be more susceptible to the number of loading sequences. However, differences in the exponent correspond to the interaction term, fm_{ij}, which is not statistically significant. The "cycle effect" observed cannot be explained by strength reduction due to adiabatic heating in the 10 Hz tests as the slope of the regression lines does not increase when the 10 Hz data are excluded from the regression. Though not global, the relations between log(N) and log(f) as presented in Fig. 8 are reliable in the frequency region investigated and the following conclusions can be drawn:

- The number of cycles to failure increases in a non-linear way with increasing frequency in the range from 0.01 Hz to 10 Hz, i.e. an increase of f results in increasing N but also reduced time to failure.
- The number of cycles to failure decreases with increasing moisture content even though the maximum stress is chosen as the same fraction of the moisture dependent short term strength.

4.2
Failure criterion on N or T

The number of cycles decreases from an order of 10^3 at 10 Hz to an order of 10 at 0.01 Hz. Consequently, Wöhler curves, (1), are useless in compressive fatigue description without a third dimension representing frequency. The results also show that time to failure decreases for increasing frequency. Hence, a failure criterion cannot be expressed as a duration of load criterion, (2).

4.3
Strain and stiffness development

At the microstructural level non-recoverable viscous strain has been identified as slip planes by Hoffmeyer (1993) and Hoffmeyer and Davidson (1989). At a high intensity of this type of microstructural damage fatal compression bands form. Stiffness reduction is a natural consequence of slip planes due to the change in material properties. The monitoring of stiffness reduction may reveal the formation of compression bands before they become visible, and a correlation between residual strain and stiffness reduction is expected.

From Table 3 it is seen that the stiffness initially increases. The stiffness increase may be explained by permanent set during load application in the first load

cycles, i.e. a consolidation process. Apart from this the stiffness is reduced during the fatigue life for all frequencies at both moisture contents. The stiffness reductions observed for the moist specimens are systematically larger than for the dry specimens. The larger stiffness reductions for the moist specimens correspond to the larger levels of residual strain observed for these specimens, Table 4.

The development of stiffness reduction follow the overall shape of the accumulation of residual strain as shown in Fig. 7; i.e. the stiffness reduction is a function of accumulated damage independent of test frequency. In Fig. 9 the stiffness reduction is given as function of residual strain for four frequencies; the frequency invariance is obvious.

4.4
Origin of residual strain

The residual strain is the strain measured at the end of the unloaded sequences. As the unloaded sequences have finite duration, full creep recovery is not possible and some of the residual strain is recoverable. However, from an early stage of the fatigue life the creep recovery is an order of magnitude smaller than the residual strain as both reported by Bach (1975) and indicated by pilot tests. Hence, the residual strain is believed to express non-recoverable strain or damage.

Development of viscous strain is known to be dependent upon stress level, time, moisture content and fluctuations as well as the creep level itself. In this context these parameters do not fully explain the frequency dependency of the residual strain developments seen in Fig. 7. Some of the accumulation of the residual strain must be reckoned as time dependent creep, identified as slip plane formation on a microstructural level. The viscous strain rate, $\dot{\varepsilon}_V$, is assumed to be dependent of the level of accumulated residual strain, $\dot{\varepsilon}_V(\varepsilon_{res})$. During cyclic square wave loading at a given stress level, the accumulation of time dependent viscous strain, ε_V, is expressed by the formula:

$$\varepsilon_V = \sum_{n=1}^{N} \int_0^{1/2f} \dot{\varepsilon}_V(\varepsilon_{res}) dt \qquad (11)$$

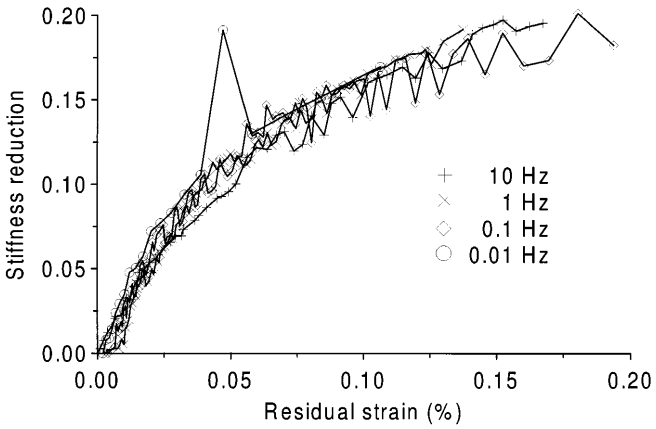

Fig. 9. Stiffness reduction as function of residual strain, 85% RH specimens

However, as the time under load to failure, $T = N/2f$, decreases for increasing frequency Eq. (11) does not consider the more rapid accumulation of residual strain in high frequency tests. To explain the frequency dependent accumulation of residual strain, time independent strain residuals, $\Delta\varepsilon_N$, introduced in the loading sequences must be invoked. Letting this strain increment be dependent on the level of residual strain, $\Delta\varepsilon_N(\varepsilon_{res})$, a simple formula for the accumulation of ε_N due to N square wave load cycles at a given stress level would be:

$$\varepsilon_N = \sum_{n=1}^{N} \Delta\varepsilon_N(\varepsilon_{res}) \tag{12}$$

The experimental evidence for the existence of time independent strain residuals $\Delta\varepsilon_N(\varepsilon_{res})$ is the different Young's moduli in loading and unloading, i.e. the stiffness ratio. From Table 3 it is seen that up to 10% of the apparent elastic strain gained in loading is not regained in unloading. In Fig. 6 it is seen how the stiffness ratio is an increasing function of the fatigue life, which verifies that $\Delta\varepsilon_N$ is dependent on the level of residual strain.

The consequence of $\Delta\varepsilon_N$ is that the mere loading sequences contribute to the accumulation of damage. Combining (11) and (12) gives an expression for the two sources of accumulation of residual strain:

$$\varepsilon_{res} = \varepsilon_V + \varepsilon_N = \sum_{n=1}^{N} \int_{0}^{1/2f} \dot{\varepsilon}_V(\varepsilon_{res})dt + \sum_{n=1}^{N} \Delta\varepsilon_N(\varepsilon_{res}) \tag{13}$$

Though heuristic in form, the algorithm (13) explains the experimental observations as the first term dominates the accumulation of residual strain in high frequency tests, leading to shorter fatigue lives, whereas the second term dominates in low frequency tests. The moisture induced reduction of time to failure is explained by higher creep rates in moist wood, i.e. by facilitated formation of slip planes (e.g. Hoffmeyer, 1990; Hoffmeyer and Davidson, 1989).

Figure 10 shows a schematic version of the developments of the residual strain curves given in Fig. 7. The sloping lines model ε_V under constant load, i.e. the

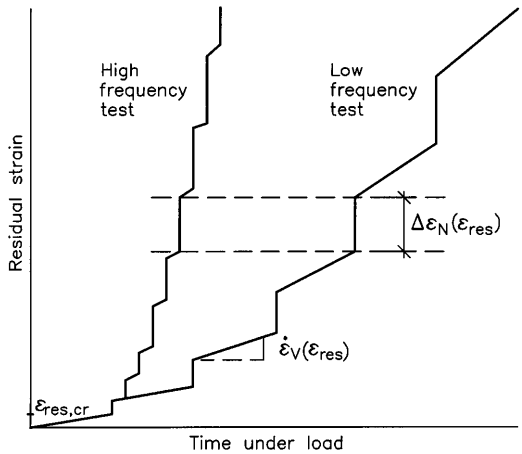

Fig. 10. Schematic development of residual strain for high and low frequency tested specimen

slope is a linearisation of $\dot{\varepsilon}_V(\varepsilon_{res})$. The vertical lines model ε_N introduced in the loading sequences.

The critical residual strain level, $\varepsilon_{res,cr}$, in Fig. 10 corresponds to the occurrence of the first premature failure zone, i.e. the first cluster of slip planes. From this stage on the development towards failure is frequency dependent:

- In low frequency testing the accumulation of residual strain is dominated by creep (11), i.e. formation of slip planes in periods with constant load.
- In high frequency testing the accumulation of residual strain is dominated by damage induced in the loading sequences (12), i.e. time independent residual strain increments.

It is unlikely that the damage introduced in the loading sequences, ε_N, is formation of additional slip planes, as slip plane formation is generally recognised as a time dependent process identified with viscous creep, ε_V, (Hoffmeyer, 1993) or (Hoffmeyer and Davidson, 1989). Hence, the additional damage in the loading sequences may be seen as the effect of the loading process working on existing slip planes. This interpretation of the damage introduced in the loading sequences is confirmed by the visible failure morphology. In low frequency tests the failure zones form randomly in the specimen as function of time and load leading to the higher number of fine-meshed failures, Table 2. Conversely, the failure of the high frequency tested specimens are confined to one compression band due to loading sequence induced enlargement of the first premature failure zone.

4.5
Energy based failure criterion

A failure criterion expressed in terms of the total work is rejected as the work on the specimens at 0.9 fatigue life, Table 5, in high frequency testing is found to be 70–100 times the work on the specimens in low frequency testing. Contrary to the work density the modified work density is of the same order of magnitude for tests at different frequencies. The moist specimens that are exposed to lower absolute stresses than the dry specimens exhibit larger values of the maximum strain near failure, Table 4. This is of course a necessary consequence of the modified work density criterion, as this essentially is a stress level dependent criterion on the maximum strain as illustrated in Fig. 11. The idealisation in Fig. 11 is verified by the values from Table 5. Initially, at 0.1 fatigue life, the modified work density is significantly lower for the moist specimens, however near failure, at 0.9 fatigue life, the moisture dependency is no longer significant.

4.6
Strain-stability failure criterion

The consequence of the modified work density failure criterion is that failure at low stress levels will occur at higher strain levels than failure at high stress levels, as idealised in Fig. 11. The observation of accumulated residual strain confirms this conjecture. Observations of overall compression failures support the view that failure is initiated at a higher level of microstructural damage at lower stress levels. The description of compression failure such as presented in (Hoffmeyer, 1990) reveals that the overall compression failure is initiated by cell wall buckling in earlywood preceded by slip plane formation in latewood, Fig. 12.

The moist and dry specimens were loaded equally severely relative to the short term strength values. However, relative to the stiffness the moist specimens were loaded less severely than the dry specimens. Hence, it is not unlikely that more

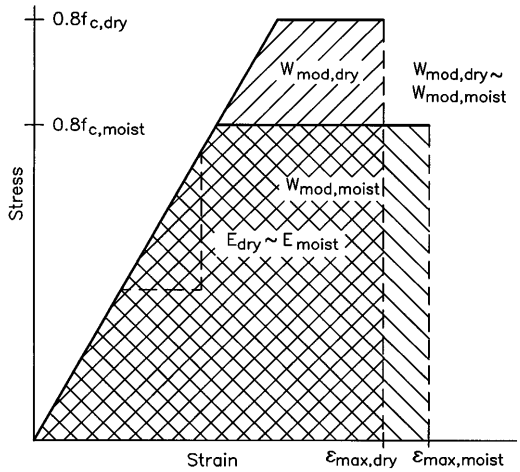

Fig. 11. Consequence of the modified work density failure criterion idealised in a stress strain diagram

damage is needed to introduce overall failure of the wood in the moist case if the final formation of compression bands is a cell wall buckling phenomenon governed by the overall stiffness of the material. This damage–stability interaction offers a micromechanical explanation to the modified work density criterion.

5 Conclusion

From the present compressive fatigue test the following is concluded with respect to modelling of fatigue failure:

- Number of cycles is an inadequate measure of wood fatigue life as it is highly dependent on test frequency.
- Total time under load to failure decreases with increasing test frequency.

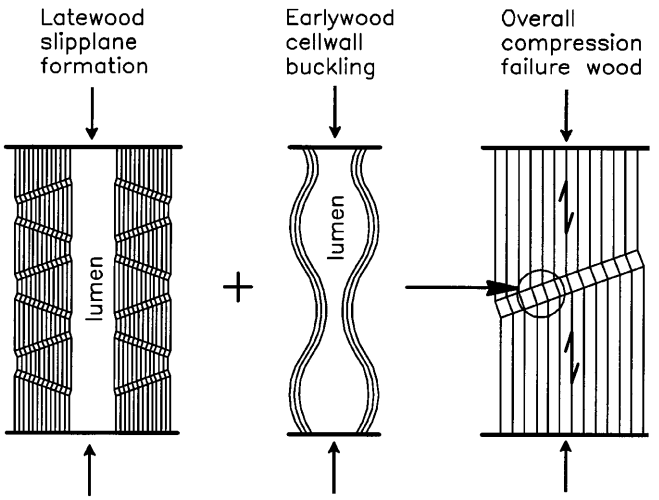

Fig. 12. Slip plane formation in latewood precedes cell wall buckling in earlywood resulting in overall compression failure

- Total work density can not explain fatigue failure as it is highly dependent on test frequency.
- A modified work density criterion, in effect a stress level dependent criterion on the maximum strain, is more promising.
- A conjecture to explain a stress level dependent strain criterion is made based on damage level and stability considerations.

A damage mechanical approach is suggested resting on damage accumulated as:

- Time dependent creep, i.e. slip planes developed during constant load periods.
- Permanent set introduced in the loading sequences, probably introduced as further damage of already formed slip planes.

The approach has the merit of being able qualitatively to explain why the time to failure is reduced with increasing test frequency. Further, there is phenomenological evidence from the visible failure morphology that two modes of damage accumulation are present in compressive wood fatigue, and that permanent set from the loading sequences dominates high frequency fatigue tests.

References

Ansell MP (1987) Laymans guide to fatigue. In: Galt JM (Ed.) Wind Energy Conversion 1987, pp. 39–54, Mechanical Engineering Publications Ltd
Ansell MP (1995) Fatigue design for timber and wood-based materials, step lecture E22. In: Blass HJ et al. (Eds.) Timber Engineering STEP 2, pp. E22/1–E22/8, Centrum Hout
Bach L (1967) Static fatigue of wood under constant strain, Information Report VP-X-24, Canadian Forest Prod. Lab., Vancouver B.C., Canada
Bach L (1973) Reiner-Weisenberg's theory applied to time-dependent fracture of wood subjected to various modes of mechanical loading. Wood Sci. 5(3): 161–171
Bach L (1975) Frequency-Dependent Fracture in Wood under Pulsating Loading, In FPRS-Annual meeting Proceedings, June 15, 1975, Portland, Oregon, USA
Bonfield PW (1991) Fatigue evaluation of wood laminates for the design of wind turbine blades, PhD thesis, University of Bath
Bonfield PW, Ansell MP (1991) The fatigue properties of wood in tension, compression and shear. J. Materials Sci. 26: 4765–4773
Bonfield PW, Ansell MP, Dinwoodie JM (1994) Fatigue testing of wood, A detailed guide for the development of life prediction formulae from fatigue data. In Proceedings of IUFRO S5.02, International Timber Engineering Conference. pp. 163–174, Sidney, Australia
Gerhards CC (1982) Effect of moisture content and temperature on the mechanical properties of wood: an analysis of immediate effects. Wood and Fiber 14(1): 4–36
Hoffmeyer P (1990) Failure of wood as influenced by moisture and duration of load, PhD thesis, State University of New York, Syracuse, New York
Hoffmeyer P (1993) Non-linear creep caused by slip plane formation. Wood Sci. Technol. 27: 321–335
Hoffmeyer P, Davidson RW (1989) Mechano-sorptive creep mechanism of wood in compression and bending. Wood Sci. Technol. 23: 215–227
Liu JY, Ross RJ (1995) Energy criterion for fatigue strength of wood structural members. In Proceedings of the 1995 ASME meeting, Mechanics of Cellulosic Materials. Vol. AMD 209/MD 60, pp. 125–133. Los Angeles
Madsen B (1992) Structural Behaviour of Timber, 1st edn., Vancouver, Canada: Timber Engineering ltd
Montgomery DC (1997) Design and analysis of experiments, 4th edn., New York: John Wiley & Sons
Philpot TA, Fridley KJ, Rosowsky DV (1994) Energy-based failure criterion for wood. J. Materials in Civil Engineering, ASCE. 6(4): 578–594
Reiner M, Weisenberg K (1939) A thermodynamic theory of the strength of materials. Rheological leaflet 10(12)

STRENGTH OF GLUED-IN BOLTS AFTER FULL-SCALE LOADING

By M. Uhre Pedersen,[1] C. O. Clorius,[2] L. Damkilde,[3] and P. Hoffmeyer[4]

ABSTRACT: In 1993 after 9 years of use, one of the wooden blades of a windmill was struck by lightning. After demounting, the damaged blade was handed over to the Technical University of Denmark, Lyngby, for the investigation of potential fatigue damage. This paper presents an experimental determination of the residual strength of the glued-in bolts that served as the blade to rotor hub connection in the windmill. The load history of the bolts, the test method, the observed fracture modes, and the force displacement curves are presented along with the recorded residual strength of the bolts. The bolts with a length of 500 mm had a special hollow tapering giving them a higher load-bearing capacity than solid bolts of equal dimensions. An FEM analysis confirms the higher load-bearing capacity. The mean residual stength was found to be 362 kN with a standard deviation of 37 kN, which is 95% of the predicted strength based on short-term tests on similar bolts. At fracture, a displacement between 0.4 and 1.0 mm was observed. In the majority of failures, the bolts were pulled out like a cork from a bottle.

INTRODUCTION

Glued-in bolts in glulam make stiff and strong connections. Contrary to traditional timber connections, they transfer section forces directly into the inner part of the cross section. Traditional connections act through shear at the surface, which limits their load-bearing capacity and thus restricts the potential of wood structures. Though glued-in bolts have been known since the 1960s, they are only sparsely used, primarily due to the limited knowledge of the long-term strength.

The aim of this paper is to present an experimental assessment of the long-term strength as a function of full-scale loading (i.e., load duration, varying load levels, moisture fluctuations, and low frequency fatigue). The assessment is based on a number of pullout tests performed on glued-in bolts having served for 9 years in a large windmill as connectors between the blade and rotor-hub. A more demanding application of glued-in bolts is difficult to imagine with the forces being reversed at every rotation of the rotor and the blades being exposed to varying weather conditions. The wind and gravity load give mainly bending in the connection, and this results in axial load in the single bolt. The axial load changes between tension and compression during the rotation.

WOODEN BLADES OF NIBE-B WINDMILL

During the early 1980s a group of Danish glulam manufacturers were inspired by American experience to develop a wooden construction for large aerogenerator rotor blades. This coincided with the desire for an alternative blade technology that could challenge the traditional fiberglass blade manufactures. In 1984 the first full-scale results were obtained as the fiberglass blades of the 20-m-radius rotor of the Nibe-B windmill were replaced by wooden blades by the Danish electricity company ELKRAFT.

The blades were 18 m long and had a solid leading edge of Swedish spruce glulam extending for about 30% of the blade chord (Fig. 1). The trailing edge was built up with ribs, stringers, and a 7-mm birch plywood coating. The blades were sealed with a 1-mm polyurethane covering allowing some moisture diffusion. The blades had a final weight of 2,500 kg each. The connection between blade and hub was established by 28 glued-in bolts in each root section. The bolts were arranged in a circle with a diameter of 710 mm in the solid root section leaving 30 mm of glulam spacing between the bolts. The cylindrical glulam root section had a diameter of 860 mm, which left 50 mm of glulam from the bolt perimeter to the outer circumference.

Fig. 2 shows the geometry of the hollow tapered bolts. The glued-in length of the bolts was 500 mm and the diameter was 48 mm. The drilled holes in the glulam were 2 mm oversized and a two-component epoxy glue was used to bond the shot-blasted surface of the bolt to the glulam. The glue was prevented from entering the hollow tapering by inserting a wood plug into the end of the bolt. This is seen in Fig. 3 showing a photograph of a glued-in bolt. The bolt has been milled down to one-half.

BACKGROUND

Static Strength

The hollow tapered bolt used in the blade to hub connection of the Nibe-B windmill (Fig. 3) was developed at the Tech-

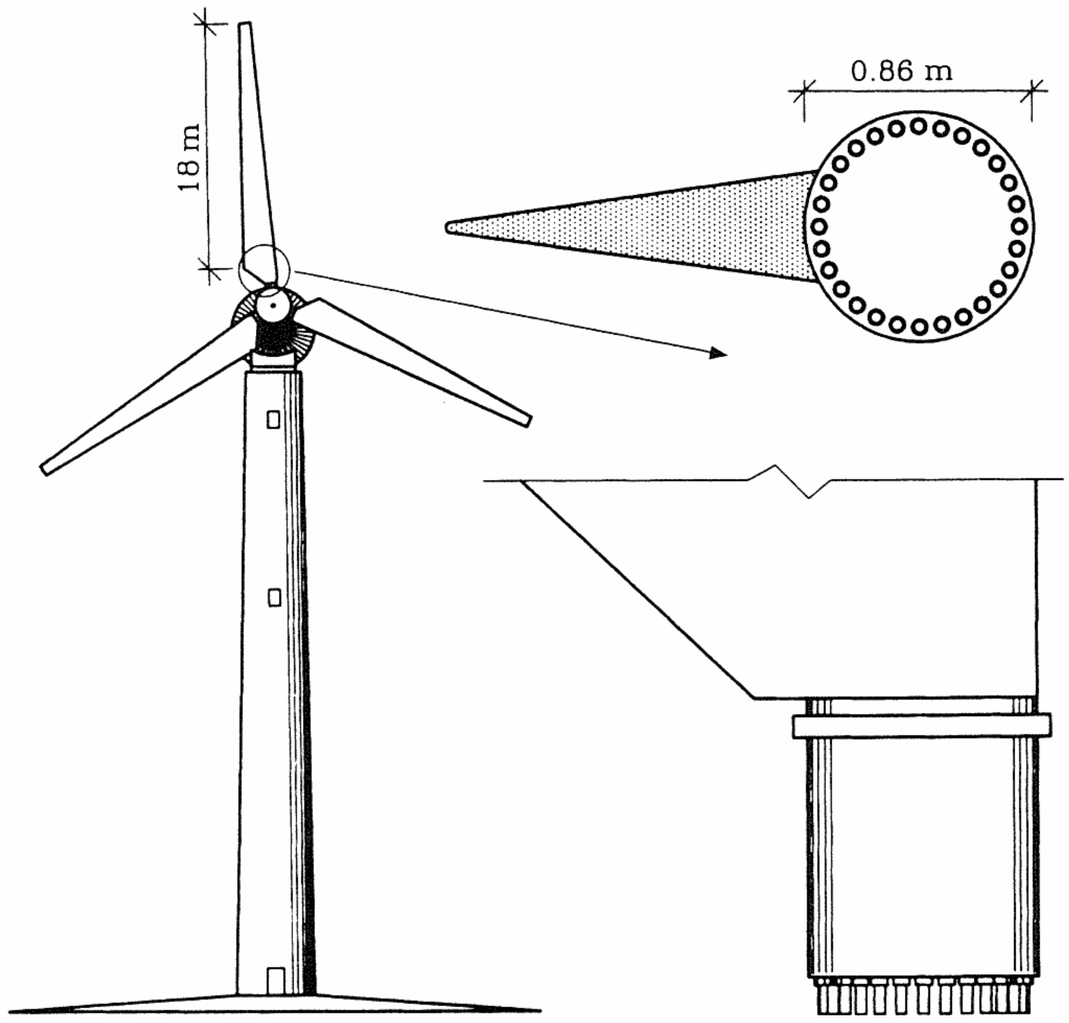

FIG. 1. Nibe-B Windmill with Detail from Blade to Hub Connection

[1]PhD Student, Dept. of Struct. Engrg. and Mat., Tech. Univ. of Denmark, DK-2800 Lyngby, Denmark. E-mail: mup@bkm.dtu.dk

[2]PhD Student, Dept. of Struct. Engrg. and Mat., Tech. Univ. of Denmark, DK-2800 Lyngby, Denmark.

[3]Assoc. Prof., Dept. of Struct. Engrg. and Mat., Tech. Univ. of Denmark, DK-2800 Lyngby, Denmark.

[4]Assoc. Prof., Dept. of Struct. Engrg. and Mat., Tech. Univ. of Denmark, DK-2800 Lyngby, Denmark.

Note. Discussion open until January 1, 2000. To extend the closing date one month, a written request must be filed with the ASCE Manager of Journals. The manuscript for this paper was submitted for review and possible publication on November 11, 1997. This paper is part of the ***Journal of Performance of Constructed Facilities***, Vol. 13, No. 3, August, 1999. ©ASCE, ISSN 0887-3828/99/0003-0107–0113/$8.00 + $.50 per page. Paper No. 16967.

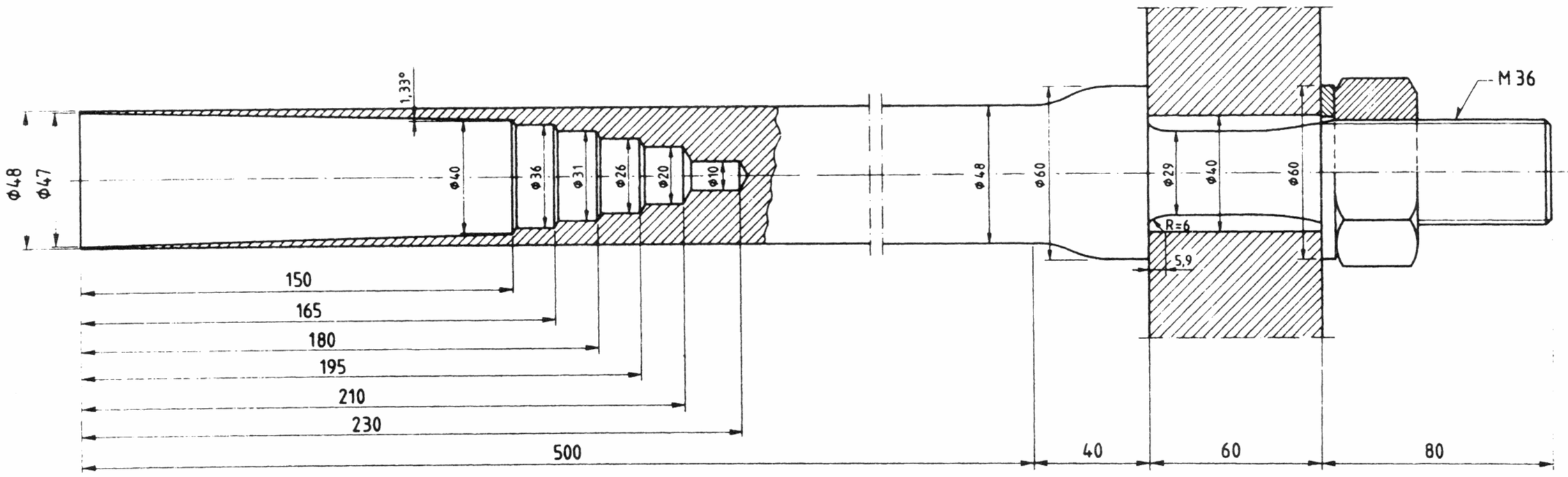

FIG. 2. Geometry of Hollow Tapered Bolts

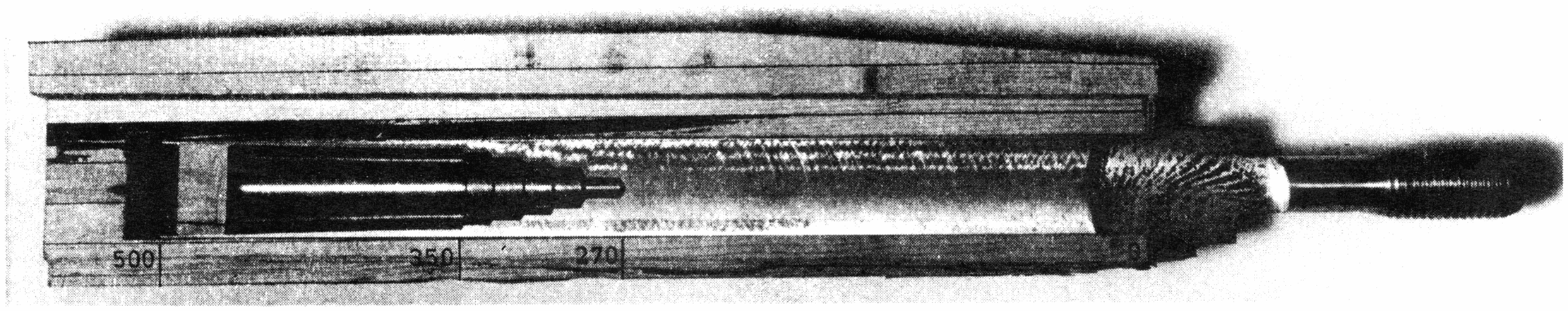

FIG. 3. Sectional View of Hollow Tapered Bolt (Measures in mm)

TABLE 1. Stiffness Parameters used in FEM

Parameter (1)	E_l (GPa) (2)	E_r (MPa) (3)	G_{rl} (MPa) (4)	ν_{lr} (5)
Wood	14	500	500	0.45
Glue	4	—	—	0.3
Steel	210	—	—	0.2

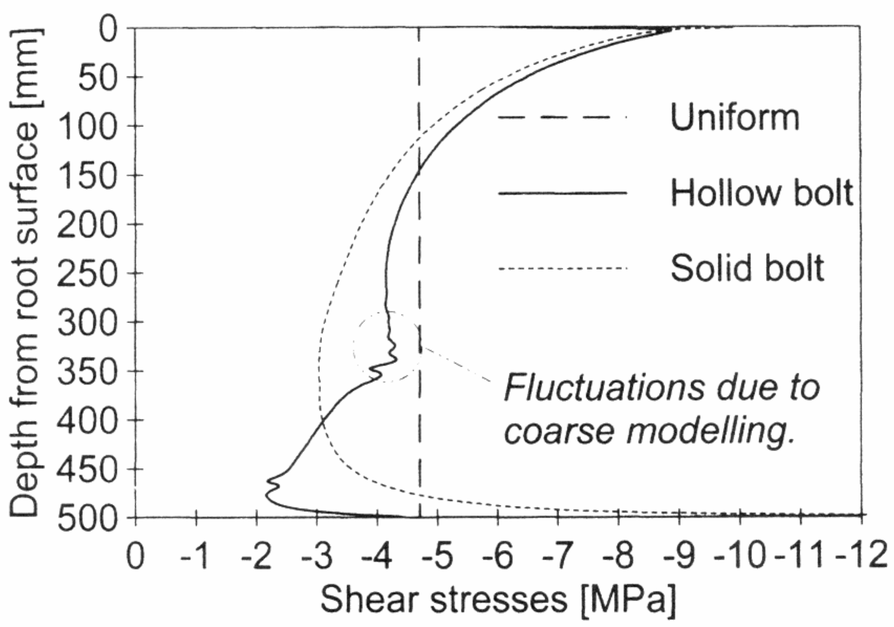

FIG. 4. Shear Stress Distribution along Hollow Tapered Bolt and Solid Bolt, respectively

nical University of Denmark, Lyngby, particularly for this purpose (Riberholt and Spøer 1983). Experimentally, Riberholt and Spøer established that the load-bearing capacity in axial tension is increased 20% by making the bolt hollow. This phenomenon is presumably explained by a stress peak leveling effect of the tapering. An accurate linear elastic finite-element analysis of the shear stress distribution along a glued-in bolt has been performed on solid and hollow tapered bolts. The stiffness parameters used in the rotational symmetrical modeling are given in Table 1. The wood parameters have been determined experimentally.

Fig. 4 shows the shear stress distribution in the middle of the glue bond. The shear stresses correspond to a bolt force of 360 kN. The following three observations are made:

1. The magnitude of the shear stress peaks at the top and at the bottom end are smaller for the hollowed bolt.
2. The extension of the area with excessive stresses at the end is smaller for the hollowed bolt.
3. The stresses along the hollowed bolt are close to the uniform stress distribution over a larger area.

The first item should not be overemphasized as the peaks represent singularities not adequately evaluated by a linear elastic modeling. A strain softening model such as presented by Johansson et al. (1995) must be invoked to explain the material behavior at these singularities. However, the two last items constitute an explanation to the larger load-bearing capacity observed in the hollowed bolts.

The short term static strength of the hollow tapered bolts can be assessed on the basis of experiments by Riberholt and Spøer (1983). They reported the static strength of hollow tapered bolts to be 346 kN with a standard deviation of 31 kN. Riberholt and Spøer used a tapered geometry similar to the geometry used in the Nibe-B blades; however, the diameter of the Nibe-B bolts is 20% larger. Furthermore, the moisture content (MC) of the surrounding wood was 12.5% on average during testing of the Nibe-B bolts, whereas Riberholt and Spøer reported MC between 9 and 11% in the test specimens. The strength is assumed to be linear in the diameter, and the shear strength of the wood is assumed to decrease 3% for a 0.01 increase in MC. The short-term strength of the Nibe-B bolts is predicted by adjusting the values from Riberholt and Spøer (1983) for size k_d and moisture k_{MC}

$$k_d = 1.20; \quad k_{MC} = 1 - 2.5 \cdot 0.03 = 0.92$$

The adjusted data predict the virgin static short-term strength, F_{static}, of the bolts to be

TABLE 2. Laboratory Fatigue Tests on Glued-In Bolts

Test (1)	Load range $\{\alpha_1, \alpha_2\}$ (%) (2)	N (10^6) (3)
I	{1, 60}	0.33
II	{2, 60}	0.13
III	{1, 60}	0.14
IV	{−20, 20}	12
V	{1, 30}	11
	{−20, 20}	30
VI	{1, 20}	12
	{1, 30}	44

$$F_{\text{static}} = k_d \cdot k_{\text{MC}} \cdot 346 \text{ kN} = 382 \text{ kN} \quad (1)$$

with a standard deviation of 34 kN.

Fatigue Performance

Fatigue tests were carried out in the design phase on hollow tapered bolts (Riberholt and Spøer 1983). Six specimens failed in fatigue at a frequency of 8.3 Hz. In Table 2 the number of cycles to failure N are listed, along with the range of the imposed load level $\{\alpha_1, \alpha_2\}$, where

$$\alpha_1 = \frac{F_{\text{fatigue,min}}}{F_{\text{static}}}; \quad \alpha_2 = \frac{F_{\text{fatigue,max}}}{F_{\text{static}}} \quad (2a,b)$$

The two last tests quoted in Table 2 were carried out as a combination of two load levels.

The fatigue testing shows that two decades of load cycles are gained when the span of the imposed axial forces is halved. The wooden blades were planned to have a 20-year service life yielding a total of 2.6×10^8 load cycles (Øye 1982). For a load variation within 15% of the axial tensile strength, failure is expected after 10^8 load cycles by simple extrapolation of the data in Table 2.

Fatigue Reduction of Static Strength

The fatigue tested specimens (Table 2) contained a glued-in bolt in each end. After fatigue failure of one of the bolts in the test specimen, it was possible to pull out the other bolt in a static tension test. Hence, the fatigue tests gave two kinds of results: (1) The number of load cycles leading to failure for a given load excitation; and (2) the residual strength of the bolt that was exposed to the same load history but had not failed. Treated as a homogeneous entity the residual strength values of the bolts that did not fail in fatigue testing had a mean value of 327 kN with a standard deviation of 22 kN. An insignificant 5% reduction is observed compared with the static short-term strength of similar bolts. An explanation could be that fatigue damage accumulates around the weakest point of the test specimen, leaving the rest of the test specimens uninfluenced by the fatigue load.

LOAD HISTORY

The rotor of the Nibe-B windmill was rigged with wooden blades for 9 years. During that time, the blades were in revolution for ~3 years or 25×10^3 h (Friis 1984; Rasmussen 1993), with a revolution frequency of 0.55 Hz. In total, the wooden rotor has been exposed to 50×10^6 load cycles and an additional 6 years of dead load.

Fig. 5 shows the principle in establishing the load history. The maxima and minima, $M_{\max}$ and $M_{\min}$, respectively, for the bending moment acting about the severest loaded axis in the connection have been determined as functions of the wind velocity (Øye 1982). The location of the severest loaded axis is given by the angle β. The bending moments were carried by the bolts as either tension or compression axial forces, denoted as $\pm F_{\max}$ and $\pm F_{\min}$, respectively. The most severely axially loaded bolts are found perpendicular to the direction of the bending moment. One-third of all bolts are exposed to more than 85% of the largest bolt force.

Limits for the axial forces are listed in Tables 3 and 4 for different wind velocity intervals and in some special situations. The numbers in Fig. 5 and Tables 3 and 4 identify the bolts that experience maximum compression or tension, respectively. The loads obtained during special operation situations are either not dramatically different from the normal loads or they occur in such low numbers that they can be ignored. The majority of load cycles obtained during normal operation is represented in the first six rows of Table 3. The windmill was in a nonoperating state for a total of 6 years. However, the most severe static force does not attain larger values than the forces encountered under dynamic loading, and the most severe forces from both dynamic and static loading act on almost the same bolts.

Fluctuations in MC in the wood are part of the load history of the bolts. Large fluctuation may introduce damage in the wood surrounding the bolt. However, observations of the moisture fluctuations showed that the solid root section had a huge moisture buffer capacity. This buffer capacity and the semidiffusion tight coating secured a relatively constant MC of the wood.

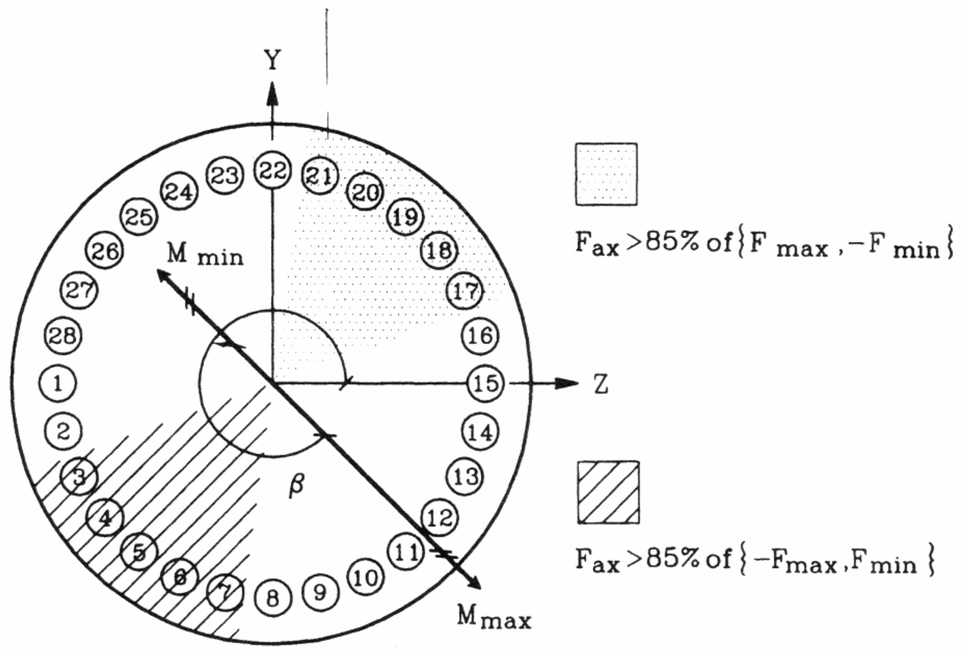

FIG. 5. Location of Most Severe Load History

TABLE 3. Axial Forces during Normal Operation

Wind (m/s) (1)	β (degrees) (2)	Cycles (10^6) (3)	$F_{\max}$ (kN) (4)	$F_{\min}$ (kN) (5)	Max tension (bolt number) (6)
5–7	355	12.9	19	−17	7–8
7–9	341	12.2	21	−15	6–7
9–11	331	9.8	26	−9	5–6
11–13	308	6.9	44	6	4
13–15	306	4.3	51	9	4
15–17	316	2.3	38	−4	4–5
17–19	322	1.2	33	−10	5
19–21	328	0.6	30	−14	5–6
21–23	331	0.2	31	−16	5–6
23–25	330	0.05	31	−21	5–6

TABLE 4. Axial Forces during Special Situations

Condition start/stop (1)	Cycles (2)	$F_{\max}$ (kN) (3)	$F_{\min}$ (kN) (4)	Max tension (bolt number) (5)
Light wind	18,000	25	−30	4–5
Strong wind	4,500	47	−65	4
Emergency	9	102	−95	3–4
Hurricane	1	106	−77	4–5

DETERMINATION OF RESIDUAL STRENGTH

The root section of the blades had a solid circular cross section extending for ~1 m. The test specimen was cut from the root section of the damaged blade. This produced a 0.8-m-high solid glulam cylinder with a diameter of 0.86 m containing the 28 glued-in bolts.

Experimental Setup

The saw-cut surface of the test specimen was leveled, made parallel to the plane spanned by the bolts, covered with Teflon film, equipped with a center tap, and finally placed upright on a steel plate. These arrangements made it possible to rotate the test specimen about its center axis. Two steel straps were tightened around the cylinder to counteract tensile stresses perpendicular to the grain introduced during testing. Four steel columns were erected surrounding the test specimen on the strong-floor of the laboratory, and a set of U-profiles were mounted on the columns providing support for the hydraulic equipment as shown in Fig. 6.

The pullout force was delivered by a 500-kN servohydraulic double acting actuator. Due to the high strength of the steel used for the bolts the shaft of the bolts could withstand the necessary forces, and it was possible to pull out a bolt using only a threaded rod and a long socket as the connection between bolt and actuator (Fig. 7). The connection between bolt and actuator allowed for some rotation, and the bolt was accurately positioned under the actuator. Hence, the pullout force was a pure axial force. To restrict the wood cylinder from moving during testing, the cylinder was prestressed between the strong-floor and the rigid test setup. The pressure was introduced using an 880-kN Hydrocam hydraulic press and a charnier between a steel beam and a 30-mm steel plate covering the upper surface of the wood cylinder.

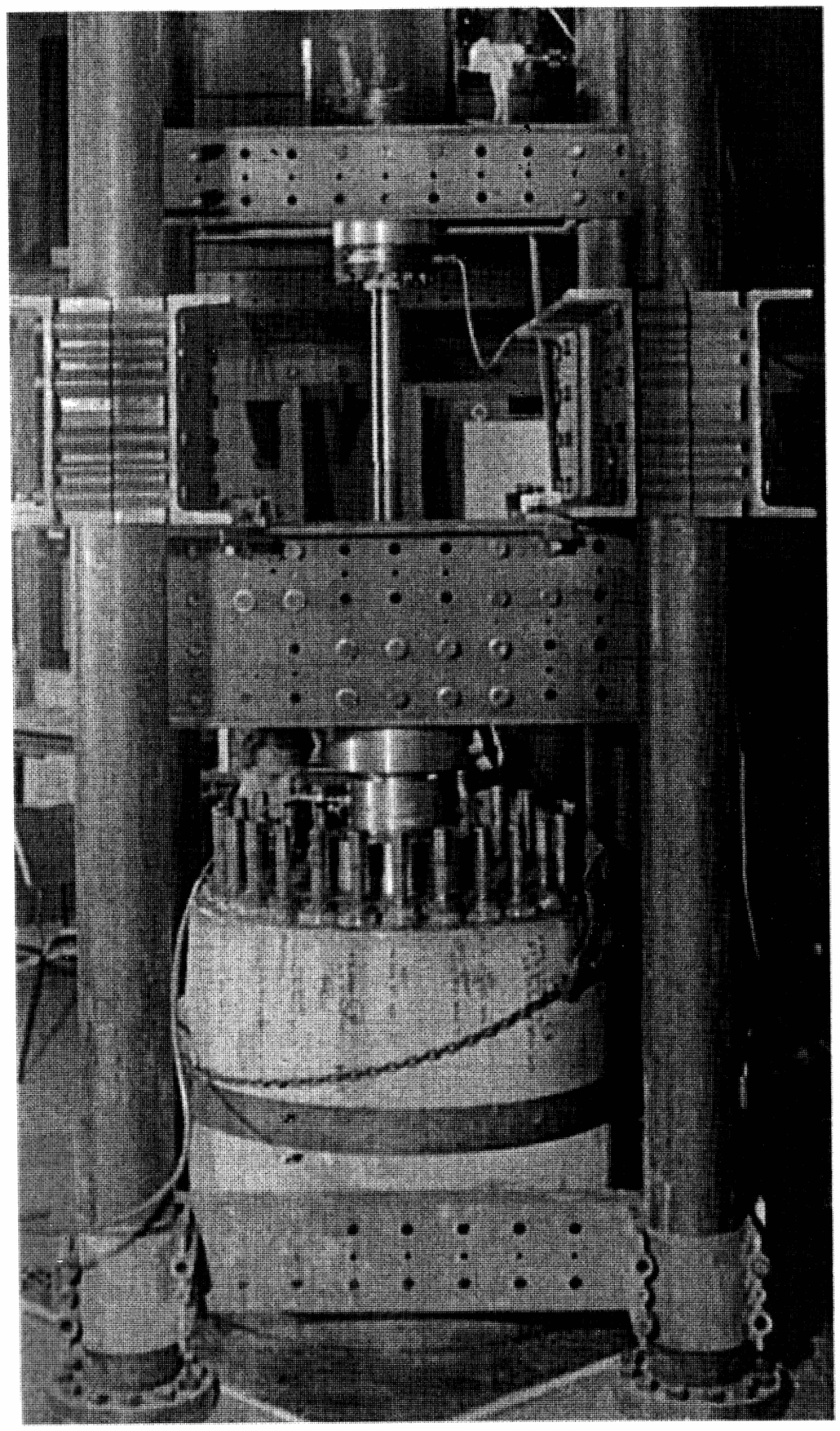

FIG. 6. Test Setup

Displacement Monitoring

Displacement of the whole test specimen was measured using three displacement transducers—one acting on the loaded bolt and the other two acting on neighboring bolts (Figure 7). Signals from the displacement transducers and from the load cell of the actuator were recorded every 2 s.

The displacement transducers measured the absolute movements of the loaded bolt and two neighboring nonloaded bolts.

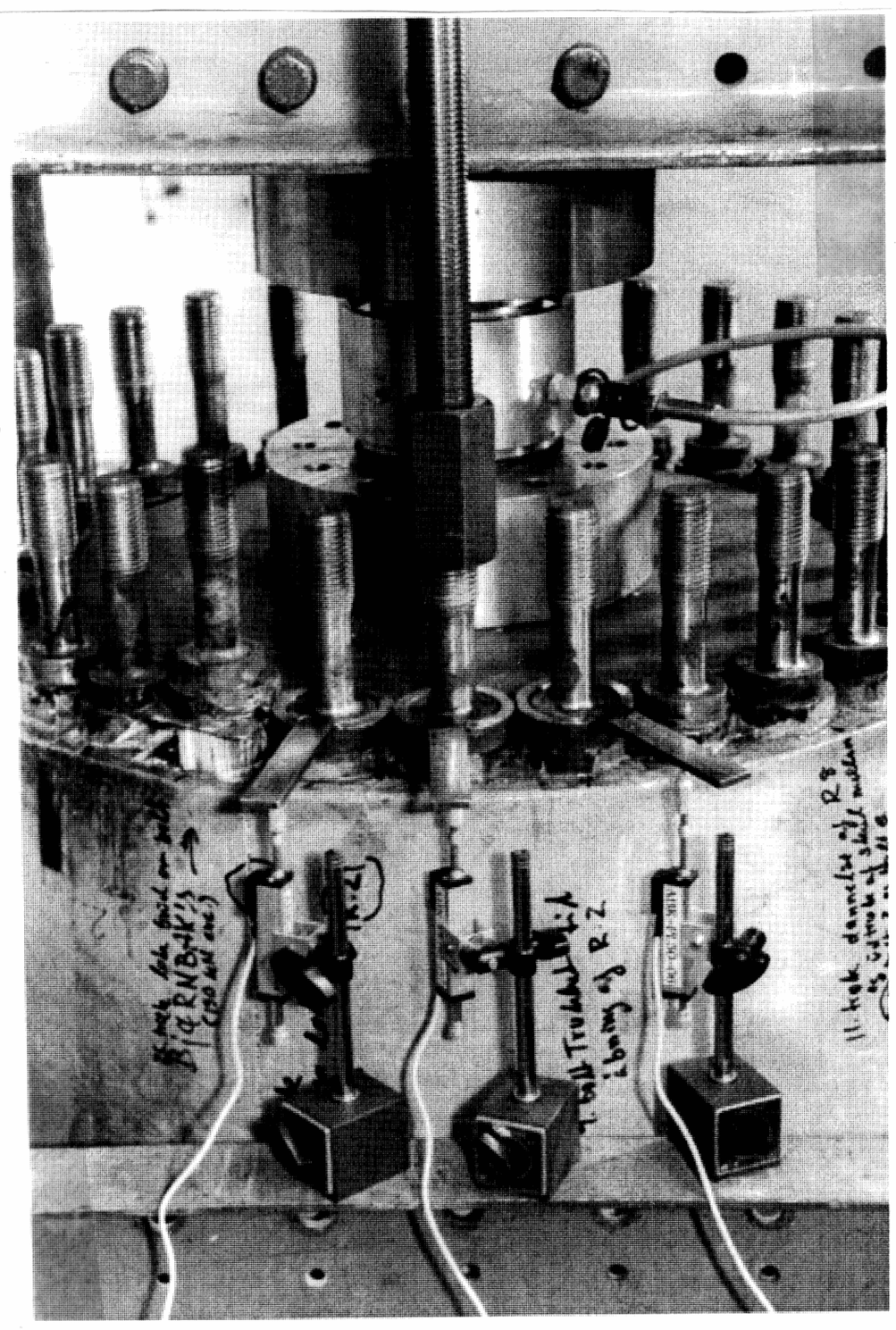

FIG. 7. Setup of Displacement Transducers

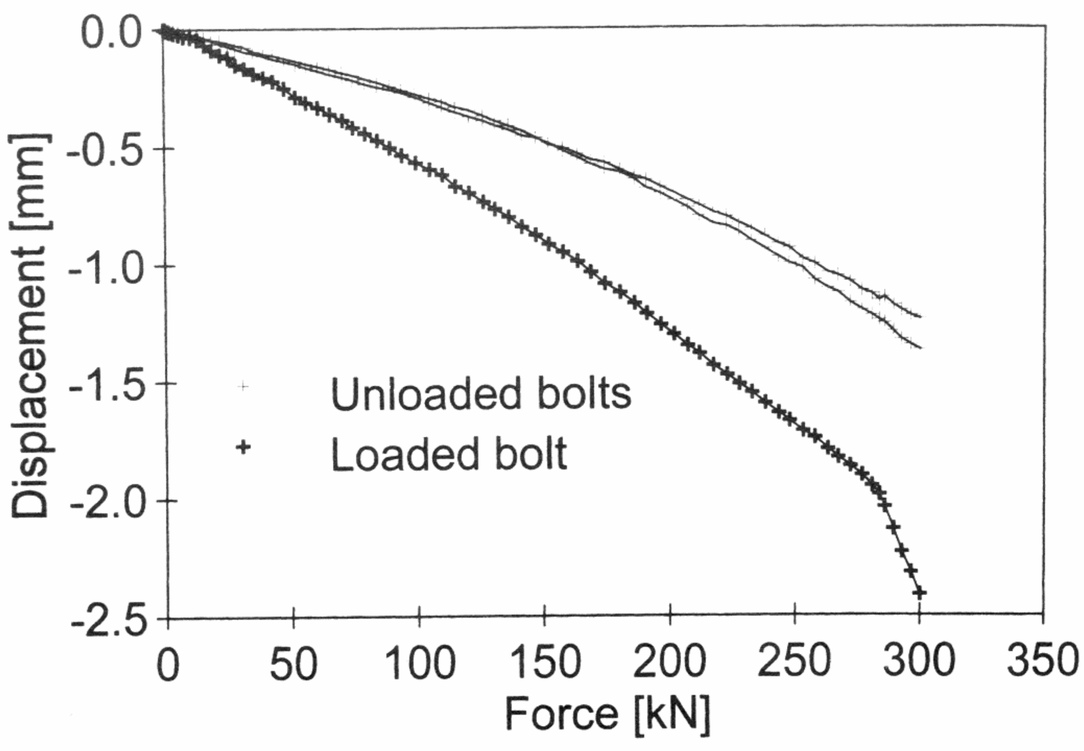

FIG. 8. Absolute Displacements of Three Neighboring Bolts

Fig. 8 shows an example of these displacement measurements. Subtraction of the displacements of the nonloaded bolts from the displacement of the loaded bolt is a measure of the displacement of the loaded bolt relative to the test specimen. This displacement measure is not restricted to the bolt and glue bond; it comprises the displacement of the wood in the proximity of the bolt as well.

Measurements with double instrumentation were made to estimate the uncertainty of the displacement measurements. The uncertainty was found to be one order of magnitude smaller than the displacement of the bolts measured relative to the test specimen.

Conduction of Tests

The bolts were spaced apart by only 30 mm of glulam, and there was a potential danger of successive progression of fractures if neighboring bolts were tested one after another. Hence, the testing was conducted in the following two series:

- First series of pullout tests bringing every second bolt to failure
- Second series of pullout tests bringing the remaining bolts to failure

The first series of pullout tests form the main results for the entire investigation. The tests were displacement controlled with a 4-min duration of each test. A total of 11 bolts were pulled out in this series. The results obtained in the second test series are of a more informative character as they may be influenced by the first test series. A total of 10 bolts were pulled out in this series.

RESULTS

Fracture Modes

In the majority of failures the bolts were pulled out like a cork from a bottle (i.e., a local brittle failure in the proximity of the bolt). Fig. 9 shows typical examples of failed bolts. Seven bolts were never tested as they were pulled off in one piece (Fig. 10). This was because of a drying crack along the inner perimeter of the bolt circle. The failure of a bolt can be described by dividing the fracture location into three categories:

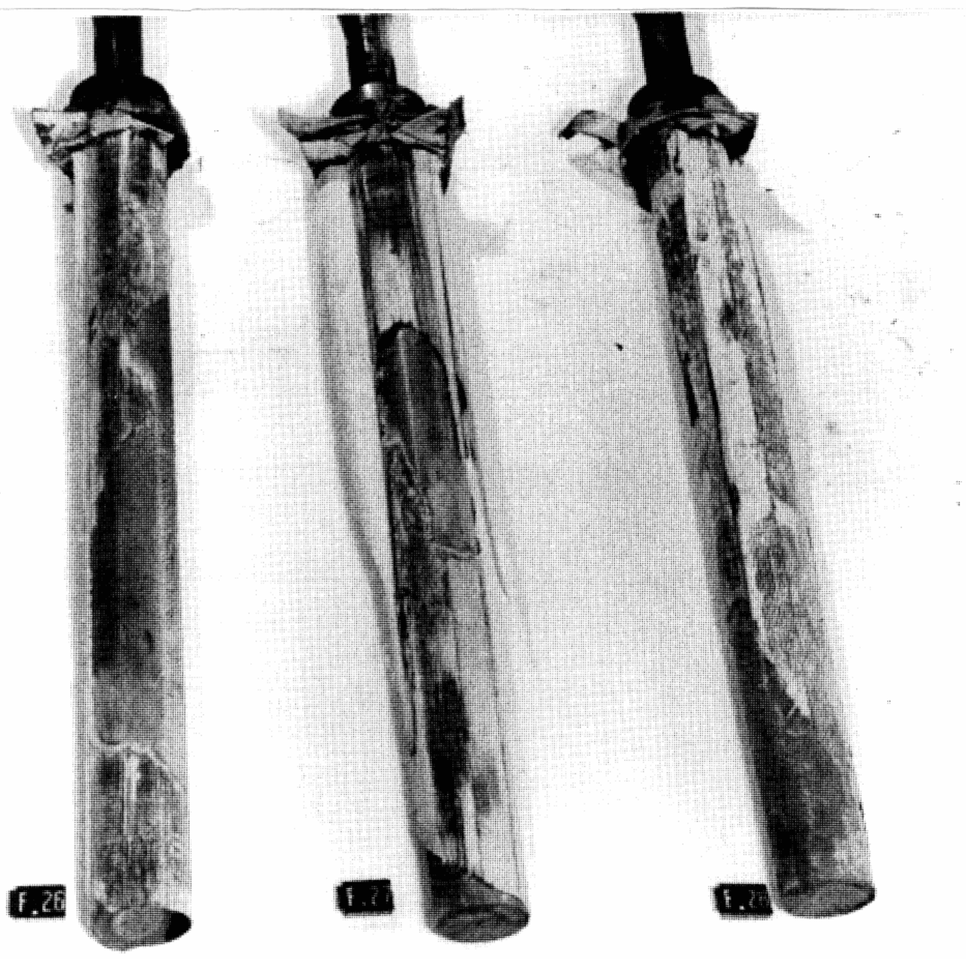

FIG. 9. Failed Bolts

- A—Fracture between bolt and glue
- B—Fracture between glue and glulam
- C—Fracture in wood in the proximity of the bolt

Fractures exposing the bolt surface occurred only in a few cases. The majority of fractures were between the glue and wood or in the wood only. The relative fracture locations are evaluated according to Categories A, B, and C in Table 5.

The bolts pulled out in the first series show the most characteristic "cork from a bottle" mode of failure. Testing and failure of one bolt influence the two neighboring bolts, which is verified by the data in Table 5. The fractures of bolts pulled in the second series tend to be in the wood surrounding the bolt rather than close to the bolt, suggesting that damage of the glulam was introduced during the first series of pullout tests. However, in each series there is no progressive shift from failure Categories A and B toward Category C.

No major flaws in the glue bond were observed on the exposed surface of the failed bolts. Few and small air voids were observed. A bolt, taken from the shell sections that failed in one part, was milled off exposing the sectional view shown in Fig. 3. This revealed slight inclination of the bolt in its hole and few air voids in the glue bond.

Strength and Stiffness

The pronounced difference in fracture phenomenology for the two series of pullout was also present for the ultimate strength. The first series of tests show a mean strength 20% higher than that obtained for the remaining bolts pulled out between the failed bolts. The results from the second test series are therefore excluded with respect to the determination of the remaining strength of the bolts.

The results of the first series of pullout tests are shown in Table 6. The value of the ultimate strength F_{ult} is given along with the ultimate displacement δ_{ult} of the loaded bolt relative to the test specimen. The mean of the obtained strength values is 362 kN with a standard deviation of 37 kN. The strength of the bolts was not negatively correlated to the progression of tests. This observation is crucial. It makes it reasonable to believe that the values of strength obtained in the first series

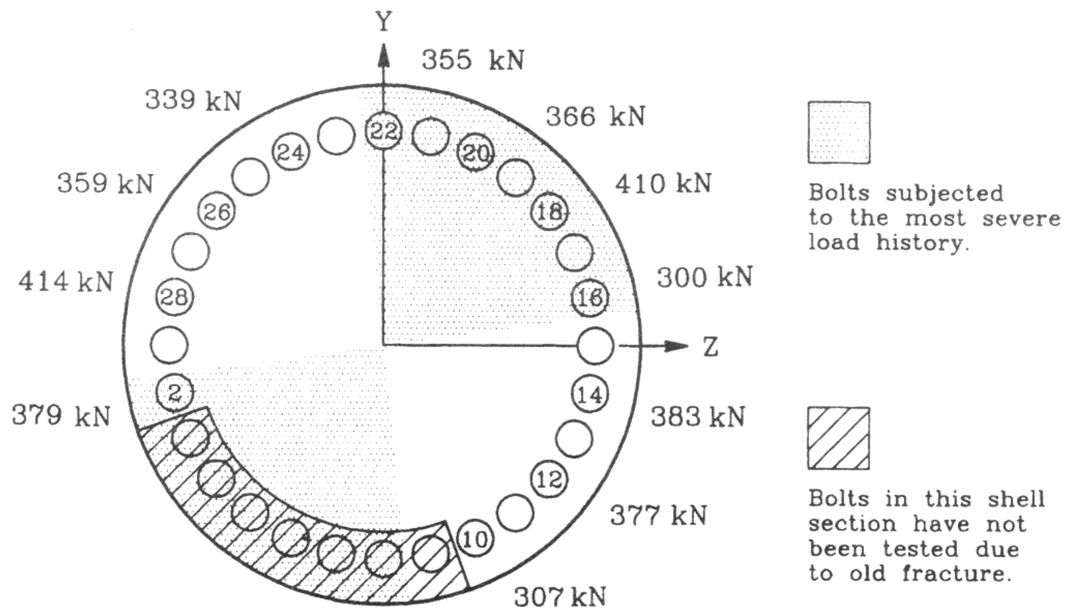

FIG. 10. Load History and Strength of Bolts Taken to Failure in First Test Series

TABLE 5. Fracture Location in Two Test Series

Series[a] (1)	Category A (%) (2)	B (%) (3)	C (%) (4)
First	14	52	34
Second	2	48	50

[a]Series in which bolts were tested.

TABLE 6. Results of First Series of Pullout Tests

Bolt number (1)	F_{ult} (kN) (2)	δ_{ult} (mm) (3)	F/δ (kN/mm) (4)	R^2 (5)
2	379	0.54	860	0.99
10	307	0.56	512	0.99
12	377	0.81	600	0.92
14	383	0.68	610	0.99
16	300	1.11	351	0.99
18	410	0.80	794	0.89
20	366	0.67	768	0.99
22	355	0.85	425	0.99
24	339	0.67	496	0.99
26	359	0.99	398	0.99
28	414	0.36	1,231	0.98

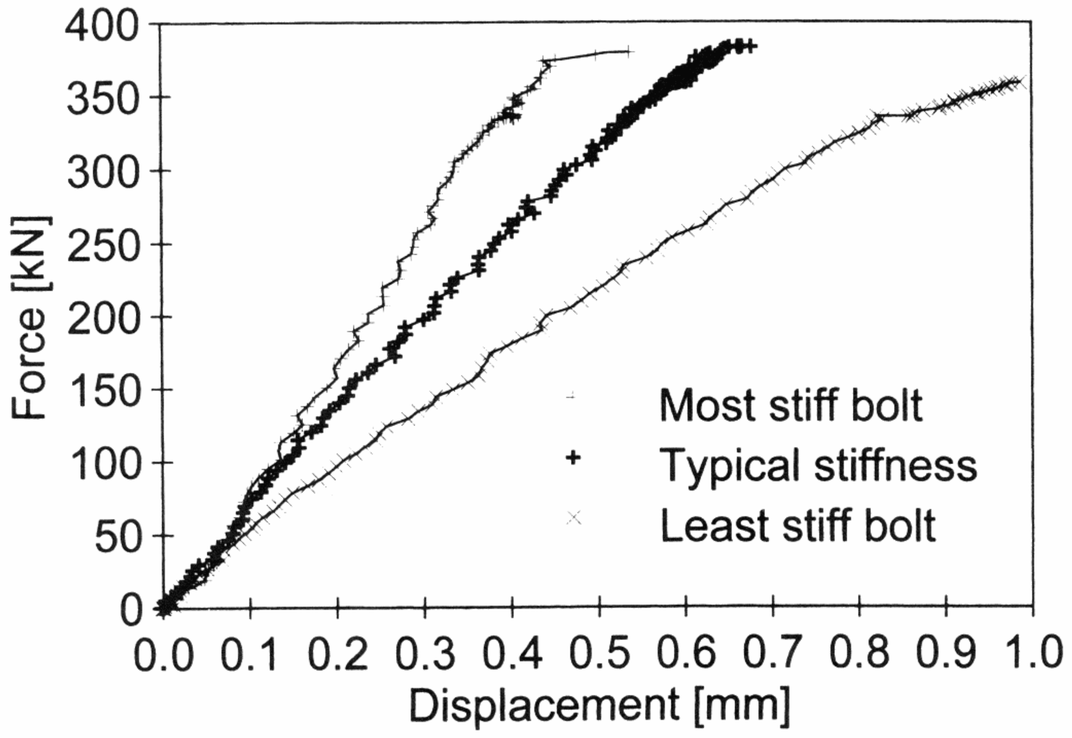

FIG. 11. Load-Displacement Curves

of pullout tests were unaffected by the test procedure. Thus, the strength values express the strength of the bolts after 9 years in situ loading. In the second test series the mean of the strength values is 304 kN with a standard deviation of 30 kN. The 20% loss of strength introduced by the testing procedure is distributed surprisingly homogeneously.

The stiffness F/δ of the connections, shown in Table 6, has been calculated on basis of the linear part of the load-displacement curves. The coefficients of determination, $R^2 > 0.98$ in most cases, verify the linearity. In Fig. 11 representative load displacement curves are shown. The curves follow the initial stiffness to failure and show no sign of plastic capacity of the connections.

DISCUSSION

Based on results from Riberholt and Spøer (1983) the predicted mean value of the virgin static short-term strength is 382 kN with a standard deviation of 34 kN [(1)]. The mean value of the residual strength obtained in the first test series shows a 5% strength reduction compared with this predicted virgin strength of the bolts. The difference in mean strengths can be confirmed at a 73% level of confidence. Although this confirms a difference between the compared mean values, it is important to note that the difference is of the same magnitude as the uncertainty introduced by the adjustment of the static short-term strength [(1)]. Hence, the strength reduction observed is not decisive in a discussion of potential fatigue damage.

The load history of the connection revealed that in terms of axial forces and load span the bolts were not subjected to the same load history. A relatively well-defined group of bolts was exposed to the most severe load history. In Fig. 10 the most severely loaded bolts are accentuated, and the values of

TABLE 7. Fatigue Data from Laboratory Tests and Condensed Version of In Situ Load History

Laboratory Tests—Low Level Fatigue on Three Bolts		In Situ Loading on Most Severely Loaded Bolt	
Load range $\{\alpha_1, \alpha_2\}$ (%) (1)	$N_{failure}$ (10^6) (2)	Load range $\{\alpha_1, \alpha_2\}$ (%) (3)	$N_{in\ situ}$ (10^6) (4)
$\{-20, 20\}$	12	$\{-5, 5\}$	13
$\{1. 30\}$	11	$\{-4, 6\}$	12
$\{-20, 20\}$	30	$\{-2, 7\}$	10
$\{1, 20\}$	12	$\{2, 12\}$	7
$\{1, 30\}$	44	$\{2, 14\}$	4

strength obtained in the first series of pullout tests are presented along with the bolt position. The graphical representation reveals no correlation between position and strength (i.e., load history and strength). As the mean strength values of the bolts in the two groups are the same, fatigue damage is not observed by this comparison.

Table 7 quotes data for three low-level laboratory fatigue failures obtained in the design phase (Riberholt and Spøer 1983) along with a condensed version of the fatigue load history of the most severely loaded bolt tested in the present investigation. A linear extrapolation of the laboratory fatigue data into 10^8 load cycles—corresponding to 20 years of service life—predicts the safe load range to be below 15% of the static tensile strength. Although the number of load cycles leading to failure in the laboratory fatigue tests is of the same magnitude as for the in situ loaded bolts, the load span is smaller. In a careful comparison, however, the number of cycles must be viewed in the light of the frequency of the load cycles, as a pure number of cycles approach to wood fatigue may be inappropriate due to the time-dependent strength properties of wood.

The frequency used in the laboratory tests (Riberholt and Spøer 1983) was 8.3 Hz, whereas the frequency of the in situ load cycles of the investigated bolts was 0.55 Hz (i.e., 15 times lower). The influence of the frequency of loading on fatigue failure in wood is not well known, but Bach (1975) reported that the number of cycles to failure is a poor measure of fatigue resistance during low frequency pulsation of clear wood. The results presented in Clorius et al. (1996) suggest that a decade of cycles to failure is lost when the frequency is lowered 15 times. If this frequency dependency is also present for glued-in bolts, the number of in situ load cycles quoted in Table 7 corresponds to 10 times as many laboratory loads cycles.

CONCLUSIONS

A total of 11 glued-in bolts have been pulled out from the root section of the wooden Nibe-B blade. The bolts experienced 9 years in situ load including a total of 50×10^6 load cycles, subjecting the bolts to axial loads ranging within 15% of the static short-term strength. The mean value of the residual static strength is 362 kN with a mean displacement at failure of 0.73 mm. An approximate load history has been reconstructed and the virgin short-term strength predicted. The following two observations are made:

1. No difference in residual strength is observed as a function of the load history.
2. The mean strength of the bolts is in accordance with the predicted short-term static strength.

It can be concluded that the bolts investigated maintain full strength after 9 years in situ loading.

ACKNOWLEDGMENTS

The research was founded by the Danish Ministery of Energy and the Danish electricity company ELKRAFT.

APPENDIX. REFERENCES

Bach, L. (1975). "Frequency-dependent fracture in wood under pulsating loading." *Proc., FPRS—Annu. Meeting.*

Clorius, C. O., Pedersen, M. U., Hoffmeyer, P., and Damkilde, L. (1996). "Fatigue damage in wood." *Proc., 1996 Int. Conf. on Wood Mech.*, 227–248.

Friis, P. (1984). "Nibe Møllerne, operation status March 1982–October 1983." *EEV. 84-03*, DEFU, Denmark (in Danish).

Johansson, C.-J., Serrano, E., Gustafsson, P.-J., and Enquist, B. (1995). "Axial strength of glued-in bolts. Calculation model based on non-linear fracture mechanics—A preliminary study." *Proc., CIB/W18 Meeting*, 28-7-9.

Øye, S. (1982). "Oscillating load calculation, Nibe-B wooden blade." *Notat VK-79-8202051*, DTH, AFM, Denmark (in Danish).

Rasmussen, B. (1993). "The wooden blade technology, state of the art 1982–1992." *EEV. 93-03*, DEFU, Denmark (in Danish).

Riberholt, H., and Spøer, P. (1983). "Glued-in bolts for the root to hub connection, Nibe-B windmill." *Tech. Rep. Ser. R No. 167*, Dept. of Struct. Engrg., DTU, Denmark (in Danish).

A Simple Size Effect Model for Tension Perpendicular to the Grain

M. Uhre Pedersen, C. O. Clorius, L. Damkilde & P. Hoffmeyer

Department of Civil Engineering, Technical University of Denmark. DK-2800 Lyngby

The strength in tension perpendicular to the grain is known to decrease with an increase in the stressed volume. Usually this size effect is explained on a stochastic basis, that is an explanation relying on an increased probability of encountering a strength reducing flaw when the volume of the material under stress is increased. This paper presents an experimental investigation on specimens with well defined structural orientation of the material. The experiments exhibit a large size effect and the nature of the failures encountered suggests that the size effect can be explained on a deterministic basis. Arguments for such a simple deterministic explanation of size effect is found in finite element modelling using the orthotropic stiffness characteristics in the transverse plane of wood.

1 Background

Size effect in tension perpendicular to the grain may be approached in one of the following ways:

- Weakest link theory, i.e. a stochastic failure model assuming that failure is determined by Weibull distributed weak elements.
- Damage relevant Weibull stresses, i.e. a stochastic approach taking into account stress peaks introduced by the transverse elastic anisotropy.
- Fracture mechanical size effect, i.e. a model based on the ratio between the release of potential energy and the energy consumption in the fracture process.
- Simple stress criterion on stress peaks introduced by the transverse elastic anisotropy.

1.1 Weakest link theory

Size effect in wood is traditionally explained with stochastic arguments that can be summarized as follows:

- Assume that strength reducing flaws are distributed so that the probability of encountering strength higher than x in a unit volume is $1 - F(x)$.
- The number of flaws is proportional to the volume.
- The strength of a given volume of wood is determined by the strength of the weakest spot. This assumption is equal to a brittle failure theory and makes it possible to establish a relation between the strength of a given volume and a chain of n unit volumes.
- The probability of encountering strength higher than x in a chain of n unit volumes is $[1 - F(x)]^n$.

One of the solutions to the above extreme value problem is a Weibull distribution, which takes the following form:

$$F_V(x) = 1 - exp[-\{(x - \epsilon)/\delta\}^k V], \tag{1}$$

where k is the shape parameter, V the volume, δ is a scale factor and ϵ is a lower limit of strength. When $\epsilon = 0$, the lower limit of strength is zero and (1) is a 2-parameter Weibull distribution.

The volume in (1) is assumed to be uniformly stressed. The volume dependent strength can be predicted from the strength distribution for a specific volume, V_0, as the probability of strength values lower than x at the volume V is set equal to the known probability $F_{V_0}(x_0)$:

$$1 - exp[-\{x/\delta\}^k V] = 1 - exp[-\{x_0/\delta\}^k V_0], \tag{2}$$

whereof

$$x = x_0 \{\frac{V_0}{V}\}^{\frac{1}{k}} \tag{3}$$

The consequence of (3) is that the strength should decrease with increase in volume. In a double logarithmic diagram the relation is linear with slope $-1/k$.

In (Barrett 1974) different experimenters' results on tension perpendicular to grain are explained by use of the weakest link theory. The strength decreases with volume according to (3) and the shape parameter is found to be larger for clear than for commercial material. It is concluded that the strength distribution at constant volume may be due to a parent Weibull distribution. In (Larsen & Riberholt 1981) a size effect for Scandinavian wood is presented. The findings are similar to those in (Barrett 1974) and it is concluded that the strength variation with volume may be described by a parent two parameter Weibull strength distribution with shape parameter of about 5. In (Mistler 1998) a comprehensive investigation of numerous experimental results is presented. It is suggested that volume is replaced by height in the design equations as the strength is found to vary more with specimen height than with specimen volume.

1.2 Damage relevant Weibull stresses

In (Ranta-Maunus 1996) it is suggested to use an integration of the tension stress state perpendicular to the grain in order to incorporate the non-uniform stress state introduced by the transverse anisotropy and transient moisture induced stresses in a failure model. The effective stresses, or damage relevant Weibull stresses, are calculated according to:

$$\sigma_{t,90,Wei} = \left(\frac{1}{V} \int_V \sigma_{t,90}^k \, dV \right)^{\frac{1}{k}} \tag{4}$$

The Weibull stress, $\sigma_{t,90,Wei}$, is the value of constant stress that gives the same probability of failure as the actual stress distribution. In (4) k is the shape parameter of the Weibull distribution. The idea of damage relevant stresses is to weigh local stress peaks according to the Weibull theory.

The non-uniform stress state introduced by the anisotropy is reported in (Hanhijärvi & Ranta-Maunus 1996) and (Castéra & Lac 1997) and the approach using damage relevant Weibull stresses as given in (4) is used in e.g. (Aicher, Dill-Langer & Ranta-Maunus 1998) with the modification that the integral over the stressed volume is replaced with an integral along a line.

1.3 Fracture mechanical size effect

Decreasing nominal strength, σ_N, for increased structural size can be explained both within linear and non-linear fracture mechanics. An approximate non-linear size effect model (5) is offered by Bažant & Pfeiffer (1987) and used in (Aicher & Reinhardt 1993, Aicher, Reinhardt & Klöck 1993) to model experiments on single edge notched wood specimens.

$$\sigma_N = B \, f_t \sqrt{1 + \frac{d}{D_0}}, \tag{5}$$

where σ_N is the nominal strength, B is an empirical constant depending on the geometry of the test specimen, f_t is tension strength in a pure strength failure criterion, d is a typical specimen dimension and D_0 is an empirical constant containing the length of the fracture process zone. The ratio d/D_0 expresses the brittleness of the specimen, for low values of the ratio the specimen fails according to a strength failure criterion and for high values the nominal strength is proportional to $d^{-\frac{1}{2}}$ as in linear elastic fracture mechanics. For intermediate values the softening properties governs the relation between nominal strength and size.

1.4 Simple maximum stress failure criterion

The model using damage relevant Weibull stresses incorporates stress peaks due to material anisotropy in a stochastic failure model. However, a simple maximum stress failure criterion uses the stress peaks

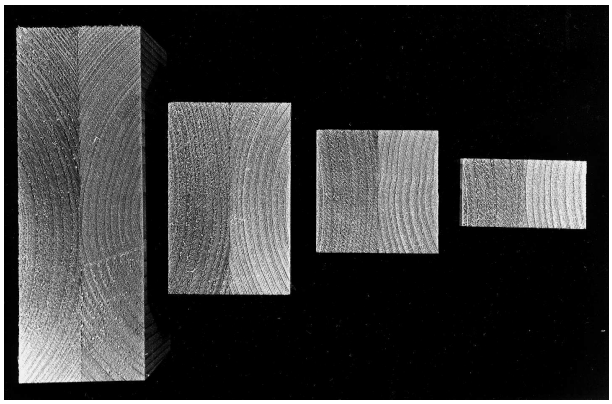

Figure 1: *Endview of specimens showing the intended double symmetry.*

directly in a stress failure model. The occurrence of stress peaks is due to cylindrical orthotropic material stiffness and in case of glulam also the regular pattern of lamination. This stiffness distribution gives rise to stress concentrations which may increase with increase in specimen size and hence give rise to a deterministic size effect. The simple maximum stress criterion states that the nominal strength is a function of stiffness orthotropy, geometry and an inherent material strength, $f_{t,90}$:

$$\sigma_N = f(\textit{stiffness orthotropy, geometry, } f_{t,90}) \tag{6}$$

The experimental observations and FEM-modelling presented in the present investigation lend themselves to a such simple stress failure criterion.

2 Experiments

2.1 Specimens

The clear wood material is taken from a large population of boards of Norwegian grown spruce, *Picea abies*. The boards were subdivided into three groups using an annual ring width criterion. In each group the boards were paired and glued sapwood to sapwood forming planks with symmetrical cross sections. Three planks, one from each annual ring width group, were chosen for the size effect investigation. After conditioning to 65% RH, 22° C, the planks were planed to 45 x 130 mm and cut to lengths of 70 mm avoiding knots and other visible flaws. Twelve clear specimens with a base of 70 x 45 mm and a height of 130 mm were taken from each plank. In random order these were shortened to heights of 25, 45, 70, 130 mm giving four groups of specimens with double symmetry, Figure 1. The base of the specimens was glued to a 20 mm thick aluminium plate using an epoxy glue. The plate had a groove for fixation in the test machine, Figure 2. In order to prevent failure in the wood-aluminium interface the specimens

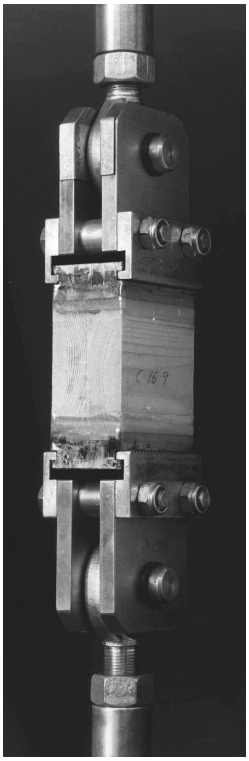

Figure 2: *A 70 mm high specimen mounted in the test machine.*

were locally reinforced with a thin strip of glass fibre in epoxy wrapped about the specimens along the interface.

The clear wood specimens are designed to be used in a fatigue test program providing information about the fatigue strength of wood in tension perpendicular to the grain. The specimen design secures failure at the free length of the specimen in a radial plane as shown in Figures 3 and 4. The design gives a lower bound estimate of the material strength as the tangential strength is smaller than the radial strength.

LVL specimens with a base of 70 x 45 mm were cut in random order from an LVL beam producing specimens with heights in the transverse direction of 25, 45, 112 and 230 mm. Six specimens at each height were tested in tension perpendicular to the grain in the same way as the clear wood specimens.

2.2 Tests

Both clear wood specimens and LVL specimens were taken to tension failure perpendicular to the grain in a 100 kN servo hydraulic Instron test machine. The load was applied in a double charnier set up, Figure 2. The tests were load controlled with a load application rate of 0.026 MPa/s giving mean times to failure of 100 seconds.

Height	Strength $[MPa]$										
$[mm]$	Series A			Series B			Series C			Mean	Stdev.
25	3.40	3.23	3.03	3.94	3.21	3.61	2.93	3.98	4.05	3.49	0.43
45	2.48	2.57	2.09	2.62	2.65	2.92	3.02	2.86	3.00	2.69	0.30
70	1.79	1.96	1.55	2.19	2.44	2.54	1.68	1.98	2.86	2.11	0.43
130	1.48	1.45	1.27	1.73	1.75	2.02	1.57	1.52	1.82	1.62	0.23
Mean	2.19			2.64			2.61				
ρ $[kg/m^3]$	418			460			479				

Table 1: *Strength values and density for three series of clear wood specimens.*

To get an estimate of the strength in the radial direction each of the 45 mm high specimens were matched with a specimen rotated 90° and tested in tension in the radial direction.

The stiffness in the radial and tangential direction of the clear wood has been determined in a test series comprising 43 specimens with dimensions 20 x 20 x 20 mm. Material from both boards in all three planks was used. The stiffnesses were determined in compression.

3 Test Results

3.1 Clear wood tests

The strength values for the four different specimen heights within each of the three series are presented in Table 1. The strength is seen to decrease more than 50% when specimen height is increased approximately 5 times. The material presented covers three test series A, B and C. Specimens within a series originate from the same plank forming a unity with respect to density and other inherent properties, hence each series constitutes a statistical block. The strength variation between series is reflected in the mean density, ρ, at 65% RH, Table 1.

3.1.1 Failure location

Independent of specimen height all specimens fail in mid section planes as shown in Figure 3. Due to the specimen design the mid section of the specimens form a radial plane, Figure 4.

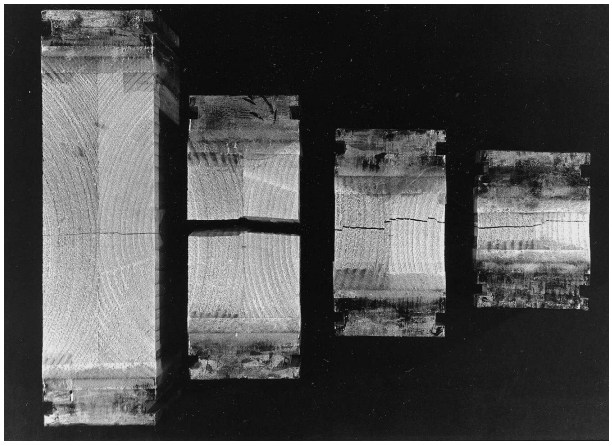

Figure 3: *All specimens fail in mid section radial planes.*

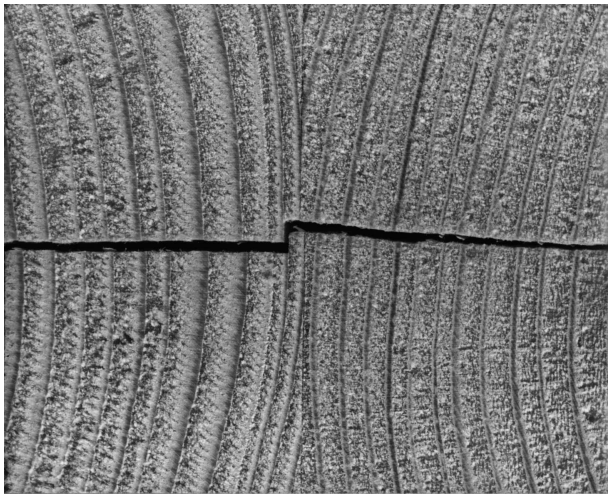

Figure 4: *Close-up of failure zone.*

Stress direction	Mean strength	Stdev.	Mean stiffness	Stdev.
Tangential	2.7	0.3	637	175
Radial	3.3	1.1	851	213

Table 2: *Strength and stiffness in tangential and radial directions, [MPa].*

Height [mm]	Strength [MPa]						Mean	Stdev.
25	1.82	1.86	1.85	1.61	1.42	1.89	1.74	0.19
45	1.47	1.50	1.43	1.61	1.52	1.48	1.50	0.06
112	1.39	1.57	1.50	1.55	1.18	1.60	1.46	0.16
230	1.30	1.46	1.75	1.48	1.44	1.32	1.46	0.16

Table 3: *Strength values for LVL specimens.*

3.1.2 Radial and tangential strength and stiffness

The consistent failure location is a result of the difference in strength in radial versus tangential direction. Table 2 lists the tension strength results from tests in radial and tangential direction. The stiffness determination from small oriented compressive tests is also given. As seen from Table 2 the strength in the radial direction is approximately 20% higher than the strength in the tangential direction. Most of the failures in the radial directions were in or initiated in the glue line. However, significantly higher strength were obtained for failure outside the glue line indicating that the radial strength is even higher than apparent from Table 2.

3.2 LVL tests

The material used for the LVL specimens have a mean density of 504 kg/m^3 at 65% RH. Table 3 shows strength values for all tested specimens. No major change in strength as function of height is observed. No systematic failure location was observed.

4 Finite element modelling

A plane finite element modelling of the specimens is used to model the stress distribution as function of specimen height and the influence of differences in tangential and radial stiffnesses. The stiffnesses are given in polar coordinates according to Figure 5. The origo for the polar coordinates lies in the pith which has been determined to lie 85 mm from the centre of the specimens as a mean for all six boards involved. With reference to the experimental values in Table 2, E_r and E_t are chosen to 900 MPa and

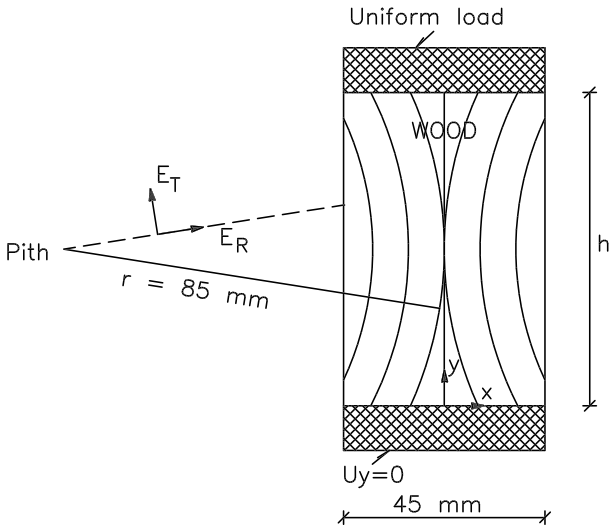

Figure 5: *Specifications for FE modelling.*

600 MPa respectively. Hearmon (1948) here quoted from (Kollmann & Côté 1984) reports a value of G_{rt} of 30 MPa for equivalent values of E_r and E_t. Poissons ratio, ν_{rt}, is set to 0.3.

Eight node isoparametric elements in plane stress are used. The specimen is meshed with 22 elements in the x-direction and 100 elements in the y-direction. A uniform load is applied to an aluminium plate similar to the experimental setup. The boundary conditions are given in Figure 5.

4.1 Results of FEM modelling

The differences in stiffness in tangential and radial direction leads to an inhomogeneous stress distribution. Figure 6 shows a contour plot of the tangential stress, σ_t, for a 130 mm high specimen. The stress peak at the corner of the specimen is due to the restriction of transverse deformation introduced by the stiff aluminium plate. In practice failure initiated by this peak was prevented by the described reinforcement of the glue line interface.

Failure is located in the mid section where the stress distribution depends on the test specimen height and the cylindrical orthotropy. For a very short specimen the influence from the cylindrical orthotropy is less pronounced and the stress distribution converges towards a homogeneous distribution. Conversely, the higher the specimen the more pronounced is the inhomogeneous stress distribution generated by the stiffness difference in radial and tangential directions. The distribution of tangential stresses plotted in Figure 7 is the outcome of a modelling with stiffness parameters as given in Section 4. The ratio between E_r and E_t is chosen as 1.5; in the literature the ratio is often set to 2. Generally an increase in this ratio will augment the difference between stress distribution for the four specimen heights. The ability

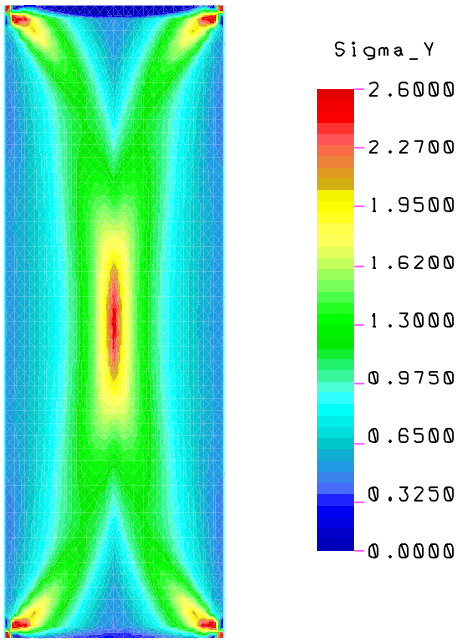

Figure 6: *Contour plot of tangential stresses in 130 mm specimen for an applied uniform external stress of 1 MPa, stress in aluminium interface not shown.*

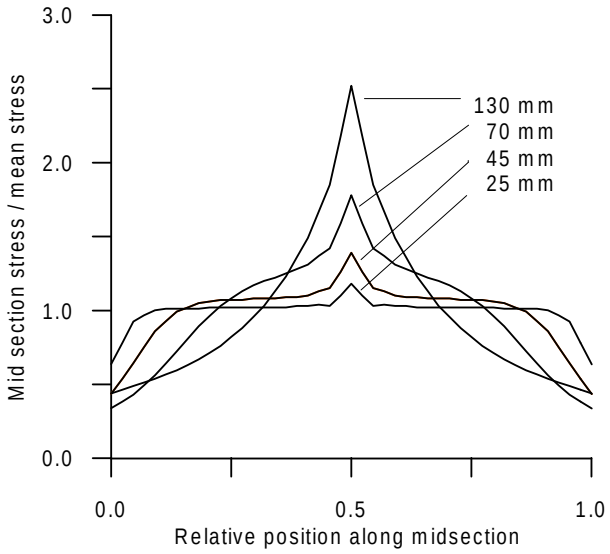

Figure 7: *Plot of tangential stresses along the mid section for the different specimen heights.*

to generate an inhomogeneous distribution is also dependent on the magnitude of the shear modulus; the general observation is that an increase of shear modulus will reduce the effect of the ratio between E_r and E_t.

5 Discussion

5.1 Statistical treatment of results

The strength of the clear wood specimens decreases with specimen height, whereas the influence of density difference between planks is reflected in the increase in mean strength from series A to C. Strength values and density are shown in Table 1. A linear two-factor statistical model is used to analyse the strength response, Y_{ijk}, as the sum of overall mean, μ, effect of plank, p_i, effect of height, h_j, and random error of the individual specimen, E_{ijk}:

$$Y_{ijk} = \mu + p_i + h_j + E_{ijk} \tag{7}$$

Both p_i and h_j are significant with levels of confidence in excess of 99.9%. A Newman-Keuls test on the differences between the effects of height shows that $h_1 \neq h_2 \neq h_3 \neq h_4$ at a level of confidence higher than 99%.

The analysis implies that the data is normally distributed. This assumption is confirmed by a normal probability test on the residuals, E_{ijk}, from the analysis. The data proves to fit slightly better to a log-normal distribution, $X_{ijk} = \log Y_{ijk}$. However, this transformation has little practical implication as the strength response Y_{ijk} covers a relatively narrow range. In Figure 8 (a) the strength values given in Table 1 are shown as function of specimen height in a double logarithmic diagram. The data has been cleaned for the scatter between series introduced by the effect of plank, i.e. the corrected values $Y_{jk} = Y_{ijk} - p_i$ are plotted against height. The graphs show that a linear correlation in a double logarithmic plot provides a good empirical fit to the data.

The LVL specimens do not show a consistent strength variation with height. Though the higher strength of the 25 mm high specimens is statistically significant there is no significant trend in the data, Figure 8 (b).

5.2 Modelling

5.2.1 Weibull weakest link

According to the Weibull weakest link theory the probability of encountering a weak spot is increased with increased volume. However, independent of specimen height, all clear wood specimens fail in the

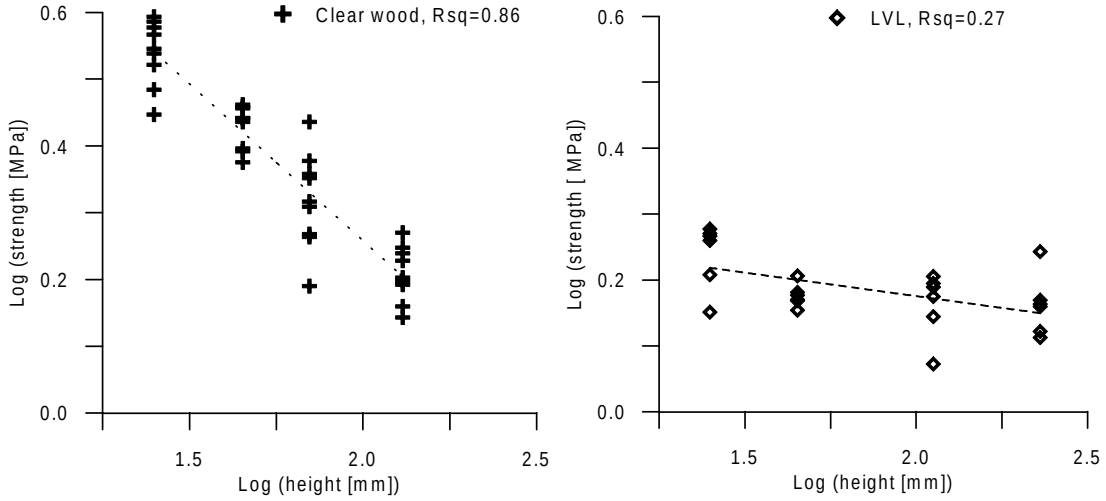

(a) Clear Wood

(b) LVL

Figure 8: *Log(strength) versus log(height).*

mid section radial plane as shown in Figure 3. The consequence of this deterministic failure location is that the strength cannot depend on the strength distribution in the material outside the failure zone. As the mid section radial plane is the weakest, the strength distribution outside this zone is of no importance to the strength of the specimen, and the strength decrease with increased volume cannot be explained by the Weibull theory. Furthermore, the LVL specimens show practically no strength variation with volume in the investigated range, even though LVL is a prime example of a Weibull material as it is full of strength reducing flaws. In Figure 9 the mean strength for both clear wood and LVL specimens are plotted together with results from (Larsen & Riberholt 1981). Larsen & Riberholt (1981) find a slope of approximately -0.2 corresponding to a shape parameter $k = 5$ in the Weibull distribution. This is the commonly recognized value of k also reported in (Barrett 1974) for commercial timber, and used in (EC5-1 1995). The clear wood specimens follow a different trend as the slope of the results is approximately -0.5. If the size effect observed for clear wood specimens was governed by a weakest link phenomenon this would correspond to the shape parameter $k = 2$. A Weibull distribution with shape parameter $k = 2$ has a larger variance than a distribution with $k = 5$ as the distribution contracts for higher values of the shape parameter. However, in this investigation the coefficient of variation is of the same order as in e.g. (Larsen & Riberholt 1981), namely 10% to 30%.

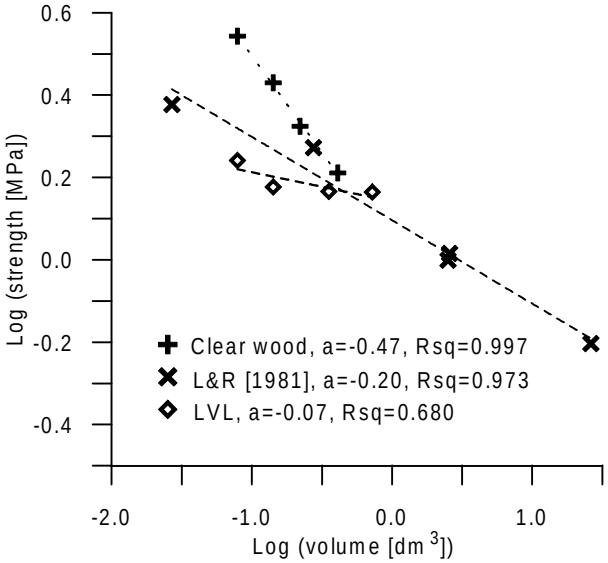

Figure 9: *Mean values from this investigation and mean values from (Larsen & Riberholt 1981).*

5.2.2 Damage relevant Weibull stresses

The concept of Weibull damage relevant stresses is appealing as it offers a means of taking into account non-uniform stress state in a volume where the strength at uniform stress is Weibull distributed.

When the non-uniform stress state is generated by external factors such as specimen geometry or loading configuration, correction to the effective volume is clearly necessary. Stress peaks in a necked tension specimen or in a simple bending specimen where the ultimate strength is governed by tension perpendicular to the grain are less harmful as they cover a limited volume. Corrections for such non-uniform stress distribution have been made in (Barrett 1974) by use of the same principle as given in (4).

Interaction between the Weibull strength distribution and non-uniform stress distribution is easily understood when the non-uniform stress is due to external factors. However, in (Ranta-Maunus 1996) the suggestion is to use (4) to include stress peaks generated by internal factors, i.e. the stiffness distribution. The authors see two problems connected to the concept of damage relevant Weibull stresses:

- The damage relevant Weibull stresses use a deterministic determination of stress distribution due to internal stiffness distribution. This stress distribution is then used in a stochastic model which originally tacitly included the same non-uniform stress distribution as a stochastic phenomenon.

- The shape parameter used in the damage relevant Weibull stress model cannot be determined directly in experiments, as it is correlated to an ideally uniformly stressed material and not the values for tests on the real material in itself influenced by local stress peaks.

Height	Damage relevant Weibull stresses $[MPa]$			
$[mm]$	$k = 2$	$k = 5$	$k = 10$	$k = 100$
25	3.49	3.53	3.57	3.98
45	2.73	2.84	2.96	3.61
70	2.22	2.50	2.79	3.60
130	1.79	2.35	2.89	3.88

Table 4: *Value of the damage relevant Weibull stress for different values of the shape parameter.*

The failure criterion in (4), as proposed in (Aicher et al. 1998), is implemented using the experimental mean strength for each height and the stress distribution along the mid section shown in Figure 7. The emerging damage relevant Weibull stresses are shown in Table 4. If the stress integration in (4) yields a reliable failure criterion a shape parameter must exist such that the damage relevant Weibull stresses take a constant value independent of specimen height. A value of $\sigma_{t,90,Wei}$ that deviates in the order 10% takes a shape parameter in the order of 100. This value of the shape parameter fitted to correspond to the ideally uniformly stressed material practically excludes size effect in this material as the slope in a log(strength)–log(volume) depiction takes the slope $-1/100$.

5.2.3 Fracture mechanical size effect

The size effect observed for the wood specimens conforms with the size effect expected from linear elastic fracture mechanics, i.e. $\sigma_N \propto d^{-\frac{1}{2}}$. However, the LVL specimens show no such variation with size. The clear wood and the LVL specimens were geometrically similar. According to (Fonselius 1986) the fracture toughness in the relevant radial plane is approximately 267 $kNm^{-3/2}$ for clear spruce and approximately 300 $kNm^{-3/2}$ for LVL and Gustafsson, Hoffmeyer & Valentin (1998) finds the values 272 J/m^2 and 310 J/m^2 for the fracture energy perpendicular to grain, G_{fy}, for glulam and LVL respectively. For these reasons the brittleness expressed as d/D_0 in Equation (5) is equal for the clear wood and LVL specimens of equal size. Hence, the size effect for the clear wood specimens cannot be of fracture mechanical origin as it is not seen for the – in relevant aspects – similar LVL specimens.

5.2.4 Simple maximum stress failure criterion

In the preceding sections three existing models have been questioned as explanatory basis for the observed size effect. The elaborate models are suggested replaced by a simple maximum stress failure criterion based on the following arguments:

- The stiffness orthotropy in the transverse plane introduces a regular, inhomogeneous pattern of stress.
- This regular pattern leads to an increasing stress inhomogeneity for increasing size, thus giving rise to the size effect.

In this explanation the regularity of the wood structure, rather than weak spots and flaws as supposed in the weakest link theory, is responsible for strength reduction with increasing size.

The experimental evidence is the decrease in nominal strength with increased specimen height for the cylindrical orthotropic clear wood specimens and the absence of size effect for LVL specimens. The stiffness distribution of the LVL specimens differs from that of the clear wood in that the cylindrical orthotropy has been straightened out to a cartesian in the manufacturing process. Further the FEM simulations show increase in the stress inhomogeneity with increased height, Figure 7, for the cylindrical orthotropic wood specimens. In order to compare experiments and simulations it is assumed that failure occurs when the stress at any point, σ, reaches an inherent failure strength:

$$\sigma = f_{t,90} \tag{8}$$

By use of (8) a nominal strength, $\sigma_{N,FEM}$, can be calculated from the stress intensification factor, α. The stress intensification factor is determined as the ratio between the maximum stress, $\sigma_{max,FEM}$, and the applied external stress, $\sigma_{applied,FEM}$:

$$\sigma_{N,FEM} = \frac{\sigma_{applied,FEM}}{\sigma_{max,FEM}} f_{t,90} = \frac{1}{\alpha} f_{t,90} \tag{9}$$

As a means of comparison between experimentally determined nominal strength, σ_N, and modelled nominal strength, $\sigma_{N,FEM}$, the values of the nominal strength have been normalised with the value for the 130 mm high specimens in Table 5. In this way the unknown inherent failure strength $f_{t,90}$ vanishes. The experimental values of normalized nominal strength, $\frac{\sigma_N}{\sigma_{N,130}}$, and the modelled normalized nominal strength values, $\frac{\sigma_{N,FEM}}{\sigma_{N,130,FEM}}$ coincide within approx. 10%. The consequence is that the stress inhomogeneity which increases for increased specimen height can explain the size effect observed. The good agreement between experimental observations and numerical simulations shown in Table 5 is the outcome of a specific choice of elastic constants and a simple maximum stress failure criterion. It may be argued that a more realistic failure criterion is an integration of stresses in excess of a critical value. This, however, would not change the general picture. The finite element model is fairly stable to perturbations of the values of the elastic constants, and a more refined stress failure criterion could be applied without violating the main point, namely that a given mean stress generates higher stresses in higher specimens.

Height	Experiments		FEM simulations	
$[mm]$	$\sigma_N\ [MPa]$	$\frac{\sigma_N}{\sigma_{N,130}}$	$\frac{1}{\alpha}=\frac{\sigma_{applied,FEM}}{\sigma_{max,FEM}}$	$\frac{\sigma_{N,FEM}}{\sigma_{N,130,FEM}}$
25	3.5	2.2	0.85	2.1
45	2.7	1.7	0.72	1.8
70	2.1	1.3	0.56	1.4
130	1.6	1	0.40	1

Table 5: *Normalized nominal strength from experiments and simulation (index FEM).*

5.3 Implications

The difference between a simple maximum stress failure criterion and the traditional Weibull approach is whether the strength perpendicular to the grain is a deterministic or stochastic parameter. In the weakest link theory the material is assumed to fail when the mean stress reaches a stochastic volume dependent strength:

$$\sigma_{mean} = f_{t,90}(\textit{strength distribution, volume}) \tag{10}$$

The simple maximum stress failure criterion operates with a deterministic material strength, $f_{t,90}$, and a deterministic stress distribution depending upon stiffness orthotropy and geometry variables including dimension of the loaded wood member as well as annual ring pattern. Failure is reached when the maximum value of the stresses reaches the material strength:

$$\sigma_{max}(\sigma_{mean},\ \textit{stiffness orthotropy, geometry}) = f_{t,90} \tag{11}$$

Due to the character of the failure criterion (11) the observed relation between specimen height and strength, Figure 9, is just an accidental function of the chosen test specimens, their height and special symmetrical geometry, Figure 1. For other specimen geometries other relations between size and strength are expected. As an example, it is well documented in the literature that a standard glulam cross section yields $\sigma_N \propto \text{volume}^{-0.2}$.

The practical implication of the proposed failure criterion may be that the stress distribution e.g. in a standard glulam cross section can be manipulated to yield higher nominal strength. In a glulam cross section all lamellas except the outer have the same orientation. This high degree of global cross sectional regularity combined with the regularity of stiffness distribution within each lamella can make the cross section concentrate the carrying stresses in a wedge shape pattern. In (Hoffmeyer, Damkilde & Pedersen 2000) this is shown in compression for an idealized cross section of six lamellas with the same pith distance and location; a stress intensification of $\alpha = 4$ is observed over 6 lamellas. Other references

e.g. (Aicher & Dill-Langer 1997) do not see this global interaction between lamella and cross sectional lay-out as different pith location for each lamella reduces the development of a regular wedge shaped pattern of carrying stresses. In (Castéra & Lac 1997) both an idealized and a more random cross section is modelled. A wedge shaped pattern of carrying stresses is a function of the lamellas concentrating stresses in the same direction, and can be avoided if every second lamella is reversed. This may of course be prohibitive in other respects but would diminish if not remove a deterministic stress peak induced size effect.

6 Conclusion

The paper reports tension perpendicular to the grain tests on small clear spruce and LVL specimens from which the following observations are made:

- There is a large size effect for small clear specimens.
- The failure location is predetermined independent of specimen size.
- Geometrical similar specimens of LVL show no size effect.
- A FEM analysis shows the stress inhomogeneity to increase with specimen height.

The observations are attempted explained within the Weibull weakest link model, a damage relevant Weibull stress model and a fracture mechanical size effect model but the most promising is a simple stress failure criterion:

- The Weibull weakest link model is rejected as the failure location is predetermined. Further, a size effect $\propto \text{volume}^{-0.5}$ is found, indicating that the material strength does not follow the commonly recognized Weibull strength distribution with shape parameter $k = 5$. Lastly, though a prime example of a Weibull material full of strength reducing flaws, LVL specimens show no size effect.
- A failure model using damage relevant Weibull stresses is questioned for theoretical reasons. Based on the experiments it is rejected as the stress giving the same failure probability for uniform stress state becomes volume independent only for values of k so high that no size effect is allowed in the uniformly stressed material.
- The observed size effect $\propto \text{volume}^{-0.5}$ is identical to the brittle fracture mechanical size effect. However, fracture mechanics cannot explain the observations as the LVL specimens which have similar fracture properties show no size effect.

- A maximum stress failure criterion is promising when stress distribution determined by the use of cylindrical orthotropy is used. FEM modelling shows the stress inhomogeneity to increase with increased height for a constant mean stress and the normalized nominal strength from FEM modelling and experiments coincide.

The simple stress failure criterion apply to the investigated specimens. In a broader context the result of the investigation questions the correctness of the traditional stochastic explanation of size effect in tension perpendicular to the grain.

References

Aicher, S. & Dill-Langer, G. (1997), 'Climate induced stresses perpendicular to the grain in glulam', *Otto-Graf-journal* **8**, 209–231. FMPA - Otto-Graf-Institute, Stuttgart.

Aicher, S. & Reinhardt, H. W. (1993), 'Einfluss der Bauteilgrösse in der linearen und nichtlinearen (Holz-)Bruchmechanik', *Holz als Roh- und Werkstoff* **51**, 215–220.

Aicher, S., Dill-Langer, G. & Ranta-Maunus, A. (1998), 'Duration of load effect in tension perpendicular to the grain of glulam in different climates', *Holz als Roh- und Werkstoff* **56**, 295–305.

Aicher, S., Reinhardt, H. W. & Klöck, W. (1993), 'Nichtlinearen Bruchmechanik-Maßstabsgesetz für Fichte bei Zugbeanspruchung senkrecht zur Faserrichtung', *Holz als Roh- und Werkstoff* **51**, 385–394.

Barrett, J. D. (1974), 'Effect of Size on Tension Perpendicular-to-Grain Strength of Douglas-Fir', *Wood and Fiber* **6**(2), 126–143.

Bažant, Z. P. & Pfeiffer, P. A. (1987), 'Determination of fracture energy from size effect and brittleness number', *ACI Materials Journal* pp. 463–480.

Castéra, P. & Lac, P. (1997), 'Effet d'échelle en traction perpendiculaire pour un multicouche composé de lamelles orthotropes: cas du bois lamellé collé', *French Journal of Timber Engineering, Annales GC Bois* **2**, 15–24.

EC5-1 (1995), Eurocode 5 – Design of timber structures – Part 1–1: General rules and rules for buildings, Preliminary building code prENV 1995-1-1, European Committee for Standardization.

Fonselius, M. (1986), Brottmekanisk studie på gran ock skiktträ, Report 80, Helsinki University of Technology, Department of Civil Engineering, Division of Structural Engineering, Espoo, Finland. (In Swedish).

Gustafsson, P. J., Hoffmeyer, P. & Valentin, G. (1998), 'Dol behaviour of end-notched beams', *Holz als Roh- und Werkstoff* **56**, 307–317.

Hanhijärvi, A. & Ranta-Maunus, A. (1996), Computational analysis of the effect of transverse anisotropy and annual ring pattern in cross-sections of curved glulam beams on the size effect of strengths., *in* 'Proceedings of European Workshop on application of statistics and probabilities in Wood Mechanics, Bordeaux, France, February 22–23, 1996'.

Hearmon, R. F. S. (1948), The elasticity of wood and plywood, Special Report 7, Forest Products Research, London.

Hoffmeyer, P., Damkilde, L. & Pedersen, T. N. (2000), 'Structural timber and glulam in compression perpendicular to grain', *Holz als Roh- und Werkstoff*.

Kollmann, F. F. P. & Côté, W. A. (1984), *Principles of Wood Science and Technology*, Vol. I: Solid Wood, reprint edn, Springer-Verlag.

Larsen, H. J. & Riberholt, H. (1981), Strength of Glued Laminated Beams. Part 4, Technical Report 8110, Institute of Building Technology and Structural Engineering, Aalborg University Centre, Aalborg, Denmark.

Mistler, H. (1998), 'Querzug-Bemessung von BSH-Trägern nach EC 5. Ein Vergleich mit Forschungsergebnissen', *Holz als Roh- und Werkstoff* **56**, 51–59.

Ranta-Maunus, A. (1996), The influence of changing state of stress caused by mechano-sorptive creep on the duration of load effect, *in* S. Aicher, ed., 'Proceedings of the 1996 International Conference on Wood Mechanics, Stuttgart, Germany, May 14–16, 1996', pp. 187–201.